PHYSICS REPORTS

NORTH-HOLLAND

PHYSICS REPORTS
A Review Section of Physics Letters

Aims and scope: Physics Reports keeps the active physicist up-to-date on developments in a wide range of topics by publishing timely reviews which are more extensive than just literature surveys but normally less than a full monograph. Each Report deals with one specific subject. These reviews are specialist in nature but contain enough introductory material to make the main points intelligible to a non-specialist. The reader will not only be able to distinguish important developments and trends but will also find a sufficient number of references to the original literature.

Abstracted/indexed in: Current Contents: Physical, Chemical & Earth Sciences/INSPEC/Physics Briefs.

Subscription information: Physics Reports (ISSN 0370-1573) is published weekly. For 1996, Volumes 264–276 (78 issues altogether) have been announced. The subscription price for these volumes is available upon request from the Publisher. A combined subscription to the 1996 issues of Physics Letters A, Physics Letters B and Physics Reports is available at a reduced rate.

Subscriptions are accepted on a prepaid basis only and are entered on a calendar year basis. Issues are sent by SAL (Surface Air Lifted) mail wherever this service is available. Airmail rates are available upon request. Please address all enquiries regarding orders and subscriptions to: Elsevier Science B.V., Order Fullfilment Department, P.O. Box 211, 1000 AE Amsterdam, The Netherlands. Tel. + 31 20 4853642, Fax: + 31 20 4852598.

Claims for issues not received should be made within six months of our publication (mailing) date.

US mailing notice: Physics Reports (ISSN 0370-1573) is published weekly by Elsevier Science B.V., P.O. Box 211, 1000 AE Amsterdam, The Netherlands. Annual subscription price in the USA is US$ 3203.00 (valid in North, Central and South America only), including air speed delivery. Second class postage paid at Jamaica, NY 11431.

USA Postmasters: Send address changes to Physics Reports, Publications Expediting, Inc., 200 Meacham Avenue, Elmont, NY 11003. Airfreight and mailing in the USA by Publications Expediting, Inc., 200 Meacham Avenue, Elmont, NY 11003.

Printed in the Netherlands

North-Holland, an imprint of Elsevier Science

PHYSICS REPORTS

ELECTROMAGNETIC PROPERTIES OF SMALL-PARTICLE COMPOSITES

Vladimir M. SHALAEV

Department of Physics, New Mexico State University, Las Cruces, NM 88003, USA

ELSEVIER

AMSTERDAM – LAUSANNE – NEW YORK – OXFORD – SHANNON – TOKYO

ELSEVIER

PHYSICS REPORTS

Physics Reports 272 (1996) 61–137

Electromagnetic properties of small-particle composites

Vladimir M. Shalaev

Department of Physics, New Mexico State University, Las Cruces, NM 88003, USA

Received September 1995; editor: A.A. Maradudin

Contents:

SSDI 0370-1573(95)00076-3

Abstract

Recent advances in the electromagnetics of composite materials are reviewed. In particular, linear and non-linear optical properties of small-particle aggregates are considered. The effects of fractal morphology, such as a localization of dipolar eigenmodes and large fluctuations of local fields, are analyzed.

PACS: 78.90.+t; 42.65.An; 61.43.Hv; 42.70.Nq

1. Introduction

Electromagnetic phenomena in metal-insulator composites (thin films, cermets, colloidal aggregates, etc.) have been intensively studied for the last two decades [1]. These media typically include small, nm-sized, particles. Nanostructured composites possess fascinating electromagnetic properties, which differ greatly from those of ordinary bulk material, and they are likely to become ever more important with the miniaturization of electronic and optoelectronic components.

Fractal structures are prevalent in composites. The emergence of fractal geometry was a significant breakthrough in the description of irregularity [2,3]. Fractal objects do not possess translational invariance and, therefore, cannot transmit running waves [3,4]. Accordingly, dynamical excitations, such as vibrational modes (fractons), tend to be localized in fractals [3–6]. Formally, this is a consequence of the fact that plane running waves are not eigenfunctions of the operator of dilation symmetry characterizing fractals. The efficiency of fractal structures in damping running waves is probably the key to a "self-stabilization" of many of the fractals found in nature [3].

The number of particles in a fractal cluster of gyration radius R_c is given by $N = (R_c/R_0)^D$, where R_0 is a typical separation between nearest neighbors, and D is the fractal (Hausdorff) dimension, which is, in general, fractional and less than the dimension of the embedding space d, i.e. $D < d$. Such a power-law dependence of N on R_c implies a spatial scale invariance (self-similarity) for the system. For the sake of brevity, we refer to fractal aggregates, or clusters, as fractals. Particle positions in fractals are correlated so that the pair correlation function $g(r) \propto r^{D-d}$, where r is the distance between two points in a cluster. This correlation makes fractals different from "truly" random systems such as salt scattered on the top of a desk. Note that the correlation becomes constant, $g(r) = const$, when $D = d$; this case corresponds to conventional media, such as crystals, gases, and liquids. The unusual morphology associated with fractional dimension results in the unique physical properties of fractals, including the localization of dynamical excitations indicated above.

Another important model used for the description of composites is percolation which is closely related to the concept of fractals. Percolation represents probably the simplest example of a disordered system. Consider a square lattice, where each site is occupied randomly with probability p (or empty with probability $1-p$). Assume that occupied sites imply electrical conductors, empty sites represent insulators, and that electrical current can flow only between nearest neighbor conductor sites. Then, there is a critical (threshold) concentration p_c above which the current can flow (percolate) from one edge of the lattice to the other; this is so-called site percolation. When the bonds between the sites are randomly occupied, we speak of bond percolation. The most common example of bond percolation is a random resistor network, where the metallic wires in a regular network are cut randomly with probability $q = 1 - p$. Again, there is a critical density $q_c = 1 - p_c$ that separates a conductive phase at low q from an insulating phase at large q. Perhaps, the most natural example of percolation is continuum percolation, such as a sheet of conductive material with circular holes punched randomly in it (Swiss cheese model). In contrast to site or bond percolation, in continuum percolation, the positions of the two components of a random mixture (in this case, presence or absence of holes) are not restricted to the discrete sites of a regular lattice.

In percolation, the concentration, p, plays a similar role as the temperature in thermal phase transitions: long-range correlations control the percolation transition and the relevant quantities near p_c are described by power laws and critical exponents.

A percolation system can be thought of as a set of clusters (consisting of connected bonds). For

$p < p_c$ only finite clusters exist; at $p = p_c$ there appears an infinite cluster. The mean size of the finite clusters, for p below and above p_c, is characterized by the correlation length $\xi(\sim R_c)$ that increases as $\xi \sim |p - p_c|^{-\nu}$ when p approaches p_c. As was first pointed out by Stanley [7], these finite clusters can be described as fractals for $r \ll \xi$. Thus, the number of sites (bonds) in the percolation clusters is $N \sim r^D$ for $r \ll \xi$ and $N \sim r^3$ for $r \gg \xi$.

The main objective of this paper is to describe electromagnetic properties of small-particle composites; we outline the main theoretical approaches and advances in this field. By "small particle" we mean a particle whose size is much less than the wavelength λ, so that the quasi-static approximation can be used to describe the response of an individual particle. (Typically, the particle size ranges from tens to hundreds of nanometers.) The particles are embedded in a host material and can be aggregated (or not) into clusters. The size of a cluster, in general, can be arbitrary with respect to λ.

The electromagnetic response can be described in terms of the complex dielectric function $\epsilon \equiv \epsilon' + i\epsilon''$, or complex conductivity $\sigma \equiv \sigma' + i\sigma''$; these two quantities are related by the formula $\epsilon = 4\pi i\sigma/\omega$. If the particles in a cluster are conductive and connected, there is a flow of conducting electrons (Ohmic current) through the system. There is also a dipolar response, which arises in Maxwell's equations through the displacement current. For a Drude metal, the Ohmic current dominates in the low-frequency region ($|\epsilon'| \ll \epsilon''$), and the displacement current (dipolar response) dominates in the high-frequency region, when $|\epsilon'| \gg \epsilon''$.

In the low-frequency region, percolation theory can be successfully used to describe the dc and ac conductivity. In particular, near the percolation threshold, scaling theory can be applied. We consider briefly the basic concepts of ac conductivity theory for percolation systems in Section 2.

In the high-frequency region, there is a non-compensated surface charge on small particles resulting in their polarization (dipolar response) and, therefore, in alteration of the field acting on the particles. One can associate with each particle a dipole moment d that "generates" a secondary field ($\propto r^{-3}$ in the near zone). The dipole-dipole interaction ($\propto r^{-3}$) is long range for conventional three-dimensional media. Thus, in the high-frequency range, there are strong dipolar interactions between particles in a cluster and clusters.

The optical (dipolar) response of inhomogeneous media can often be successfully described using various mean-field theories. We outline these theories and their application to determining optical properties of composites in Section 3.

A semi-phenomenological spectral representation that takes into account the presence of collective dipolar modes (characterized by various depolarization factors) is considered in Section 4. This theory, however, does not give, in general, a recipe for the calculation of mode strengths from first principles.

Spatial scaling that occurs for $r \ll R_c$ can dramatically affect the optical properties of fractal clusters. In Section 5 we consider the scaling of optical properties of diluted fractal clusters. In particular, dispersion relations characterizing the frequency-dependent localization of dipolar modes in fractals will be analyzed here.

Optical properties of original (non-diluted) small-particle clusters are considered in Section 6. The general solution to the coupled-dipole equations are presented and analyzed in this section. Optical properties of fractal and non-fractal small-particle composites are also compared in Section 6.

As shown in Sections 5 and 6, dipolar eigenmodes in fractal composites are substantially different from those in other media. For example, there is only one dipolar eigenstate that can be excited by a homogeneous field in a dielectric sphere (for a spheroid, there are three resonances with non-zero

total dipole moment); the total dipole moment of all other eigenstates is zero and, therefore, they can be excited only by inhomogeneous field. In contrast, fractal aggregates possess a variety of dipolar eigenmodes, distributed over a wide spectral range, which can be excited by a homogeneous field. In the case of continuous media, dipolar eigenstates (polaritons) are running plane waves that are eigenfunctions of the operator of translational symmetry. This also holds in most cases for microscopically disordered media that are, on average, homogeneous. Dipolar modes, in this case, are typically delocalized over large areas, and all monomers absorb light energy, with approximately equal rate, in regions that significantly exceed the wavelength. In contrast, fractal composites have eigenstates that are often localized in sub-wavelength regions. Absorption by monomers in these "hot zones" is much higher than by other monomers in a fractal composite. This is a consequence of the already mentioned fact that fractals do not possess translational symmetry; instead, they are symmetrical with respect to scale transformation.

In Section 7, the non-linear optical responses of small-particle composites are considered. Nanostructured composites may have much larger non-linear susceptibilities than those of ordinary bulk materials. The enhancement of the non-linear optical response in composites is basically due to strong fluctuations of local fields. These fluctuations are especially large in composites with fractal morphology. In this case, local field distributions are extremely inhomogeneous in space and include "hot zones" associated with localized modes. The non-linearities emphasize the role of fluctuations leading to huge non-linear susceptibilities. In Section 7 we consider a number of strongly enhanced optical processes in composite materials.

Brief summarizing remarks are presented in the concluding Section 8.

2. Critical behavior of the conductivity and dielectric function in a percolation system

The random resistor (R), and resistor-inductor-capacitor (RLC), network models are widely used to describe electromagnetic properties of a percolation system; they permit the study of dc and ac conductivity, respectively [8,9]. Pioneering work in this field has been carried out by Efros and Shklovskii [10] and by Straley [11]. By generalizing the scale-invariance concept from phase transition theory, and the related theory of dynamic critical phenomena (for the latter see, for example, Ref. [12]), they developed a theory of electrical transport in a metal-insulator composite near the percolation threshold.

In the quasi-static limit, the problems of finding the electrical conductivity and the dielectric function are equivalent, since the corresponding equations for the current density and conductivity σ, and for the displacement current and dielectric function ϵ are identical (see, for instance, Ref. [13]). Accordingly, electrical and dielectric properties of inhomogeneous media can be equally described in terms of either the complex conductivity, $\sigma \equiv \sigma' + i\sigma''$, or the complex dielectric function, $\epsilon \equiv \epsilon' + i\epsilon''$. As mentioned above, these two quantities are related via the equation $\epsilon = (4\pi i/\omega)\sigma$.

For a Drude metal, the dielectric constant is given by

$$\epsilon = \frac{4\pi i\sigma}{\omega} = \epsilon_0 + \frac{4\pi i\sigma(0)}{\omega[1 + i\omega\tau]}, \tag{2.1}$$

where the dc conductivity $\sigma(0)$ is related to the plasma frequency, ω_p, and the relaxation time, τ, by $\sigma(0) = \omega_p^2\tau/(4\pi)$; the quantity ϵ_0 is the contribution to ϵ due to interband electron transitions.

The properties to be considered below are different for the low- and high-frequency regions, where $\epsilon'' \gg |\epsilon'|$ and $|\epsilon'| \gg \epsilon''$, respectively. In the first case, the conduction electron response associated with the Ohmic current ($j_\Omega = \sigma' E$) dominates, while in the latter limit, dipolar response associated with the displacement current ($j_D = \epsilon' \partial E/\partial t = -i\omega\epsilon' E$) prevails. If the free charge current dominates, the susceptibility of a metallic particle in a composite is given by the bulk value, $\chi = (\epsilon - 1)/4\pi$, with ϵ defined in (2.1) (for simplicity, we assume here that the host is vacuum). However, if the current of conduction electrons is small, one must take into account non-compensated charges in opposite sides of the particle surface. This is because free electron displacements in the high-frequency range are typically less than atomic dimensions, and metal particles exhibit dielectric rather than conductive behavior. In this case, particles in the composite are polarized and the dipolar response (displacement current) dominates. The polarization is determined in general by the form of a particle. For a spherical particle, the susceptibility is given by $\chi_0 = (3/4\pi)[(\epsilon - 1)/(\epsilon + 2)]$. At $\epsilon' = -2$, there is a resonance associated with the localized surface plasmon (LSP) excitation. As shown below, the LSP resonance plays a crucial role in the optics of metal composites.

We consider first the low-frequency limit, $\epsilon'' \gg |\epsilon'|$ (i.e. $\sigma' \gg \sigma''$). For a Drude metal, this case corresponds typically to the inequality $\omega\tau \ll 1$ and the dielectric function is approximated by

$$\epsilon' = \epsilon_0 + 4\pi\sigma(0)\tau, \quad \epsilon'' = 4\pi\sigma(0)/\omega. \tag{2.2}$$

For the low-frequency region, one can also neglect contributions from interband transitions and put $\epsilon_0 = 1$ in Eq. (2.2).

We assume below that $|p - p_c| \ll p_c$ and $h \equiv \epsilon_i/\epsilon \ll 1$, where ϵ_i and ϵ are dielectric functions for the (host) insulator and metal constituents, respectively. If these two requirements are met, one can apply the theory of Refs. [10,11]. The parameter h plays in this theory the same role as a magnetic field in ferromagnetic phase transition theory [10].

The effective dielectric function of a composite material near the percolation threshold has the form [10,11,14,15]

$$\frac{\epsilon_e}{\epsilon} \sim L^{-t/\nu} F\left(\frac{\epsilon_i}{\epsilon} L^{(t+s)/\nu}\right), \tag{2.3}$$

where

$$L = \min\{l, L_\omega, \xi, q^{-1}\}. \tag{2.4}$$

Here l is the linear size of a system, ξ is the percolation correlation length, q is the wave vector, and L_ω is the coherence length, which often can be identified with the localization length. (All lengths are measured in units of a typical grain size, a, which is assumed to be small.) Below, we assume that l, $q^{-1} \gg L_\omega$, ξ (the condition $q^{-1} \gg l$ corresponds to the quasi-static limit), so that the length scale of importance is either L_ω or ξ.

The scaling function $F(z)$ in (2.3) has the limiting forms described below [10,14,15].

For large values of $|z|$, $F(z)$ is given by

$$F(z) = A_0 z^{t/(t+s)}, \quad |z| \gg 1. \tag{2.5}$$

For small $|z|$, the form depends upon whether there exists a conducting path connecting opposite sides of the sample. If such a path exists, i.e. if $p > p_c$,

$$F(z) = A_1 + A_2 z, \quad |z| \ll 1 \quad (p > p_c). \tag{2.6}$$

If there is no conducting path across the sample,

$$F(z) = A_3 z + A_4 z^2, \quad |z| \ll 1 \quad (p < p_c), \tag{2.7}$$

and the sample is insulating for a dc signal. Since $\epsilon_i \ll \epsilon$, the condition $|z| \ll 1$ corresponds to relatively small scales L, for which there is a distinction between conducting and insulating parts of a system, whereas at very large scales, $|z| \gg 1$, the existence of a conducting part becomes unimportant, and therefore ϵ_e has no dependence on L and its form is the same for $p > p_c$ and $p < p_c$.

The percolation correlation length ξ has the following critical behavior [4]:

$$\xi \sim |p - p_c|^{-\nu}. \tag{2.8}$$

The excitation (coherence) length L_ω is determined by the mean-square distance traveled in a random walk with the travel time t [4–6,16]

$$\langle r^2(t) \rangle \propto t^{2/(2+\Theta)}, \tag{2.9}$$

where $2+\Theta = d_w = 2D/\tilde{d}$ is the fractal dimension of the random walk. The exponent $\tilde{d}$ is the fracton (spectral) dimension which determines the spectral dependence of the density of vibrational states, fractons [5,6]:

$$\rho \sim \omega^{\tilde{d}-1}. \tag{2.10}$$

For homogeneous media, $\Theta = 0$ and (2.9) gives the usual diffusion law. For fractal clusters, $\Theta > 0$ reflects the slowing down of the diffusion process in fractals [5,6,16].

The frequency, ω, of the applied field determines the travel time t during which the random walk traverses the region L_ω,

$$L_\omega \propto \omega^{-1/(2+\Theta)}. \tag{2.11}$$

The "anomalous" diffusion picture [16] assumes that the random walk traverses a single cluster whose size is larger than L_ω. It is important to note that for an ac current, the above relation is valid as long as all capacitance-related impedances are much larger than that of the metallic path. This implies that there is no interaction between the clusters of a percolation systems (i.e. there are no capacitances on bonds connecting different clusters).

Below we analyze the dielectric function, ϵ, for the two limiting cases, $\xi \ll L_\omega$ and $\xi \gg L_\omega$.

We first consider the case when $\xi \ll L_\omega$, with ξ satisfying Eq. (2.8). Note that the function $F(z)$ defined in (2.5)–(2.7) results in ϵ_e which is independent of ξ in the limit $|z| \gg 1$ (this corresponds to the case of high magnetic fields in ferromagnetic phase transition theory), whereas in the limit $|z| \ll 1$ and $|p - p_c| \to 1$, one has $\epsilon_e \to \epsilon$ and $\epsilon_e \to \epsilon_i$ for $p > p_c$ and $p < p_c$, respectively. This agrees, of course, with the expected limiting behavior.

As follows from (2.5)–(2.7), scaling is quite different in the two limits, $|z| \ll 1$ and $|z| \gg 1$. Thus, the relation $|z| \sim 1$, together with Eq. (2.8), defines the crossover frequency $\omega_c \sim (\omega_p^2 \tau/\epsilon_i)|p - p_c|^{t+s}$; accordingly, the limits $|z| \ll 1$ and $|z| \gg 1$ correspond to $\omega \ll \omega_c$ and $\omega \gg \omega_c$, respectively.

In accordance with (2.3) and (2.5)–(2.7), the real part of the dielectric function has the following forms in the limit $\xi \ll L_\omega$ [14]:

$$\epsilon_e' = \begin{cases} A_0 \epsilon_i^{t/(t+s)} [\omega/4\pi\sigma(0)]^{-s/(t+s)} \cos\left(\frac{\pi}{2}\frac{s}{t+s}\right), & \text{if } |z| \gg 1 \\ A_2 \epsilon_i |p - p_c|^{-s}, & \text{if } |z| \ll 1,\ p > p_c \\ A_3 \epsilon_i |p - p_c|^{-s}, & \text{if } |z| \ll 1,\ p < p_c \end{cases} \tag{2.12}$$

According to (2.12), in the limit $|z| \ll 1$, quantity ϵ_e' has the same scaling dependence (as a function of $p - p_c$) both below and above the threshold [10]. Note also that ϵ_e' has a peak at $\omega = 0$ as a function of the frequency. The half-width of the peak $\Delta\omega \approx [4\pi\sigma(0)/\epsilon_i]|p - p_c|^{t+s}$ decreases to zero at p_c, and its height is proportional to $\epsilon_i |p - p_c|^{-s}$ (i.e. it diverges at p_c [14]).

For the imaginary part of the dielectric function, $\epsilon_e'' = (4\pi/\omega)\sigma_e'$, we obtain from (2.3) and (2.5)–(2.7) ($\xi \ll L_\omega$) [10,11,17,18]

$$\epsilon_e'' = \begin{cases} A_0 \epsilon_i^{t/(t+s)} [\omega/4\pi\sigma(0)]^{-s/(t+s)} \sin\left(\frac{\pi}{2}\frac{s}{t+s}\right), & \text{if } |z| \gg 1 \\ A_1 4\pi\sigma(0)\omega^{-1} |p - p_c|^t, & \text{if } |z| \ll 1,\ p > p_c \\ -A_4 \epsilon_i^2 \left[\frac{\omega}{4\pi\sigma(0)}\right] |p - p_c|^{-t-2s}, & \text{if } |z| \ll 1,\ p < p_c \end{cases} \tag{2.13}$$

Note that $A_4 < 0$ in (2.13).

The absorption coefficient is defined by $\alpha = 2(\omega/c)\,Im\sqrt{\epsilon_e}$. In the low-frequency limit ($\omega\tau \ll 1$) we find $\epsilon \approx i\epsilon'' \approx i\omega_p^2\tau/\omega$. Then, for $|z| \ll 1$ and $p < p_c$, using (2.12) and (2.13), we find $\epsilon_e'' \ll |\epsilon_e'|$, $\epsilon_e' \sim z$, and $\epsilon_e'' \sim z^2$. Accordingly, $\alpha \approx (\omega/c)\epsilon_e''/\sqrt{\epsilon_e'}$, and [17]

$$\alpha \sim \frac{\epsilon_i^{3/2}}{\omega_p^2 \tau c} \omega^2 |p - p_c|^{-(t+3s/2)}. \tag{2.14}$$

Eq. (2.14) gives the known quadratic frequency dependence for α (for a Drude metal, this dependence is also predicted by the effective-medium theory in the dilute limit, as shown in Section 3).

For $|z| \ll 1$ and $p > p_c$, comparing (2.12) and (2.13), we obtain that $\epsilon_e'' \gg |\epsilon_e'|$ since $\epsilon_e'' \sim O(1)$ and $\epsilon_e' \sim z$. Thus $\alpha \approx \sqrt{2}(\omega/c)\sqrt{\epsilon_e''}$ and [17]

$$\alpha \sim (\omega_p/c)(\omega\tau)^{1/2} |p - p_c|^{t/2}. \tag{2.15}$$

Eq. (2.15) gives the $\omega^{1/2}$ dependence of the Hagen-Rubens relation for conducting materials.

For $|z| \gg 1$ the absorption coefficient shows the anomalous frequency dependence

$$\alpha \sim c^{-1} (\omega_p^2 \tau)^{s/2(s+t)} \epsilon_i^{t/2(s+t)} \omega^{(s+2t)/2(s+t)}. \tag{2.16}$$

In this limit, the ac conductivity has the following frequency dependence [10,14,19]:

$$\sigma_e' = (\omega/4\pi)\epsilon_e'' \propto \omega^{t/(s+t)}.$$

We now consider the other limiting case when $L_\omega \ll \xi$, so that $L = L_\omega$ in (2.4). The condition $L_\omega \ll \xi$ means that during a period $\sim \omega^{-1}$ a random walker traverses a region smaller than the correlation length ξ.

First, note that in the frequency domain the condition $L_\omega \ll \xi$ corresponds to the requirement $\omega \gg \omega_{c1}$ where ω_{c1} is the crossover frequency which is determined by the relation $L_\omega \sim \xi$ and

which, in general, differs from the earlier introduced ω_c. For the anomalous diffusion, L_ω is given by (2.11), and we have $\omega_{c1} \sim \xi^{-(2+\Theta)}$. Note that similar to the case considered above ($\xi \ll L_\omega$), there is also a crossover frequency, ω_{c2}, corresponding to the transition from the region $|z| \ll 1$ to the region $|z| \gg 1$ (which in the case of $\xi \gg L_\omega$ defined by the relation $L_\omega \sim (\epsilon/\epsilon_i)^{\nu/(t+s)}$). Thus there is, in general, a family of different crossover frequencies associated with various dynamic regimes.

In the limit $|z| \gg 1$, we obtain from (2.3) and (2.5) the same result for ϵ_e as in the previous case ($L_\omega \gg \xi$), with $|z| \gg 1$,

$$\epsilon_e/\epsilon \sim (\epsilon_i/\epsilon)^{t/(t+s)} \tag{2.17}$$

for both $p > p_c$ and $p < p_c$.

Note that Eq. (2.17) is valid for any L in (2.4), provided $|z| \gg 1$, and it is usually associated with anomalous frequency dependence (see, for example, Ref. [19]).

For the case of $|z| \ll 1$, with $p > p_c$, we obtain from (2.3) and (2.6)

$$\epsilon_e \sim \epsilon L_\omega^{-t/\nu}. \tag{2.18}$$

With the use of (2.11), this leads to

$$\epsilon_e'' \propto \omega^{[t/\nu(2+\Theta)]-1}, \tag{2.19}$$

so that the corresponding ac conductivity is given by $\sigma' \propto \omega^{[t/\nu(2+\Theta)]}$. This result was first reported by Gefen, Aharony and Alexander [16], who developed the theory of anomalous diffusion on percolation clusters. Their method consisted of integrating (2.9) over the cluster size distribution in a percolation system. Note that, as was pointed out by the authors [16], this method does not take into account capacitances between different clusters. This is equivalent to the case when the polarization of the medium (within which the clusters are embedded) tends to zero.

Using the known relations for critical indices [4] $2+\Theta = d_w = 2D/\tilde{d}$ and $t/\nu = d-2-D+2D/\tilde{d}$ one obtains from (2.19)

$$\epsilon_e'' \propto \omega^{-(D+2-d)/d_w}. \tag{2.20}$$

In the dielectric limit, $p < p_c$ (with $|z| \ll 1$), we obtain from (2.3) and (2.7) $\epsilon_e'' \propto \omega^m$, where $m = 1-(t+2s)/(\nu d_w)$. Using the relation $t/\nu = d-2-D+d_w$, and the conjecture $s+t = d\nu$ [20], we obtain $m = 2-(D+2+d)/d_w$. Note, however, that this result is based on the use of (2.11) and thus it neglects the capacitance-related interaction between the clusters.

Thus, Eqs. (2.3)–(2.5) allow one to calculate the dielectric function of a percolation system in all limiting cases, $|z| \gg 1$ and $|z| \ll 1$, with $p > p_c$ and $p < p_c$ (metallic and dielectric behavior, respectively).

The present theory is also valid for a system consisting of a good conductor and a bad conductor. In particular, a theory similar to that described above was developed for the complex dielectric constant of a superconductor–normal conductor transition in a disordered system [14,21]. The parameter h in this case is given by $h = \sigma_n/\sigma_s$ where σ_n and σ_s are the conductivities of normal (n) and superconducting (s) metals.

Above, we assumed that $\omega\tau \ll 1$. If $\omega\tau \sim 1$, then the relation $|\epsilon| \gg \epsilon_i$ still typically holds for metal-insulator composites and, thus, the theory outlined above can be applied. However, in this case, $|\epsilon|' \sim \epsilon''$ and one has to take into account modifications due to the polarization of particles associated

with the displacement current. Accordingly, the effective dielectric constant is expected to depend on the particle form in this case.

Such dependence becomes especially important in the high-frequency limit, $\omega\tau \gg 1$, when $|\epsilon'| \gg \epsilon''$ and the displacement current dominates. At these frequencies, a more appropriate description of the optical response involves light-induced dipoles on particles and interactions between them. The dipole-dipole interaction in a three-dimensional space is long range. Accordingly, in addition to the interaction of particles within one cluster, inter-cluster interactions are also of importance in a percolation system in the high-frequency range. Spatial scaling occurs in a percolation system only within a connected fractal cluster (in the range $r \ll \xi$), while the system as a whole is, on average, three dimensional and homogeneous. (Inside the volume occupied by a fractal cluster there are many other smaller clusters; although these clusters are not geometrically connected with the larger cluster, they strongly interact with it via dipole forces.) We anticipate that fractality in the space domain results in the scaling of dynamical excitations only if the inter-cluster interactions are not too large. Because of the long-range character of the dipole-dipole interaction (prevailing in the optical range), the scaling in a percolation system probably does not play as an important role in the optical range as it does in the low-frequency limit (where the Ohmic current dominates and the capacitance-related interaction between clusters is relatively small). In accordance with this, numerical simulations [18] of absorption by percolation clusters do not show a critical dependence on $p - p_c$ in the visible part of the spectrum. (In the optical range, the mean-field theory [21] can often be used successfully to describe the optical properties of a percolation system.)

Note, however, that for a mixture of well-separated and, therefore, non-interacting, fractal clusters (such as small-particle aggregates in colloidal solutions), scaling can play a crucial role (see Section 5).

It is also worth noting that in the form presented above percolation theory cannot be directly applied to the description of optical properties in the range where LSP resonances are effective. This is because one has typically $|\epsilon|/\epsilon_i \sim 1$ in this spectral range and thus the theory requirement $|\epsilon|/\epsilon_i \gg 1$ does not hold. However, a modified theory that takes into account alterations of particle susceptibility due to its polarization and the resonant character of the excitation, can be developed in this case [22–34].

The susceptibility of a polarizable spherical particle in the optical range is $\chi_0 = (3/4\pi)(\epsilon - \epsilon_i)/(\epsilon + 2\epsilon_i) \equiv -(X + i\delta)^{-1}$, where

$$X = -Re(\chi_0)^{-1} = -\frac{4\pi}{3}\left[1 + \frac{3\epsilon_i(\epsilon' - \epsilon_i)}{|\epsilon - \epsilon_i|^2}\right], \quad \delta = -Im(\chi_0)^{-1} = 4\pi\frac{\epsilon''\epsilon_i}{|\epsilon - \epsilon_i|^2}. \tag{2.21}$$

Here X plays a role of a spectral variable and δ is a decay parameter which is small, $\delta \ll 1$, in the high-frequency range. In the vicinity of the LSP resonance ($\epsilon'(\omega_0) = -2\epsilon_i$) the value of X is also small, $|X| \ll 1$ ($X \propto (\omega - \omega_0)$. Thus, we have $|\chi_0| \gg 1$ near the LSP resonance and a scaling theory, similar to the phase transition theory for $|T - T_c|/T_c \ll 1$ and the percolation theory for $|p - p_c| \ll 1$, can be formulated. Such a theory was developed by Stockman, Shalaev and their co-workers [24–34] (see Sections 5 and 6). In this theory, the point $X = 0$ plays, in a sense, a similar role as $|T - T_c|/T_c$ in the phase transition theory, and as $|p - p_c|$ in the percolation theory. In all of these cases, the scaling behavior of physical characteristics is associated with long-range fluctuations near a critical point.

3. Mean-field theories and numerical techniques

3.1. Maxwell-Garnett and effective-medium theories

One of the appealing features of effective-medium theories is the ease with which one may calculate the dielectric constant of a composite material ϵ_e. In the case of a two-phase, d-dimensional medium, the Maxwell-Garnett theory (MGT) yields the following expression [35] for ϵ_e in terms of the dielectric constants of the host medium ϵ_2 and spherical inclusions ϵ_1 (present with volume fraction p_1):

$$\frac{\epsilon_e - \epsilon_2}{\epsilon_e + (d-1)\epsilon_2} = p_1 \frac{\epsilon_1 - \epsilon_2}{\epsilon_1 + (d-1)\epsilon_2} \tag{3.1}$$

(note that similar approaches have been also developed earlier for dielectrics by Clausius [36] and Mossotti [37], and applied in optics by Lorentz [38] and Lorentz [39]). The MGT expression is obviously non-symmetrical with respect to the exchange $\epsilon_1 \to \epsilon_2$, $\epsilon_2 \to \epsilon_1$ and is justified only in the limit of small p_1 when it can be simplified:

$$\epsilon_e = \epsilon_2 + 3p_1\epsilon_2 \frac{\epsilon_1 - \epsilon_2}{\epsilon_1 + (d-1)\epsilon_2} + O(p^2). \tag{3.2}$$

Thus, in the dilute limit, $p_1 \ll 1$, the interaction between particles is small and there is only one resonance at $\epsilon_1 = -2\epsilon_2$ (for $d = 3$), corresponding to the surface plasmon resonance of an isolated spherical particle. For metal particles in vacuum, in accordance with (2.1), the resonance occurs at $\omega = \omega_p/\sqrt{3}$.

The absorption coefficient $\alpha = 2(\omega/c)Im\sqrt{\epsilon_e}$ for $p_1 \ll 1$ is given by ($\epsilon_2 = 1$)

$$\alpha \approx 3p_1 \frac{\omega}{c} Im\left[\frac{\epsilon_1 - 1}{\epsilon_1 + 2}\right]^{1/2}. \tag{3.3}$$

Fig. 1 shows the absorption coefficient of a dilute suspension of metal spheres in vacuum, as calculated from MGT [21] (3.3). The surface plasmon resonance results in a strong absorption near $\omega = \omega_p/\sqrt{3}$. In the limit $\omega\tau \ll 1$, MGT gives an ω^2 dependence for the absorption:

$$\alpha = C\omega^2 p_1, \quad C = 9/[4\pi\sigma(0)c]. \tag{3.4}$$

While the experiment does show the predicted dependences on ω^2 and p_1, the magnitude of the absorption by a composite is typically much larger than that predicted by MGT. Enhancement of far-infrared absorption by a composite will be discussed below.

For larger values of p_1, Eq. (3.1) becomes a poor approximation. In particular, it fails to have a non-trivial percolation threshold for either of the two phases. The symmetric (in the two components) effective-medium theory (EMT), known also as coherent potential approximation, was first proposed by Bruggeman [40], and it offers the following formula for calculating ϵ_e:

$$p_1 \frac{\epsilon_1 - \epsilon_e}{\epsilon_1 + (d-1)\epsilon_e} + p_2 \frac{\epsilon_2 - \epsilon_e}{\epsilon_2 + (d-1)\epsilon_e} = 0. \tag{3.5}$$

This is a quadratic equation with the solution (see, for example, Ref. [41])

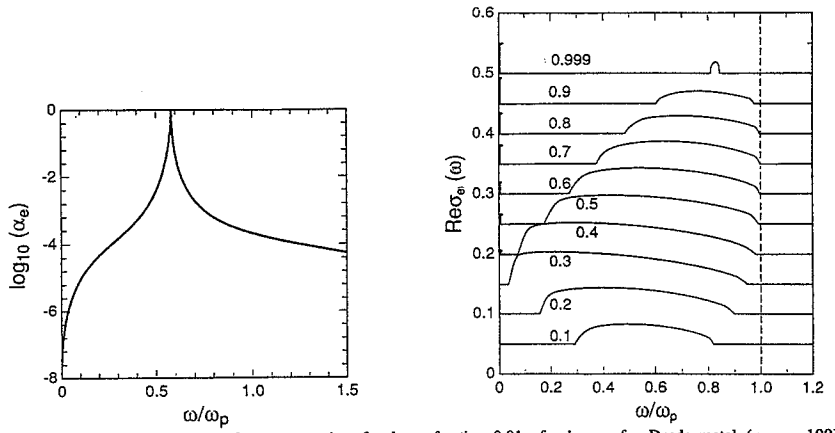

Fig. 1. Absorption coefficient, α_e, for a composite of volume fraction 0.01 of spheres of a Drude metal ($\omega_p\tau = 100$) embedded in a host medium of dielectric constant unity, as calculated in the quasi-static approximation and the dilute limit. Taken from Ref. [21].

Fig. 2. Schematic of $Re\,\sigma_e(\omega)$ of a metal-insulator composite made up of volume fraction p of a Drude metal and $1-p$ of insulator, as calculated in the EMT in the limit $\tau \to \infty$. The heavy vertical line at $\omega = 0$ denotes a δ-function, which represents the Drude peak; the integrated strength of the δ-function is proportional to the height of the δ-function. The peak at $p = 0.999$ is arbitrarily increased in height for clarity. Taken from Ref. [42].

$$\epsilon_e = \frac{1}{2(d-1)}\{d\bar{\epsilon} - \epsilon_1 - \epsilon_2 \pm [(d\bar{\epsilon} - \epsilon_1 - \epsilon_2)^2 + 4(d-1)\epsilon_1\epsilon_2]^{1/2}\}, \tag{3.6}$$

where $\bar{\epsilon} \equiv p_1\epsilon_1 + p_2\epsilon_2$. The upper sign in Eq. (3.6) should be used when ϵ_1 and ϵ_2 are both real and positive.

Fig. 2 shows $Re[\sigma_e(\omega)] = (\omega/4\pi)Im[\epsilon_e(\omega)]$, plotted against frequency for several values of p, as calculated within the EMT [42]. In contrast to a sharp peak described by the MGT expression, the EMT shows, for $p < p_c$ ($p_c = 1/3$ in the EMT), a single peak, broadened by electromagnetic interactions between individual grains. For $p > p_c$, a Drude peak, centered at $\omega = 0$ and corresponding to the dc conductivity of the composite, develops in addition to the surface plasmon band. The integrated strength of the Drude peak grows as p increases. The surface plasmon band eventually shrinks and narrows to a peak centered at $\omega = \omega_p\sqrt{2/3}$ that corresponds to a void resonance (charge oscillation in the vicinity of a spherical void in an otherwise homogeneous metal). Frequency dependences similar to those shown in Fig. 2 have been seen in experiments [43].

3.2. Differential effective-medium theory. Enhanced far-infrared absorption by fractal metal aggregates

It is well known that when a dilute distribution of small particles is placed in a dielectric host, long-wavelength absorption of the composite is proportional to the square of the frequency (see Eqs. (2.14), (3.4) and Fig. 1). What is surprising is that the magnitude of the observed absorption exceeds the classical prediction by a factor of $10^4 - 10^6$. There are many suggested explanations of this phenomenon [44–61]. Among these are quantum size effects, broad distribution of particle sizes, absorption due to resistive coating on particles, clustering of small metal particles into clumps, and formation of percolation clusters and fractal clusters.

An interesting extension of the EMT was suggested by Fuchs, who considered a diffuse-cluster model in which each aggregate is a sphere with a radially dependent filling factor [58]. At each radius r, the Bruggeman effective-medium theory was used to find the average dielectric constant $\epsilon_e(r)$ $(d=3)$

$$p_1(r)\frac{\epsilon_1-\epsilon_e(r)}{\epsilon_1+2\epsilon_e(r)}+[1-p_1(r)]\frac{\epsilon_2-\epsilon_e(r)}{\epsilon_2+2\epsilon_e(r)}=0, \tag{3.7}$$

where $p_2(r)=1-p_1(r)$. This model demonstrates that clustering broadens the dipole absorption peak and gives a low-frequency enhancement, ~100. However, the experimentally observed enhancement still significantly exceeds that predicted by the theory of Ref. [58].

Stroud and Hui developed the differential effective-medium theory (DEMT), describing far-infrared absorption by fractal clusters of metal particles embedded in a dielectric host [54]. They found that the absorption per unit mass of metal was enhanced, relative to that of isolated particles, by a factor which can equal several orders of magnitude; the enormous enhancement in the absorption occurs because of fractality.

In this model one begins by considering a cluster of radius R, with volume fraction of conductor $p(R)$ and of insulator $1-p(R)$. Then, adding metal and insulator to the cluster in such a way that the radius is increased by an amount δR, one may derive the following differential equation [54]:

$$\frac{d\epsilon_e(R)}{dR}=-\frac{3}{p(R)}\frac{dp(R)}{dR}\epsilon_e(R)\frac{\epsilon_i-\epsilon_e(R)}{\epsilon_i-\epsilon_e(R)}, \tag{3.8}$$

where ϵ_i is the dielectric constant of the insulator. Eq. (3.8) can be integrated to obtain the cubic equation

$$\frac{\epsilon_e(R)}{\epsilon_e(a)}\left[\frac{\epsilon_i-\epsilon(a)}{\epsilon_i-\epsilon_e(R)}\right]^3=\frac{1}{[p(R)]^3}, \tag{3.9}$$

where a is the radius of small metal particles forming the cluster and $\epsilon(a)$ is the dielectric constant of a metal particle. Note that similar equations have been used in DEMT of sedimentary rocks [62].

The volume fraction $p(R)$ of metal particles in a fractal cluster (embedded in a three-dimensional space, $d=3$) is given by $p(R)=(R/a)^{D-3}$, from which, using (3.9), one obtains

$$\frac{\epsilon_e(R)}{\epsilon_e(a)}\left[\frac{\epsilon_i-\epsilon(a)}{\epsilon_i-\epsilon_e(R)}\right]^3=(R/a)^{3(3-D)}. \tag{3.10}$$

The corresponding equation for the real part of the cluster conductivity, $\sigma_e'(R)$, in the low-frequency limit has the form [54]

$$\sigma_e'(R)=\sigma_e'(a)(R/a)^{-(3/2)(3-D)}. \tag{3.11}$$

As follows from Eq. (3.11), the conductivity of a cluster decreases with increasing radius leading to an enhancement of absorption.

In the low-frequency limit, the absorption α per unit mass of metal is given by [54]

$$\alpha\sim\frac{\omega^2}{\sigma(a)}(R/a)^{(5/2)(3-D)}. \tag{3.12}$$

Thus the far-infrared enhancement due to aggregation of initially isolated particles into fractal clusters is given by a factor $(R/a)^{(5/2)(3-D)}$. (The corresponding enhancement in two dimensions, $d=2$, is $(R/a)^{3(2-D)}$.) Clearly, the enhancement factors can be enormous for a large cluster.

In the end, we mention some other related papers in this field. Sheng and co-workers, through re-formulation of the coherent potential approximation, suggested a new scheme which is capable of identifying the quasi-wave modes as well as yielding their dispersion relations [63]. In earlier papers, Sheng et al. also calculated the local fields in random dielectric media characterized by uniform or percolative correlations [64], and studied the effects of multiple scattering by aggregate clusters [65]. Finally, Torquato developed a unified methodology to quantify the morphology; he analyzed various properties (such as the electric conductivity and elastic moduli) of inhomogeneous media from a general viewpoint (see Ref. [66] and references there).

3.3. Numerical calculations of the effective dielectric function

As mentioned above, the random resistor-inductor-capacitor (RLC) network model is widely used in numerical simulations of the effective conductance of inhomogeneous media and, in particular, of percolation systems [8,9,21]. A network containing complex impedances of two kinds, chosen to represent "insulating" and "conducting" particles, can describe composites of a Drude metal and a dielectric [67]. An insulating bond in this model is represented by a capacitor C' with admittance

$$\sigma_i=i\omega C'. \tag{3.13}$$

A metallic bond is represented as a series of a resistor and an inductor in parallel with a capacitor. The admittance of a metallic bond is

$$\sigma_m=\frac{1+i\omega RC-\omega^2LC}{R+i\omega L}, \tag{3.14}$$

where R is the resistance of the conducting element and L and C are its inductance and capacitance, respectively. The ratio $\sigma_m/\sigma_i=1-\omega_p^2/[\omega(\omega-i/\tau)]$ has a Drude form, with the choice $L=C=C'=1$ and $L/R=\tau$.

Among the most effective methods used for simulations of RLC networks are the transfer-matrix (TM) approach suggested by Derrida and co-workers [68] and the $Y-\Delta$ transformation developed by Frank and Lobb [69]. Note that although the $Y-\Delta$ algorithm is faster than the TM approach, it can be applied only to two-dimensional systems.

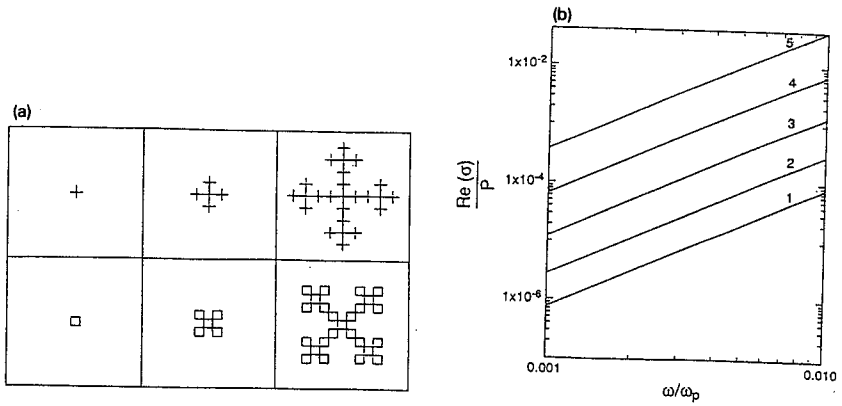

Fig. 3. (a) Schematic showing construction of the cross and square fractals, at stages 1, 2, and 3. (b) $Re\,\sigma_e(\omega)/p$ at low frequencies for stages 1–5 of a cross fractal. Taken from Ref. [70].

In the TM approach, the d-dimensional network is built by adding successive $(d-1)$-dimensional layers in a particular direction [21]. By applying an arbitrary voltage, V_j, at each surface sites of the most recently added layer, one relates the currents, I_i, that flow into these sites to the voltages in terms of a symmetric admittance matrix A_{ij} : $I_i = \sum_j A_{ij} V_j$. As new bonds are added to the network in order to complete the next layer, A_{ij} changes. Provided new bonds are added one by one, it is easy to calculate the resulting changes in A_{ij}.

The Frank and Lobb algorithm consists of a repeated application of a sequence of series, parallel and star-triangle ($Y-\Delta$) transformations to the bonds of the lattice. The final result of this sequence of transformations is to reduce any finite portion of the lattice to a single bond that has the same conductance as the entire lattice.

We briefly consider the results of absorption simulations based on the above algorithms. Hoffmann and Stroud [70], using the $Y-\Delta$ algorithm, have calculated the far-infrared absorption of a deterministic fractal embedded in a two-dimensional dielectric host. The clusters were built up in stages, starting from four metallic bonds arranged in either a cross or a square (see Fig. 3a). Subsequent stages are formed by repeating the generation process, surrounding the cluster with four additional clusters identical to the existing one. The linear dimension of the cluster increases three-fold at each stage, while the number of bonds is multiplied by five, i.e. the clusters have fractal dimension $D = \ln(5)/\ln(3)$. Fig. 3b shows $Re\,\sigma_e(\omega)$, normalized by the fraction of metallic bonds, p, for the cross fractal. As follows from the figure, $Re\,\sigma_e/p \propto \omega^2$ and increases sharply with cluster size (this was also predicted by the DEMT (see (3.11)).

Brouers and co-workers [71] applied the $Y-\Delta$ algorithm to simulate the near infra-red absorption of a two-dimensional metal-dielectric composite on the basis of the model of a square lattice occupied by bonds of metal (with probability p) and insulator (with probability $1-p$) conductance. The results of the simulations are illustrated in Fig. 4a and 4b. Fig. 4a shows the IR optical absorption $2\pi\epsilon''/\lambda$,

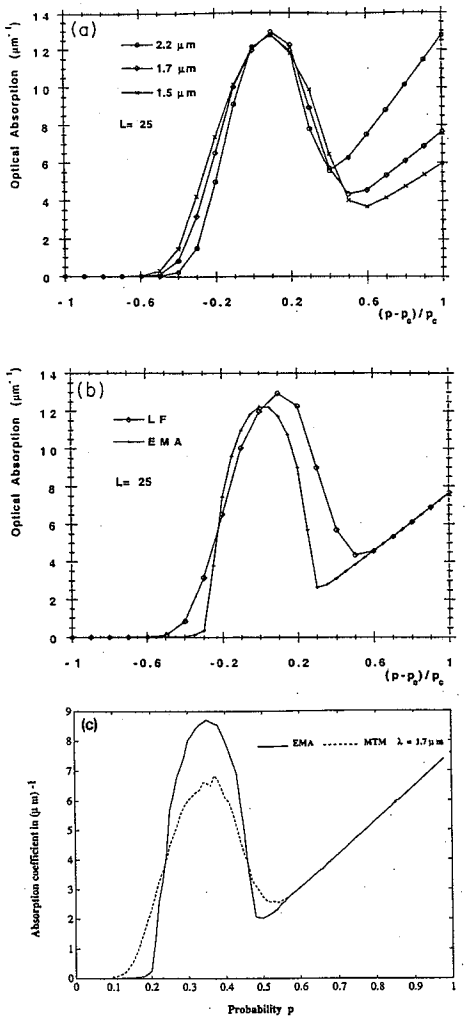

Fig. 4. (a) 2d near-infrared optical absorption for the three wavelength 2.2, 1.7 and 1.5 μm as a function of metal fraction p. (b) 2d near-infrared absorption for $\lambda = 1.7\mu$m, calculated with the Frank-Lobb (LF) algorithm ($d = 2$) and compared with the results of the effective-medium approximation (EMA). (c) 3d absorption calculated using the method of the transfer matrix (MTM) and the effective-medium approximation (EMA); for the MTM, the width of the 2d section 7×7 bonds. Taken from Refs. [71,72].

for three wavelengths $\lambda_1 = 2.2, \lambda_2 = 1.7$, and $\lambda_3 = 1.5\,\mu$m. Circuits of a linear size of 25 were averaged over 1000 circuit configurations. The optical absorption was found to be maximum for a concentration slightly higher than $p_c = 0.5$. As the wavelength increases, the contribution of conducting electrons increases, while the contribution of cluster modes (associated with the displacement current) decreases. This results in the narrowing of the central absorption curve around the origin ($p \sim p_c$), and increased absorption for $(p - p_c)/p_c \to 1$ as the wavelength increases.

Fig. 4b shows the result of two-dimensional simulations for $\lambda = 1.7\,\mu$m, compared with the EMT. The behavior is qualitatively similar for different models, although, for the EMT, the maximum is closer to $p = p_c$, and the width of the central peak is smaller. (Similar results were obtained in Ref. [72] based on the symmetrized Maxwell-Garnett approximation, which is a version of the Sheng approximation [73].) The authors ascribed this discrepancy to configuration fluctuations neglected in the EMT. Good agreement of the results of 2d simulations with EMT calculations was also reported in Ref. [74].

In Fig. 4c, a comparison between EMT and TM calculations for a three-dimensional lattice is shown [72]. Similar to the two-dimensional case, the maximum occurs at concentration $p^* \approx 0.35$, higher than the percolation threshold ($p_c \approx 0.248$). Further, the absorption maximum predicted by EMT is higher than that found in the simulations.

Zabel and Stroud [75], using an RLC network, performed two-dimensional simulations for random diffusion-limited aggregates (DLA) as well as for ordered cross and square fractals (see Fig. 3a). They showed that the fractal character of metallic bonds embedded in a dielectric host leads to a large broadening of the spectrum of surface-plasmon resonances in the optical region. In ordered fractals, an optical conductivity is shown to be self-similar in frequency; the authors have suggested that the new plasmon frequencies appearing for each iteration should decrease with the size l of the fractal "blob" [76] within a larger fractal as $l^{-\alpha}$ with $\alpha = 0.56$.

Brouers et al. [77] also studied effects similar to those reported by Zabel and Stroud [75]. These authors used a deterministic hierarchic electrical network that was constructed on a deterministic fractal lattice (DFL). (The DFL was introduced previously by Kirkpatrick [8] and Mandelbrot [2].) For the two-dimensional lattice, Brouers et al. showed that the constant B occurring in $Re[\sigma_e(\omega)] = B\omega^2 p$ (which describes the far-infrared absorption) $\propto R^x$, where R is the size of a cluster, and $x = -\ln(2^{D-1} - 1)/\ln 2$; the latter differs from the exponent, $x = 3(2 - D)$, predicted by the DEMA [54]. Their model also predicts a saturation length, $l_{sat} \propto \omega^{-y}$, above which, for a given frequency, the absorption is size independent (the authors interpreted l_{sat} as the crossover localization length: $l_{sat} \sim L_\omega \sim \omega^{-y}$). The exponent y was found to change continuously from a value $y_{RC} = (D - 2 + x)^{-1}$, in the low-frequency, resistive, (RC) range, to the value $y_{LC} = 2y_{RC}$, in the high-frequency, self-inductive, (RL) part of the spectrum. (Note that the difference in spectral dependence between the resistive and self-inductive frequency ranges, was also discussed earlier by Robin and Souillard [78]). It was shown in Ref. [77] that new frequencies appearing at each iteration follow the rule $\omega_{n+1}/\omega_n \approx L^{-\alpha}$ with $\alpha = 1/y_{LC}$.

The results of 3d numerical simulations performed by Stroud and Zhang [18] using an RLC network and the TM algorithm, are presented in Fig. 5. As follows from the figure, the effective conductivity exhibits a Drude peak at $\omega = 0$ that appears only above the percolation threshold p_c. Also, a broad spectrum of resonances, whose lower edge approaches zero frequency at p_c, is clearly seen in the figure. In accordance with speculations presented in the end of Section 2, for the high-

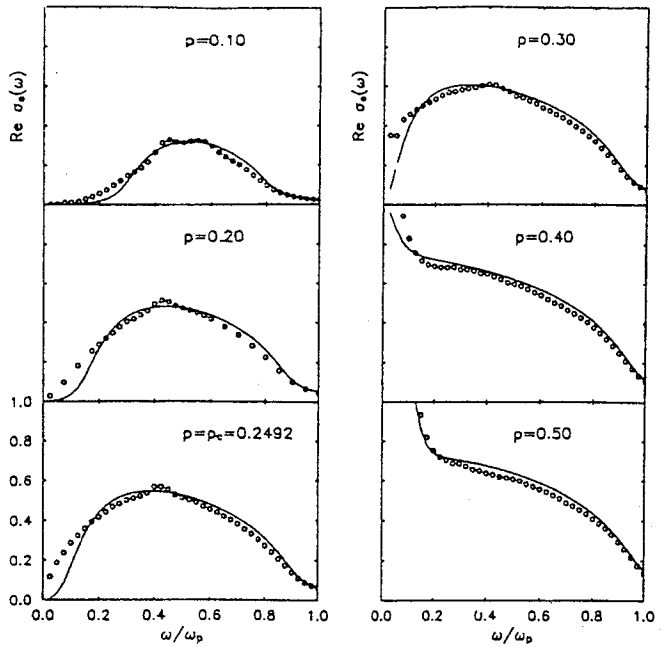

Fig. 5. $Re\,\sigma_e(\omega)$ for a ($d = 3$) $10 \times 10 \times 5000$ network of dielectric and Drude metal bonds, plotted at several metal concentrations p. Full lines denote the self-consistent EMT calculations. Taken from X. Zabel and D. Stroud, Phys. Rev. B 48 (1993) 6658.

frequency region, the absorption in Fig. 5 does not exhibit a critical behavior (as a function of $p - p_c$) near the percolation threshold.

It is important to mention that an RLC network, with its stick-like metallic bonds, significantly simplifies the actual local structure of small-particle composites. As mentioned above, the form of a particle becomes important at high frequencies. (This form strongly affects the magnitude of the dipole moment induced on the particle.) Also, in all numerical techniques that were described above, the actual Maxwell equation $\nabla \cdot D = \nabla \cdot (\epsilon E) = -\nabla \cdot (\epsilon \nabla \Phi) = 0$ is replaced by its discrete analogue, which contains differences such as $(\epsilon_i E_i - \epsilon_j E_j)/a$ (with $E_i = (\Phi_j - \Phi_i)/a$) summed over the nearest neighbors. Such a replacement is possible only if a function (Φ or E in our case) changes little over a lattice period a. At high frequencies, however, the field arises from dipoles induced on the particles, and it has a strong spatial dependence ($\propto r^{-3}$) that produces a significant change of field amplitudes on a scale of the period a. Thus, in the high-frequency region, light-induced dipoles and the corresponding dipolar (or multipolar) interaction must be taken into account; such considerations will be discussed below in Sections 5–7.

4. Spectral theory for composites and recursive spectral representation for self-similar structures

4.1. Spectral representation

The spectral representation is a very efficient approach for the calculation of the dielectric function in inhomogeneous media. It was developed by Bergman [41,79], Fuchs et al. [57,80–84] and by Milton [85]. Below we briefly consider the basic idea of the spectral theory, following Refs. [82–84]. According to the spectral representation theory, for a continuous medium consisting of two components, the effective dielectric function can be written as [81]

$$\epsilon_e/\epsilon_2 - 1 = p_1 \left\{ C_1(\epsilon_1/\epsilon_2 - 1) + \int_0^1 \frac{g_1(n)\,dn}{(\epsilon_1/\epsilon_2 - 1)^{-1} + n} \right\}, \tag{4.1}$$

or as

$$\epsilon_e/\epsilon_1 - 1 = p_2 \left\{ C_2(\epsilon_2/\epsilon_1 - 1) + \int_0^1 \frac{g_2(n)\,dn}{(\epsilon_2/\epsilon_1 - 1)^{-1} + n} \right\}, \tag{4.2}$$

where $g_1(n)$ and $g_2(n)$ are the "spectral density functions" for components 1 and 2, respectively, and C_1 and C_2 are the strengths of percolation of the respective components. Eqs. (4.1) and (4.2) are written from the point of view of component 1 in a host component 2, and component 2 in a host component 1, respectively. The $g_1(n)$ and $g_2(n)$ are related through the symmetry relation $p_1 n g_1(n) = p_2(1-n)g_2(1-n)$ [81].

The physical meaning of the spectral representation is as follows. The first term in (4.1) describes the contribution of an infinite cluster of the constituent media to the dielectric function (we assume for definiteness component 1 to be a conductor). It is associated with the dc conductivity of the percolating system. Note that the term $C_1(\epsilon_1/\epsilon_2 - 1)$ in Eq. (4.1) can also be obtained by replacing $g_1(n)$ by $g_1(n) + C_1\delta(n)$ and extending the range of integration so as to include the point $n = 0$. Thus, the existence of percolation is equivalent to a mode at $n = 0$, the percolation mode [83]. The C's can be found from the relation $p_1C_1 = \lim_{\epsilon_1\to\infty}(\epsilon_e/\epsilon_1)$, which in the low-frequency limit acquires the form $p_1C_1 = \sigma_e(0)/\sigma_1(0)$ [81].

The second terms in Eqs. (4.1), (4.2) describe contributions to the dielectric functions from different possible collective resonances of interacting particles in the composite [81]. The polarization factor n is small for needle-like geometrical structures and close to unity for plate-like objects. The function $g(n)$ gives the density, both in number and strength, of these various shape resonances.

In particular, for the MGT describing a dilute system of spherical particles ($p_1C_1 \to 0$ in the dilute limit), the spectral function is $g_1(n) = \delta(n - n_0)$, where $n_0 = (1 - p_1)/3$, and an absorption peak (corresponding to the Mie resonance) occurs at $\omega_0 = \sqrt{(1-p_1)/3}\omega_p$, provided ϵ_1 is given by the Drude formula. For a non-diluted system of particles, the interaction is expected to result in broadening of the spectral function, leading to a continuous set of surface modes characterized by different depolarization factors n.

There are three sum rules for the g's [81]:

$$\int_0^1 g_1(n)\,dn = 1 - C_1, \tag{4.3}$$

$$\int_0^1 n g_1(n)\,dn = \frac{1}{3}(1 - p_1), \tag{4.4}$$

and

$$(1-p_1)C_2 + p_1C_1 + p_2\int_0^1 \frac{g_2(n)\,dn}{1-n} = 1. \tag{4.5}$$

For a collection of N particles in vacuum, the spectral function $g(n)$ is not continuous, but consists of discrete modes with strengths c_s and depolarization factors n_s (accordingly, $g(n)$ in (4.1) can be represented as a sum of terms $c_s\delta(n - n_s)$). In this case, the total polarizability α is given by [84]

$$\alpha = \frac{Nv}{4\pi}\sum_s \frac{c_s}{(4\pi\chi)^{-1} + n_s}, \tag{4.6}$$

where v is the volume of a particle, and $\chi = (\epsilon - 1)/4\pi$. The total strength of the modes is

$$\sum_s c_s = 1; \tag{4.7}$$

they have a centroid of 1/3,

$$\sum_s c_s n_s = 1/3, \tag{4.8}$$

and lie in the range $0 < n_s < 1$. Eq. (4.6) generalizes the well-known expression for the polarizability of an isolated spherical particle of radius R_m in vacuum ($\alpha_{sph} = v\chi_{sph} = (v/4\pi)[(4\pi\chi)^{-1} + 1/3]^{-1} = R_m^3(\epsilon - 1)/(\epsilon + 2)$) to the case of a collection of interacting particles. In this case, interactions between particles result in a set of eigenmodes characterized by depolarization factors, n_s, and contributing to the total polarizability of a cluster with a weight c_s.

Note that the spectral representation expresses the effective dielectric function of a composite in terms of the spectral density, $g(n)$, but it does not provide a method for determining $g(n)$ from first principles. However, if the expression for ϵ_e is known, then $g(n)$ can be found from [81]

$$g_1(n') = \frac{1}{\pi p_1}\lim_{s\to 0} Im(\epsilon_e/\epsilon_2 - 1), \tag{4.9}$$

where the n' and s are introduced by the relation

$$(\epsilon_1/\epsilon_2 - 1)^{-1} \equiv -(n' + is), \quad s > 0. \tag{4.10}$$

For example, in the EMT, one obtains from (3.5) and (4.9), (4.10) the following expression for $g_1(n)$ [81]:

$$g_1^{EMT}(n) = \frac{1}{4\pi p_1 n}[-9n^2 + 6(1+p_1)n - (3p_1 - 1)^2]^{1/2}. \tag{4.11}$$

Introducing $\Delta p_1 \equiv p_1 - p_c$ (in the EMT $p_c = 1/3$) we rewrite $g_1(n)$ in the form

$$g_1^{EMT}(n) = \frac{3}{4\pi p_1} n^{-1}[(n - n_{1L})(n_{1U} - n)]^{1/2}, \tag{4.12}$$

if $n_{1L} < n < n_{1U}$ and $g_1^{EMT}(n) = 0$, otherwise. Here, for $|\Delta p_1| \ll 1$,

$$n_{1L} = \{4 + 3\Delta p_1 - 2[(1 + 3\Delta p_1)(4 - 6\Delta p_1)]^{1/2}\}/9 \approx 9(\Delta p_1)^2/8, \tag{4.13}$$

and

$$n_{1U} = \{4 + 3\Delta p_1 + 2[(1 + 3\Delta p_1)(4 - 6\Delta p_1)]^{1/2}\}/9 \approx (6\Delta p_1 + 8)/9. \tag{4.14}$$

Fuchs and Ghosh [81] have proposed the following generalization for $g(n)$:

$$g_1(n) = Cn^{-1}(n - n_{1L})^{1-\alpha}(n_{1U} - n)^{\beta}, \tag{4.15}$$

if $\alpha > 0$, $0 \leqslant n_{1L} \leqslant n \leqslant n_{1U} \leqslant 1$, and $g_1(n) = 0$, otherwise. With this choice for $g(n)$, they were able to reproduce (in the limit $|\epsilon_2/\epsilon_1| \ll 1$ and $|p_1 - p_c| \equiv |\Delta p_1| \ll p_c$) the results of percolation theory for the case $\xi \ll L_\omega$ (see Section 2). They found, in particular, that α in (4.15) is expressed in terms of the percolation theory indices as $\alpha = s/(t+s)$. (The expression for β is more complicated and depends on p_1, n_{1U} and α.)

Note that the theory based on the form of $g(n)$ proposed by Fuchs and Ghosh is phenomenological and contains the free parameters α, n_{1L}, and n_{1U}. The theory, however, successfully explains basic dielectric properties of rock-and-brain systems and, in particular, Archie's law [81].

4.2. *Recursive spectral representation for continuous self-similar structures*

We consider, first, self-similar continuous composites and then fractal clusters of spheres. Our considerations are close to those presented in papers by Fuchs and co-workers [83,84].

In the first stage of recursive construction, one randomly places unconnected inclusions of component 1, with volume fraction p_1, into a host of component 2. The effective dielectric function, $\epsilon_m^{(1)}$, of the mixture is

$$\epsilon_m^{(1)} = M(\epsilon_1, \epsilon_2, p_1), \tag{4.16}$$

where the form of the function M depends, in general, on the geometry of the composite.

In the next stage, larger inclusions of component 1 (with the same filling factor p_1) are incorporated into a host consisting of the first-stage composite. The effective dielectric function of the second stage, $\epsilon_m^{(2)}$, is found by replacing the host dielectric function ϵ_2 in Eq. (4.16) by $\epsilon_m^{(1)}$. Repeating this procedure recursively, the effective dielectric function after stage j is

$$\epsilon_m^{(j)} = M(\epsilon_1, \epsilon_m^{(j-1)}, p_1). \tag{4.17}$$

This approach can be applied, in particular, to brine containing rocks, in which the volume fraction, p_1, of insulator (rocks) is recursively added to a conducting host (brine).

Note that in the DEMT (see Section 3.2), an infinitely small fraction of the first component is introduced at each stage, whereas in the recursive theory this fraction can be finite. If the initial volume p_1 approaches zero, then it can be shown [87] that the recursive theory becomes equivalent to the DEMT.

Using the spectral representation (4.2), one writes Eq. (4.16) in the form

$$\frac{\epsilon_m^{(1)}}{\epsilon_1} - 1 = p_2 \left\{ C_2(\epsilon_2/\epsilon_1 - 1) + \int_0^1 \frac{g_2(n)\,dn}{(\epsilon_2/\epsilon_1 - 1)^{-1} + n} \right\}. \tag{4.18}$$

Note that Eq. (4.18) is written from the point of view of component 2. If $g_2(n)$ has a peak at $n = n_0$ (i.e. $g_2(n) = A\delta(n - n_0)$), there is a surface mode at $n = n_0'$ defined by the relation $[\epsilon_2/\epsilon_1 - 1]^{-1} + n_0 = 0$. For dilute spherical inclusions of component 1, there is only one dipole mode (which has non-zero weight) at $n_0 = 2/3$, or $\epsilon_1/\epsilon_2 = -2$.

Following Ref. [83], we introduce variables $x, x_1, \ldots, x_j$ defined by $\epsilon_2/\epsilon_1 - 1 = -1/x, \ldots$, $\epsilon_m^{(j)}/\epsilon_1 = -1/x_j$. Then, Eqs. (4.16) and (4.17) can be written as

$$x_1 = h(x), \ldots, x_j = h(x_{j-1}), \tag{4.19}$$

where

$$h(x) = \left\{ p_2 \left[C_2/x + \int_0^1 \frac{g_2(n)\,dn}{x - n} \right] \right\}^{-1}. \tag{4.20}$$

Using the recursive map given by Eqs. (4.19) and (4.20), one can calculate the variable x_j associated with the stage j of the recursive procedure.

It is instructive to introduce the spectral function $g_2(j, n)$ for the recursive structure at stage j in an expression similar to Eq. (4.18); $\epsilon_m^{(1)}$ on the left-hand side of the equation must be replaced by $\epsilon_m^{(j)}$, and on the right-hand, p_2, C_2, and $g_2(n)$ are replaced by the quantities $\phi_2^{(j)}, C_2^{(j)}$, and $g_2(j, n)$, respectively. The volume fraction of component 2 at the end of stage j is $\phi_2^{(j)} = (p_2)^j$; the percolation constant is

$$C_2^{(j)} = \phi_2^{-1} \lim_{\epsilon_2 \to \infty} (\epsilon_m^{(j)}/\epsilon_2) = (C_2)^j, \tag{4.21}$$

and the spectral function $g_2(j, n)$ is given by

$$g_2(j, n) = (\pi\phi_2^{(j)})^{-1} \lim_{s \to 0} (\epsilon_m^{(j)}/\epsilon_1), \tag{4.22}$$

where we set $\epsilon_2/\epsilon_1 = -1/x = -1/(n + is)$ in Eq. (4.22).

From the above expressions, one may determine the spectral function at the end of stage j if it is known for the first stage. In particular, for the MGT one has for the first stage: $g_2(n) = (1 - C_2)\delta(n - n_0)$ where $C_2 = 2/(2 + p_1)$ and $n_0 = (2 + p_1)/3$. By such means, one ultimately obtains the dielectric function for arbitrary stage j.

As one continues the recursive procedure, the spectral function develops an approximately self-similar structure [83], with a distribution of scaling indices associated with multifractality that can be analyzed by the procedure suggested by Halsey et al. [88].

Note that the recursive spectral theory also permits the consideration of critical behavior near the percolation threshold [83]. However, in the recursive theory [83], the percolation threshold is $\phi_{2c} = 0$ (we assume that component 2 is a conductor which surrounds the insulating inclusions

of component 1). Since $\phi_2^{(j)} > 0$, one only approaches the percolation threshold as the number of iterations increases and never actually reaches the threshold or passes through it. Fuchs and Ghosh suggested [87] that this explains the difference in critical indices found on the basis of the recursive spectral theory and those following from the standard scaling theory near the percolation threshold (see Section 2).

4.3. Recursive theory for collective modes of a fractal cluster of spheres

We now consider the iterative procedure used by Claro and Fuchs to find the polarizability of a fractal collection of spheres in terms of the polarizability of the generator [84]. In this case, a cluster of spheres (the generator) is replaced by a single equivalent sphere, which is used to construct a larger cluster in a self-similar way, and this procedure is repeated recursively. The examples of three-dimensional generators are octahedral clusters with $N = 6$ and with $N = 7$ (i.e. with and without a sphere at the center, respectively). In the octahedral cluster ($N = 6$), sphere radius a and distance $R = 2a\sigma$ between nearest neighbors, the radius of the equivalent sphere is $a^{(1)} = (1/2)R + a = a(1+\sigma)$, so that, if neighboring spheres in the generator touch each other, the equivalent spheres also touch each other and the spheres in a given generator touch the spheres in neighboring generators.

It is worth emphasizing that the recursive treatment considered below is approximate; it simplifies the actual interaction between particles in a large cluster (even within the pure dipole approximation).

The polarizability of a sphere of volume v is given by

$$\alpha_{sph} = v\chi_{sph} = \frac{v}{4\pi}[(4\pi\chi)^{-1} + 1/3]^{-1} \tag{4.23}$$

with $\chi = (\epsilon - 1)/4\pi$ the susceptibility of the sphere material. Using the spectral representation for the polarizability of the spheres in the generator, we obtain (see also (4.6))

$$\alpha^{(1)} = \alpha_{sph} = \frac{V^{(1)}}{4\pi}[(4\pi\chi_e^{(1)})^{-1} + 1/3]^{-1} = \frac{Nv}{4\pi}\sum_s \frac{C_s}{(4\pi\chi)^{-1} + n_s}, \tag{4.24}$$

where $V^{(1)}$ is the volume of the equivalent sphere and N in the number of spheres in the generator.

Repeating the procedure recursively, we have at stage j

$$\alpha^{(j)} = \frac{V^{(j)}}{4\pi}[(4\pi\chi_e^{(j)})^{-1} + 1/3]^{-1} = \frac{NV^{(j-1)}}{4\pi}\sum_s \frac{C_s}{(4\pi\chi_e^{(j-1)})^{-1} + n_s}. \tag{4.25}$$

Introducing the variables

$$y = -[(4\pi\chi)^{-1} + 1/3],\ y^{(1)} = -[(4\pi\chi_e^{(1)})^{-1} + 1/3], \ldots, y^{(j)} = -[(4\pi\chi_e^{(j)})^{-1} + 1/3],$$

Eqs. (4.24) and (4.25) can be written as

$$y^{(1)} = h(y), \ldots, \quad y^{(j)} = h(y^{(j-1)}) = h^{(j)}(y), \tag{4.26}$$

where

$$h(y) = \left[F\sum_s \frac{C_s}{y - y_s}\right]^{-1}, \tag{4.27}$$

$y_s = n_s - 1/3$, and $F = NV^{(j-1)}/V^{(j)} = Nv/V^{(1)}$ is the filling fraction of spheres in the equivalent sphere. The notation $h^{(j)}(y)$ denotes the function $h(y)$, which has been iterated j times, i.e. $h^{(1)}(y) \equiv h(y)$, $h^{(2)} = h(h(y))$, etc. Eqs. (4.26) and (4.27) define a map, which can be used iteratively to find successive variables $y^{(1)}, y^{(2)}, \ldots, y^{(j)}$ as a function of y, beginning with $y^{(1)} = h(y)$.

The collective surface mode spectrum of the final structure is defined by a strength $C_m^{(j)}$ and depolarization factors $n_m^{(j)}$ that appear in the spectral representation for $\alpha^{(j)} = -V^{(j)}/(4\pi y^{(j)})$:

$$\alpha^{(j)} = \frac{v^{(j)}}{4\pi}\sum_m \frac{C_m^{(j)}}{(4\pi\chi)^{-1} + n_m^{(j)}} = \frac{v^{(j)}}{4\pi}\sum_m \frac{C_m^{(j)}}{y - y_m^{(j)}}, \tag{4.28}$$

where $y_m^{(j)} = n_m^{(j)} - 1/3$, and $v^{(j)} = N^j v$ is the actual volume of the spheres in the final structure. (The symbol m is used as a general label for the modes at any stage of iteration, whereas the symbol s, which was used previously, is a label for the modes of the generator.) The total strength is $\sum_m C_m^{(j)} = 1$, and, since the final structure has cubic symmetry, the centroid sum rule $\sum_m C_m^{(j)} n_m^{(j)} = 1/3$ (or $\sum_m C_m^{(j)} y_m^{(j)} = 0$) is satisfied. The modes lie within the range $0 < n_m^{(j)} < 1$.

The quantity $y = -[(4\pi\chi)^{-1} + 1/3]$ is, in general, complex, $y \equiv y' + iy''$. We assume that y'' is small and different modes m do not overlap. Then, in the expression for $Im\,\alpha^{(j)}$ in (4.28), each mode is represented by a Lorentzian peak of width y'' and area $(v^{(j)}/4)C_m^{(j)}$. This determines the strength $C_m^{(j)}$.

The mode positions can be found by noting that, if y'' is small, then, $\alpha^{(j)} \to \infty$ and $y^{(j)} \to 0$ when $y \to y_m^{(j)}$. Hence, the mode positions $y_m^{(j)}$, where m labels the mode number, correspond to the zeros of $h^{(j)}(y)$:

$$h^{(j)}(y_m^{(j)}) = 0. \tag{4.29}$$

By analyzing the structures obtained with the $N = 6$ octahedral cluster as a generator, it was shown in Ref. [84] that the spectrum consists of "bars", regions in which modes must lie, and "gaps", regions from which modes are excluded. These regions suggest analogies with the Cantor fractal set. To calculate the distribution of scaling indices, $f(\alpha)$ (do not confuse the scaling index α with the polarizability), one can use the procedure suggested by Halsey et al. [88]. According to this procedure, one builds first a measure, $M(q,\delta) = \sum_i \mu_i^q \delta_i^d$, that remains finite at $\delta \to 0$ only if $d = \tau(q)$. Here, $\delta_i = (\Delta y)_i/(y_R - y_L)$ is the ratio of the width $(\Delta y)_i$ of the ith bar to the overall width of the spectrum $(y_R - y_L)$, and μ_i is the total strength of all modes lying in the ith bar ($\sum_j p_i = 1$). Then, one sets $M(\tau, q) = 1$, defining τ as a function of q. For each value q one finds $\alpha(q) = -d\tau(q)/dq$ and $f(\alpha(q)) = q\alpha(q) + \tau(q)$. The procedure gives generalized dimensions $D_q = \tau(q)/(1-q)$ as a function of q with D_0 being the Hausdorff dimension of the distribution.

Claro and Fuchs showed [84] that the surface-mode spectrum for the described recursive model is a multifractal set and found the corresponding distribution, $f(\alpha)$, of scaling indices. In particular, they obtained $D_0 \approx 0.53$.

Note that the concept of multifractality naturally appears when modes forming a fractal set have different strengths C_m (in terms of the Cantor set, different bars have non-trivial distributions of weights p_i in the measure $M(q,\tau)$). We will show in Section 5 that, in the case of an ensemble of diluted fractal clusters, all modes contribute to the optical absorption with approximately equal weight (i.e. they have the same strengths and p_i is simply proportional to δ_i). Accordingly, the absorption can be expressed in terms of a spectral density of modes, $\rho(\omega)$ (which possesses the scaling dependence

with the exponent $d_o - 1$; d_o is called the optical spectral dimension). In this case, one should put $D_0 = d_o$ and the measure $M(q, \tau)$ is finite only at $q = 0$, i.e. it is structureless (no dependence on q).

5. Scale-invariant theory of collective optical modes in fractal clusters

Below, we consider a method for obtaining the dispersion law characterizing excitations in fractals for an arbitrary interaction. The consideration is similar to that presented in the paper by Stockman, George and Shalaev [25]. In particular, this theory provides a good description of the optical spectra of diluted clusters. (We will specify what we mean by "diluted clusters" in Section 5.4. The spectra of original, non-diluted, clusters will be considered in Section 6.) The theory, which is based on scale invariance, results in a dispersion law giving the relation between localization length and frequency parameter. The corresponding exponents are expressed in terms of the spectral and Hausdorff dimensions. The expressions obtained for the dispersion-law exponent are different for vibrational (Goldstone-type) and dipolar (non-Goldstone-type) excitations. We also show that dipolar collective modes, similar to vibrational modes, are strongly localized in fractals.

Dynamical excitations of fractals possess fractal properties, and their density of states and dispersion law exhibit scaling behavior under certain conditions. Scaling of the eigenstate density, ρ, for the vibrations in fractals has been introduced by Alexander and Orbach [5] in the form

$$\rho \propto \omega^{\tilde{d}-1}, \tag{5.1}$$

where ω is the oscillation frequency and $\tilde{d}$ is an index called the fracton (or vibrational spectral) dimension [5,6]. The dispersion relation for the vibrations of fractals ("fractons") has the form [5]:

$$\omega \propto L^{-D/\tilde{d}}, \tag{5.2}$$

where L is the coherence length of the excitation. In the trivial limit ($D = \tilde{d} = d$), Eq. (5.2) reproduces the dispersion law of a wave propagating with constant speed, $\omega \propto L^{-1}$, with L as the wavelength. In fractals, the coherence length, L, simultaneously plays the roles of wavelength and localization radius (the strong localization hypothesis [5,89]). The dispersion relation (5.2) has been proven in Ref. [76] from very general mode-counting arguments, independent of any model-based considerations. However, it is clear a priori that Eq. (5.2) can only be valid for excitations of the Goldstone type, which are characterized by the absence of a gap in the spectrum, and become running waves in the trivial limit $D \to d$. For non-Goldstone excitations in fractals (e.g., of the plasmon type), one expects a dispersion law different from Eq. (5.2), in particular, possessing a spectral gap for $D \to d$. Such a law for dipolar excitations on fractals, first derived by Stockman and co-workers [24], is different from Eq. (5.2). The problem of finding the dispersion relations for fractal excitations has also been the subject of experimental studies [90–93].

The approach of Ref. [25] is based on the self-similarity of a fractal and the idea that collective excitations of relatively large coherence length L are insensitive to the details of the fractal structure at small scales. Thus, one can change the spatial resolution of a fractal structure, R_0, without changing observable quantities. We choose the work done by the probe field as the quantity whose invariance (with respect to a change of R_0) may be used to obtain the required dispersion laws. Following Ref. [25], we first apply the method to reproduce the well-known dispersion relation for vibrations in a fractal, and then apply it to dipolar excitations.

5.1. Scaling and dispersion laws

By the term "dispersion relation" we imply the dependence of the eigenvalue w of the interaction operator, W, on the excitation coherence radius, L; thus, the dispersion relation has the form $w = w(L, R_0)$. Scale invariance holds for the fractal excitation provided its coherence radius, L, satisfies the inequalities

$$R_0 \ll L \ll R_c, \tag{5.3}$$

where R_c is the gyration radius of the cluster and R_0 is the characteristic spacing between the nearest monomers. These two parameters, together with the Hausdorff dimension, determine the number of monomers in the fractal, $N = (R_c/R_0)^D$. If the condition (5.3) is met, the excitation extends over many monomers and is not sensitive to details of the fractal at small scales. Therefore, a change in the minimum scale should not modify the functional form of the dispersion relation. To meet these requirements, in the usual way, w should be a power (scaling) function of L and R_0.

We introduce the metrical dimensionality, m, of W: when all the linear dimensions (including R_0, R_c and L) are changed by the same factor, then w is changed proportionally to, say, R_0^m. For the vibrational model considered below, the dimension m can be arbitrary, with $m = 0$ being the usual choice; for the dipolar model, $m = -3$. The change of w resulting from a change of coherence length L (without changing R_0 or any other length) is given by a non-trivial index which we denote by $-\kappa$: $w \propto L^{-\kappa}$. Thus, in the scaling region (5.3), the dispersion relation has the form

$$w \sim (L/R_0)^{-\kappa} R_0^m. \tag{5.4}$$

It is clear that when L becomes large, w should become small; therefore, $\kappa > 0$. In some simple cases, the index κ can be determined analytically from the well-known decimation procedure [6,94]. For example, on the Sierpinski gasket in d dimensions, $\kappa = \ln(d+3)/\ln 2$, $D = \ln(d+1)/\ln 2$.

The main idea is to use the invariance of the work A done by the field with respect to the change of the minimum scale R_0 (without changing any other linear dimensions). Such a transformation is equivalent to unifying a group of monomers entering a fractal "blob" to form a renormalized monomer and, therefore, has been called the renormalization transformation [24,76]. The renormalized monomers constitute a fractal which is characterized by the same critical indices as the original fractal, though the strength of the interactions may change. The necessary condition for the work to have a scaling form is the small magnitude of the dissipation. In what follows, we will assume that this condition is fulfilled.

5.2. Vibrational excitations

We consider a fractal cluster consisting of N material particles positioned at points $\boldsymbol{r}_i$. The small displacements $\boldsymbol{d}_i$ of the monomers induced by an external driving force $\boldsymbol{F}_i$ ($i = 1, \ldots, N$) obey the system of equations

$$\frac{\partial^2 d_{i\alpha}}{\partial^2 t} = -u^2 \sum_j T_{i\alpha j\beta} (d_{i\beta} - d_{j\beta}) - \omega_0^2 d_{i\alpha} - \gamma \frac{\partial d_{i\alpha}}{\partial t} + F_{i\alpha}. \tag{5.5}$$

Here Greek letters denote Cartesian components (summation over repeated Greek indices is implied), u is a characteristic frequency (of the order of the Debye frequency), T is the interaction matrix

whose elements do not depend on the interaction strength (in the simplest case, $T_{i\alpha j\beta} \propto \delta_{\alpha\beta}$ and is unity for nearest neighbors and zero otherwise), ω_0 is the restoring frequency which can originate from interaction of the monomers with the embedding host medium (for a self-supporting fractal, $\omega_0 = 0$), γ is a relaxation constant, and $F_{i\alpha}$ is the component of the weak (probe) force acting on the ith monomer. Assuming the probe force to have the temporal dependence $\boldsymbol{F} \propto e^{-i\omega t}$, we can, in a routine manner, introduce for each quantity the corresponding amplitude. Such amplitudes will be denoted below by the same symbols.

We define the vector $|d)$ in a $3N$-dimensional linear space with components $(i\alpha|d) = d_{i\alpha}$; similarly we define corresponding vectors for other quantities. Then, the system of Eqs. (5.5) can be written as

$$(Z + W)|d) = |E^{(0)}), \tag{5.6}$$

where

$$Z \equiv -X - i\delta, \quad X = \frac{\omega^2 - \omega_0^2}{u^2}, \quad \delta = \frac{\omega\gamma}{u^2}, \quad |E^{(0)}) = \frac{1}{u^2}|F), \tag{5.7}$$

and the operator W is determined by its matrix elements,

$$(i\alpha|W|j\beta) = T_{i\alpha j\beta} - \delta_{ij}\sum_k T_{i\alpha k\beta}. \tag{5.8}$$

This operator is symmetrical and obeys the condition

$$\sum_j (i\alpha|W|j\beta) = 0. \tag{5.9}$$

It follows from Eq. (5.9) that the homogeneous vectors $|0\alpha)$, with components $(i\alpha|0\beta) = \delta_{\alpha\beta}N^{-1/2}$, are eigenvectors of W, with zero eigenvalues. This is an exact condition for the excitations to be of the Goldstone type. The homogeneous excitation is simply a shift of the system as a whole, and brings about a gapless excitation spectrum with the excitation frequency tending to zero for $L \to \infty$.

We now introduce the eigenvectors, $|n)$, of the operator W corresponding to the eigenvalues, w_n. Since W is a symmetric operator, all eigenvalues and components of the eigenvectors, $(i\alpha|n)$, are real. The solution of Eq. (5.6) is expressed in terms of the linear response function α,

$$d_{i\alpha} = \sum_j \alpha_{ij,\alpha\beta} E_{j\beta}, \tag{5.10}$$

where

$$\alpha_{ij,\alpha\beta} = \sum_n \frac{(i\alpha|n)(n|j\beta)}{(Z + w_n)}. \tag{5.11}$$

From this expression and the completeness of the set $|n)$, an exact sum rule [25] follows:

$$\int \alpha_{ij,\alpha\beta} dX = \pi\delta_{ij}\delta_{\alpha\beta}. \tag{5.12}$$

The contributions of the uniform eigenvectors $(i\alpha|0\beta)$ should be excluded from (5.11) since these contributions correspond to the movement of the system as a whole, and not to the internal excitations.

Thus, we put $n \neq 0$ in Eq. (5.11). The condition of orthogonality to the uniform eigenvectors has the form [76]

$$\sum_i (i\alpha|n) = 0 \quad (n \neq 0). \tag{5.13}$$

As a consequence of Eq. (5.13), the polarizability, Eq. (5.11), obeys the condition

$$\sum_j \alpha_{ij,\alpha\beta} = 0. \tag{5.14}$$

This condition shows that the constant component of the probe field, $E^{(0)}$ (or F), vanishes from the solution Eqs. (5.10), (5.11).

The work done by the probe field A (more exactly, the power of the external field dissipated by the system) is given by

$$A = \left\langle \sum_i \overline{\frac{\partial \boldsymbol{d}_i(t)}{\partial t} \boldsymbol{F}_i(t)} \right\rangle, \tag{5.15}$$

where $\langle \ldots \rangle$ denotes averaging over an ensemble of fractals and $\overline{(\ldots)}$ over space variations of the driving field; the observable quantity $\boldsymbol{d}_i(t) = \boldsymbol{d}_i e^{i\omega t} + \text{c.c.}$, and similarly for $\boldsymbol{F}_i(t)$. Using the definitions (5.7), (5.10) and the rotational symmetry of the cluster as a whole, we obtain from Eq. (5.15)

$$A = \frac{2\omega}{\omega^2 - \omega_0^2} X \left\langle \sum_{ij} Im\, \alpha_{ij} \overline{\boldsymbol{F}(\boldsymbol{r}_i)\boldsymbol{F}^*(\boldsymbol{r}_j)} \right\rangle, \tag{5.16}$$

where $\alpha_{ij} \equiv \frac{1}{3}\alpha_{i\alpha j\alpha}$, and we assume a potential driving field; the latter means that the force $\boldsymbol{F}$ depends on the particle coordinate only, i.e. $\boldsymbol{F}_i = \boldsymbol{F}(\boldsymbol{r}_i)$.

When the probe field is applied, the fractal is characterized by an additional large scale distance: the field correlation length, L_f. To bring about scaling of the work done by the field, we assume that the coherence radius is much less than both R_c and L_f (i.e. in addition to (5.3), we require $L \ll L_f$).

As shown in Ref. [25], the expression (5.16) for A can ultimately be transformed to

$$A \sim \frac{\omega}{\omega^2 - \omega_0^2} \overline{|\boldsymbol{F}|^2} \left(\frac{L}{L_f}\right)^2 NX\rho(X), \tag{5.17}$$

where the density of eigenmodes, i.e. the number of eigenmodes per unit interval of X, is defined by

$$\rho(X) = N^{-1} \left\langle \sum_n \delta(X - w_n) \right\rangle. \tag{5.18}$$

Expression (5.17) possesses the property which is generally characteristic of Goldstone excitations: the field work tends to zero when the field correlation length becomes large. In the limit $L_f \to \infty$, the field becomes homogeneous and only induces a shift of the system as a whole; it cannot excite internal Goldstone modes.

If X is in the scaling region (i.e. $L(X)$ obeys (5.3)), the probe field interacts with fractal modes delocalized over many monomers, and a change of the minimum scale, R_0, of the fractal should

not affect the work done by the field. Hence, A in (5.17) should not depend on R_0. The driving field frequency, ω, obviously, does not depend on R_0. The restoring frequency ω_0 also does not depend on R_0: when some monomers are unified to a new (renormalized) monomer, their total mass and restoring force are increased in proportion to their number. The excitation coherence length, L, should not depend on R_0 either. Thus, taking the dependence $N \propto R_0^{-D}$ into account, we obtain from Eq. (5.17)

$$R_0^{-D} X \rho(X) \propto R_0^0, \tag{5.19}$$

where the proportionality should be understood in the sense of the overall functional dependence on R_0.

As suggested in a number of papers and confirmed by model calculations, in the intermediate region (5.3), the density of states obeys scaling, which, taking into account the metrical dimensionality of W and X, has the form

$$\rho(X) \sim R_0^{-m} |R_0^{-m} X|^{d_X - 1}. \tag{5.20}$$

The index d_X is called the spectral dimension. Substituting (5.20) into (5.19), we obtain the transformation law

$$|X| \propto R_0^{(D+md_X)/d_X}. \tag{5.21}$$

The probe field excites the resonant fractal modes, with $w = X$. Taking this into account and comparing the power of R_0 in Eqs. (5.4) and (5.21), we obtain $\kappa = D/d_X$ and

$$|X| \sim (L/R_0)^{-D/d_X} R_0^m. \tag{5.22}$$

This relation, with X as the independent variable instead of ω and the notation d_X instead of $\tilde{d}$, is the same as Alexander and Orbach's law (5.2). We point out that the value of the critical index d_X depends on the definition of the critical variable X (see also below). Also, note that κ does not depend on the metrical dimension m.

Using (5.7) and expressing X in terms of frequency, we transform Eq. (5.22) to

$$|\omega^2 - \omega_0^2| \sim (L/R_0)^{-D/d_X} u^2 R_0^a. \tag{5.23}$$

In the long-wavelength limit ($L \to \infty$), we found from (5.23) that $\omega \to \omega_0$. For $\omega_0 \neq 0$, according to (5.23), the scaling law is

$$|\omega - \omega_0| \propto L^{-D/d_X}. \tag{5.24}$$

For the case $\omega_0 = 0$ (vibrations in a self-supporting fractal), we find from (5.22) and (5.23) that $X \propto \omega^2$; in this case, it is natural to use ω as an independent variable. Transforming the density of states and using the equality $\rho(\omega)\,d\omega = \rho(X)\,dX$, we obtain from (5.22)

$$\omega \propto L^{-D/2d_X}, \tag{5.25}$$

where, as follows from a comparison with Eq. (5.2),

$$d_X = \tilde{d}/2. \tag{5.26}$$

It is interesting to note that the presence of a gap, ω_0, results in a change (by a factor 2) of the exponent governing the dispersion relation, as compared with the "usual" gapless case, $\omega_0 = 0$ (cf. Eqs. (5.24) and (5.25)).

In the trivial limit ($\tilde{d} = D = d$), the dispersion law (5.23) acquires the familiar form $\omega = (\omega_0^2 + ck^2)^{1/2}$, where the wave vector $k \sim L^{-1}$ and $|c| \sim u^2 R_0^{2+m}$; this relation describes the different branches of elementary excitations in condensed media.

Finally, we mention that, under certain conditions, fractons in a percolation cluster manifest multifractal properties [95–97].

5.3. Dipolar excitations

Now we consider a model which describes dipolar excitations. In this model, a cluster consists of polarizable monomers with the dipole interactions between them at the driving frequency ω. The cluster is subjected to an external electric field, with amplitude $\boldsymbol{E}_i^{(0)}$ at the site of the ith monomer. The amplitudes, $\boldsymbol{d}_i$ ($i = 1, \ldots, N$) of the light-induced dipole moments obey the system of equations

$$Z d_{i\alpha} = E_{i\alpha}^{(0)} - \sum_j (i\alpha|W|j\beta) d_{j\beta}, \tag{5.27}$$

where $Z \equiv -X - i\delta = \alpha_0^{-1}$ and α_0 is the polarizability of an isolated monomer (not to be confused with the tensor components and with the absorption coefficient). Note that hereafter X and δ differ (by a simple pre-factor) from the corresponding quantities introduced in (2.21).

The quantity W in (5.27) is an operator of the light-induced dipolar interactions between particles in a cluster. In particular, for the dipole-dipole interaction in the near zone ($R_c \ll \lambda$), we have

$$W_{\alpha\beta}^{ij} \equiv (i\alpha|W|j\beta) = \left[\delta_{\alpha\beta} - 3\frac{(r_{ij})_\alpha (r_{ij})_\beta}{r_{ij}^2}\right] \frac{1}{r_{ij}^3}, \tag{5.28}$$

with $\boldsymbol{r}_{ij} \equiv \boldsymbol{r}_i - \boldsymbol{r}_j$ ($W^{ij} = 0$ for $i = j$). In the $3N$-dimensional vector space, the system (5.27) acquires exactly the form (5.6). (However, the meaning of the quantities is different: the operator W is determined by (5.28), $Z \equiv -X - \iota\delta = \alpha_0^{-1}$ and $\boldsymbol{E}_i^{(0)}$ is the external field, which is not renormalized as is the case in (5.7).) Thus, the linear-response expressions (5.10) and (5.11) are valid and the polarizability of an ith monomer is given by

$$\alpha_{i,\alpha\beta} = \sum_{j,n} \frac{(i\alpha|n)(n|j\beta)}{Z + w_n}. \tag{5.29}$$

The solution (5.29) is similar to that given by Eq. (4.6), which was obtained using the spectral representation. However, in contrast to the spectral-representation theory, Eq. (5.29) provides a recipe for calculation of the mode strengths, c_s, in terms of eigenfunctions of the interaction operator. According to (5.29), the polarizability of a particle in a cluster is given by the sum of the eigenmodes having different eigenfrequencies, w_n, and contributing to the polarizability with a weight given by the product of the corresponding eigenfunctions.

As follows from (5.29), the conventional Kramers-Kronig formula is valid in terms of X:

$$Re\,\alpha_{i,\alpha\beta} = \frac{1}{\pi} P \int_{-\infty}^{\infty} \frac{Im\,\alpha_{i,\alpha,\beta}(X')\,dX'}{X' - X},$$

where P denotes the principal value of the integral. Provided the eigenvalues, w_n, are real and the decay constant δ is positive, other exact relations hold [24]:

$$\frac{1}{\pi}\int_{-\infty}^{\infty} Im\,\alpha_{i,\alpha,\beta}(X)\,dX = \delta_{\alpha,\beta}, \quad P\int_{-\infty}^{\infty} Re\,\alpha_{i,\alpha,\beta}(X)\,dX = 0, \tag{5.30}$$

and

$$P\int_{-\infty}^{\infty} X\,Im\,\alpha(X)\,dX = 0. \tag{5.31}$$

Note that the solution (5.29) of the coupled-dipole equations (5.27) and the sum rules (5.30) and (5.31), are general, and valid for arbitrary clusters (fractal or non-fractal).

The work done by the field has a form similar to Eq. (5.15), with the difference that it is performed by the original field $\boldsymbol{E}_i$:

$$A = 2\omega \left\langle \sum_{ij} Im\,\alpha_{ij}\overline{E^{(0)}(r_i)E^{(0)*}(r_j)} \right\rangle. \tag{5.32}$$

This expression is different from its counterpart (5.16) for the Goldstone (vibration) excitations.

Unlike Goldstone excitations, in the case of dipolar excitations, the polarizability does not obey the condition (5.14). Thus, the relevant expression (5.32) for the work does not vanish for the uniform field $\boldsymbol{E}^{(0)}$. Such a field corresponds to the excitation of a cluster by electromagnetic radiation with the wavelength much larger than the cluster size, R_c. In this case, the work (5.32) becomes

$$A = 2\omega N|E^{(0)}|^2 Im\,\alpha, \tag{5.33}$$

where $\alpha \equiv \langle (3N)^{-1}\sum_j \alpha_{ij,\alpha\alpha}\rangle$.

Stockman and co-workers formulated the scaling hypothesis [24], which states that in the intermediate region, $R_0 \ll L_X \ll R_c$, the absorption contour $Im\,\alpha(X)$ possesses scaling and should have a power-law dependence on the "frequency" parameter X:

$$Im\,\alpha(X) \sim R_0^3 (R_0^3|X|)^{d_o - 1}, \tag{5.34}$$

where d_o, which is called the optical spectral dimension, is the counterpart of the spectral dimension $\tilde{d}$ in the case of vibrational excitations ($0 \leqslant d_o \leqslant 1$).

Assuming $|X| \gg \delta$, we obtain from (5.29)

$$Im\,\alpha(X) = \frac{\pi}{3}\rho(X) + \frac{\pi}{3N}\sum_{i\neq j,n}\langle (i\alpha|n)(n|j\alpha)\delta(X - w_n)\rangle, \tag{5.35}$$

where the density of dipolar collective modes has the form of Eq. (5.18) and w_n are the eigenfrequencies of the dipolar operator W. The density of dipolar eigenmodes satisfies the following sum rules:

$$\int_{-\infty}^{\infty} \rho(X)\,dX = 3, \quad \int_{-\infty}^{\infty} X\rho(X)\,dX = Tr\,W = 0. \tag{5.36}$$

Note that the first term in (5.35) satisfies both sum rules for $Im\,\alpha$, (5.30) and (5.31). Correspondingly, the zeroth and first moments (in terms of X) of the second term in (5.35) are exactly zero. In the scaling region, this term is expected to have a power-law dependence. Thus, if the scaling region gives the dominant contribution to the sum rules (5.30) and (5.31), the second term in (5.35) should be small after the averaging and [24]

$$Im\,\alpha(X) \approx \frac{\pi}{3}\rho(X) \sim R_0^3|R_0^3 X|^{d_o - 1}. \tag{5.37}$$

According to (5.37), all eigenmodes contribute to the absorption with equal weights and, therefore, the absorption and the density of the eigenmodes are described by the same scaling dependence. Note that although this result is approximately valid for random diluted clusters, it fails for original, non-diluted, clusters (see Section 6). This is because the assumption of the dominant contribution of the scaling region to the sum rule is not valid in the general case. Besides, symmetry properties of the eigenmodes and related selection rules can be important for non-diluted fractal clusters (see Section 6). However, we first assume that (5.37) is valid; spectra of non-diluted clusters, when (5.37) does not hold, will be considered in Sections 6 and 7.

From (5.33) and (5.37), we obtain the required expression for the work,

$$A \approx \frac{2\pi}{3}\omega\overline{|E^{(0)}|^2} N\rho(X). \tag{5.38}$$

Using the scaling formula (5.21) and the relation $N = (R_c/R_0)^D$, we arrive at the conclusion that the A-scale-invariance requirement applied to Eq. (5.38) leads to the transformation law, $|X| \propto R_0^{(D+md_X)/(d_X-1)}$ which, after comparison with (5.4), gives $\kappa = (D+m)/(d_X - 1)$. Accordingly, the dispersion relation is

$$|X| \sim \left(\frac{L}{R_0}\right)^{-(D+m)/(d_X-1)} R_0^m. \tag{5.39}$$

Eq. (5.39) clearly differs from Eq. (5.22) for vibrational excitations. Note that now κ does depend on m. Eq. (5.39) gives X as a function of L and, through the dependence $X = -Re\,\alpha_0^{-1}(\omega)$, the relation between the eigenfrequency ω and L. The last relation (distinct from $X(L)$) does not necessarily scale. For the optical field, the interaction is given by Eq. (5.28), so that its metrical dimension is $m = -3$. In this case, the dispersion law (5.39) becomes

$$|X| \sim \left(\frac{L}{R_0}\right)^{-(3-D)/(1-d_o)} R_0^{-3}, \tag{5.40}$$

where d_o is the notation for d_X in the dipole case [24,25]. This formula can be also rewritten as

$$L_X \sim R_0 (R_0^3|X|)^{(d_o-1)/(3-D)}. \tag{5.41}$$

As follows from (5.41), in the vicinity of the center ($R_0^3|X| \ll 1$), the eigenmodes are delocalized over a large part of a cluster ($L_X \gg R_0$), whereas towards the wings of the absorption contour (at $R_0^3|X| \sim 1$) the modes are strongly localized ($L_X \sim R_0$).

At resonance, the polarizability, α_0, has a pole, and in its vicinity $X \approx K(\omega - \omega_0)$, where ω_0 is the resonance frequency and $K = const$. For example, for a two-level system, the constant $K = \hbar/|\boldsymbol{d}_{12}|^2$, where $\boldsymbol{d}_{12}$ is the dipole matrix element of the resonant transition in the monomer. Accordingly, in the vicinity of the resonance, Eq. (5.40) becomes [cf. Eq. (5.24)]

$$|\omega - \omega_0| \sim \left(\frac{L}{R_0}\right)^{-(3-D)/(1-d_o)} R_0^{-3}|\boldsymbol{d}_{12}|^2/\hbar. \tag{5.42}$$

Note that the scaling condition (5.3), when using (5.41), acquires the form

$$N^{-(3/D-1)/(1-d_o)} \ll R_0^3|X| \ll 1. \tag{5.43}$$

Thus, the scaling region is restricted to small $|X|$, i.e. occupies the center of the absorption band. In addition to (5.43), there is another necessary condition for scaling:

$$|X| \gg \delta, \tag{5.44}$$

which is compatible with (5.43) only if the decay constant is small ($R_0^3\delta \ll 1$).

Now we briefly discuss the physical origins for the difference in dispersion relations for the two problems considered. By the choice of the spectral variable, $Z = -X - i\delta$, the basic equations, (5.5) and (5.27), for the two problems are reduced to the common equation (5.6) in the $3N$-dimensional vector space. However, there are two differences between the two problems. First, for vibrations, the field $\boldsymbol{E}$, which appears in the basic equation (5.6), is not the physical field ($\boldsymbol{F}$), whereas, for polar excitations, it is. Second, for vibrations, the interaction obeys the Goldstone requirement (5.13), which brings about the conditions (5.14). As a result of these differences, the expressions for the field work for the two problems are different [cf. Eqs. (5.17) and (5.38)]. In particular, for vibrations, as for any Goldstone excitation, the field work (5.17) tends to zero in the limit of constant exciting field ($L_f \to \infty$); however, this is not the case for non-Goldstone excitations. Therefore, it is not surprising that the dispersion laws (5.22) and (5.39), obtained from the scale-invariance requirements for the corresponding field-work expressions, are different.

5.4. Scaling and localization of collective dipolar modes in diluted fractals. Results of numerical simulations

In this section we consider the results of numerical simulations of optical properties of diluted (randomly decimated) clusters. A diluted cluster is obtained by random removal of monomers from the cluster and successive reduction in cluster size, so that the average distance between nearest neighbors remains the same as in the original cluster. This procedure leads to improved spatial scaling at small distances while the global fractal morphology of the cluster remains unchanged [24]. Specifically, each monomer in a cluster consisting of a large number of particles is either kept in its place, with probability $\beta \ll 1$, or removed from the fractal, with probability $1 - \beta$. Then, the cluster as a whole is reduced in size by a factor $(1/\beta)^{1/D}$. The power-law behavior of the correlation function, $g(r) \propto r^{D-3}$, holds for the diluted fractal down to smaller distances, $r_0 = \beta^{1/D}R_0 \ll R_0$.

Note that the model of diluted clusters can describe some real systems, such as metallic nanoparticles in a fractal (e.g., polymer) host.[1]

Two types of fractals were studied [26]: random-walk clusters (RW), with $D = 2$ and $R_0 = a/(6)^{1/2}$, and cluster-cluster aggregates (CCA) [98], with $D \simeq 1.78$ and $R_0 \approx a/3$, where a is the lattice period. All clusters were subjected to 32-fold decimation, i.e. $\beta \approx 0.03$. (As simulations showed, the further decreasing of β does not affect the spectra.) The calculated values were averaged over a large ensemble of clusters ($\sim 10^3$). The polarizability was computed from (5.29) by diagonalizing the matrix (5.28).

In Fig. 6a, the quantity $Im\,\alpha$ for diluted cluster-cluster aggregates (DCCA) is plotted as a function of X for two different values of δ: $\delta = 0.001$ and $\delta = 0.005$ (the number of particles in each clusters was $N = 64$). The results are presented in units, where $R_0 = 1$. Clearly, there is strong inhomogeneous broadening associated with the interaction of particles. The resultant spectral width is much larger than δ and, accordingly, there is no dependence of the spectra on δ. The scaling properties of $Im\,\alpha$ and ρ are analyzed in Figs. 6b and 6c. In accordance with (5.37), both quantities show approximately the same scaling, with the exponent $d_o = 0.3 \pm 0.1$. (Note, however, that because of the strong statistical noise in the simulations, the obtained scaling was disputed in Ref. [34].)

Similar results, with $d_o = 0.4 \pm 0.1$, were obtained for the RW clusters; these simulations were performed for $N = 128$ and $N = 256$ [26].

Note that the scaling behavior obtained near the "critical" point, $X = 0$, has a similar physical nature as the scaling in percolation systems (see Section 2). In both cases, long-range fluctuations near the critical point ($X = 0$, for the optical absorption by diluted fractals, and $p = p_c$, for a percolation system) result in the scaling of observable characteristics.

We now consider in more detail the predicted localization of collective dipolar modes in fractals (see Eq. (5.41)). It is worth noting that localization of dipolar excitations in fractals is a non-trivial fact since in "usual" media ($D \to 3$) dipolar excitations are typically delocalized.

In Fig. 7a, three different dipole modes of the fractal are presented [29]. Each mode is determined by a certain value of the dimensionless spectral variable, $R_0^3|X|(R_0 \equiv 1)$. The cluster was simulated using 2d cluster-cluster aggregation (CCA) [98]. The points in the figure correspond to the centers of particles touching each other and forming the cluster. The radii of the circles drawn around the particles give the values of dipole moments induced on them. These dipole moments were calculated by calculating the eigenvectors of the interaction operator, W, and substituting them in Eq. (5.29). As seen in the figure, the dipole modes are localized.

Fractal clusters resulting from cluster-cluster aggregation are random. Spatial localization of dipolar modes and the corresponding local fields can be also obtained for geometrically ordered fractals. Figs. 7b and 7c, showing the distribution of local field intensities for the Viscek fractal, also indicate the localization. The symmetry breaking results from the incommensurate structure of the light field with respect to that of the cluster. Specifically, it is the introduction of the two vectors $\boldsymbol{E}^{(0)}$ and $\boldsymbol{k}$ (that do not coincide with the fractal axes), with the tensor character of the dipole-dipole interaction, that breaks the symmetry.

The mean coherence length, L_X, is defined as [25,29]

[1] The basic hypothesis formulated in Ref. [24] was that the dilution does not affect the optical properties in the scaling region and the optical excitations of the original and diluted clusters are the same. In the next section we will see that although these properties are qualitatively similar, there is also a significant difference.

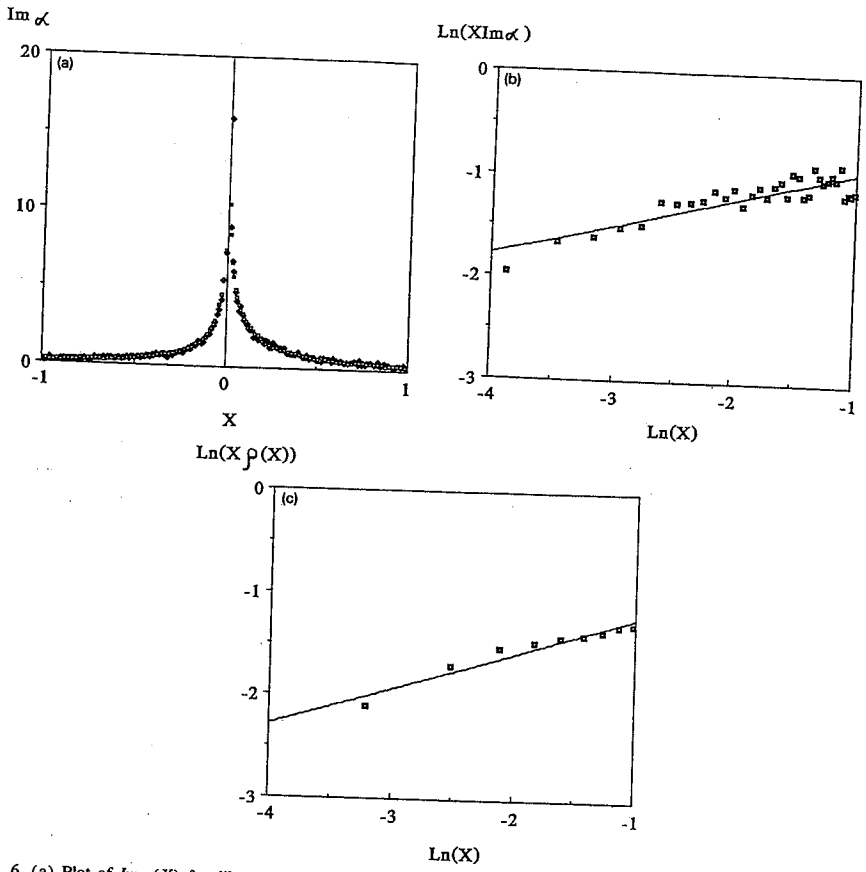

Fig. 6. (a) Plot of $Im\,\alpha(X)$ for diluted cluster-cluster aggregates (DCCA). Diamonds and boxes refer to $\delta = 0.001$ and $\delta = 0.005$, respectively. (b) ln–ln plot of $X\,Im\,\alpha(X)$. The slop $d_o = 0.28$ is plotted. (c) ln–ln plot of $X\rho(X)$. The slope $d_o = 0.35$ is plotted. Taken from V.M. Shalaev et al., Phys. Rev. B 44 (1991) 12216.

$$L^2(X) = \frac{\langle \sum_n \delta(X - w_n) \{ \sum_i (i\alpha|n)^2 r_i^2 - [\sum_i (i\alpha|n)^2 r_i]^2 \} \rangle}{\langle \sum_n \delta(X - w_n) \rangle}. \tag{5.45}$$

This definition has a clear quantum-mechanical analogy with $(i\alpha|n)$ as the wave function (the wave functions are normalized, $\sum_i (i\alpha|n)^2 = 1$).

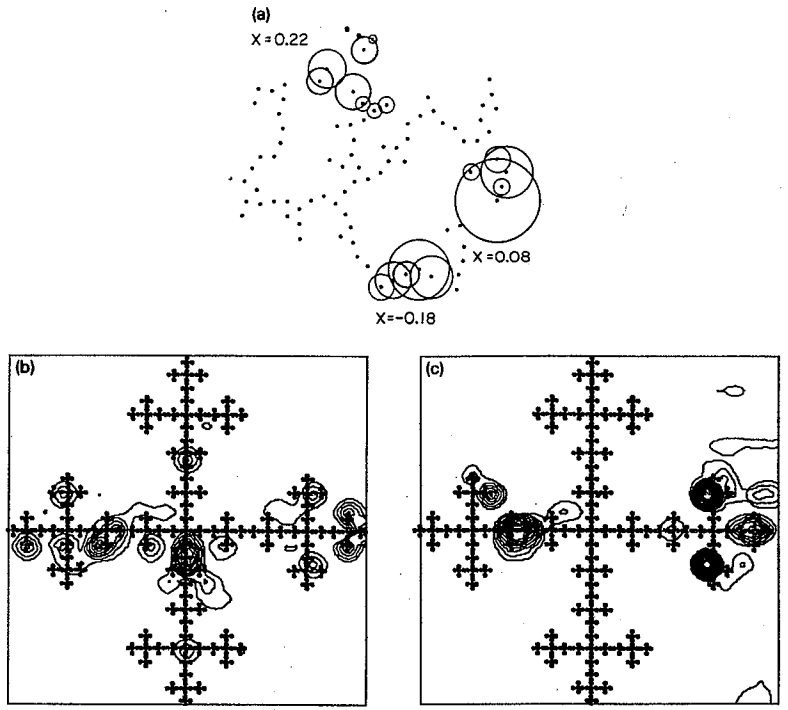

Fig. 7. (a) Localized dipole modes on the fractal. (Taken from Ref. [29].) (b) and (c): Local field intensity of the light-induced dipole modes on a Viscek fractal for s-polarization and $X = -0.1$ (b) and $X = -0.25$ (c). Taken from Shalaev et al., Physica A 207 (1994) 197.

We have examined the diluted cluster-cluster aggregates [29], with the 32-fold decimation ($\beta \simeq 0.03$) has been used.

The localization length, L_X, in diluted cluster-cluster aggregates is shown in Fig. 8 as a function of the dimensionless spectral variable $R_0^3|X|(R_0 \equiv 1)$ for both positive and negative X [29]. The number of particles in each diluted cluster is $N = 128$. The calculated points lie along straight lines, with the slopes -0.53 ± 0.07 and -0.56 ± 0.06 for $X > 0$ and $X < 0$, respectively. The corresponding value of the optical spectral dimension is $d_o = 0.33 \pm 0.08$, in accordance with (5.41). This value agrees with $d_o = 0.3 \pm 0.1$ found from the density of states and the absorption (Fig. 6b,c) [26].

Thus, strong localization of dipole collective excitations occurs in fractals. The localization results in very high local fields leading to huge enhancements of resonant Rayleigh [26], Raman [28] and, especially, non-linear scattering, e.g., degenerate four-wave mixing [30,99,100]. We will consider

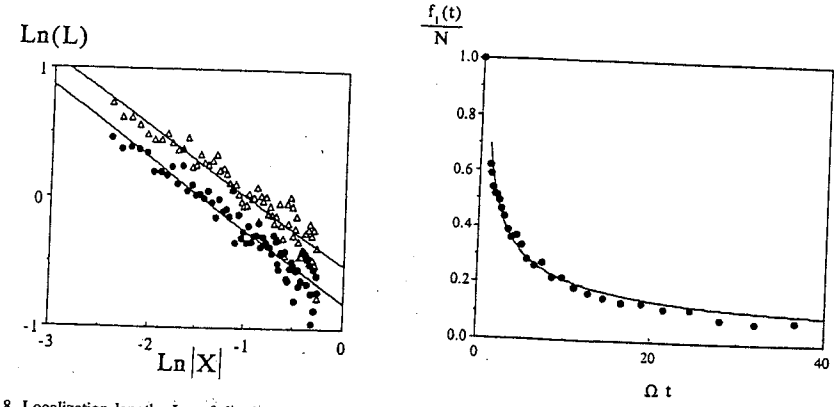

Fig. 8. Localization length, L_X, of dipole excitations on DCCA for $X > 0$ (triangles) and $X < 0$ (circles). Taken from Ref. [29].

Fig. 9. Function $f_1(t)/N$ describing the decay of the optical free-induction (polarization) for $\gamma t \ll 1$. The solid line is the $0.75(\Omega t)^{-0.55}$ dependence. The exponent gives the value of the spectral dependence $d_o = 0.55$. The simulations are made for diluted ballistic cluster-cluster aggregates ($D \approx 1.9$). Taken from Ref. [32].

below enhanced optical effects in small-particle aggregates (see Section 7).

In the end of this section, we briefly consider optical free-induction decay (OFID) in fractals. Under certain conditions, spatial self-similarity of fractal clusters leads to scaling in the time domain. Martin et al. studied dynamics of the sol-gel transition probed by light scattering and reported the observation of a power-law time decay of the intensity autocorrelation function [101]. Fractal time processes often imply a self-similar distribution of the eigenfrequencies [19]. Shalaev and Botet showed that the scaling in the mode distribution (see Eq. (5.37)) can result in the scaling of the OFID [32].

As shown in Ref. [32], a wide-band excitation, with $E^{(0)}(t) \propto E^{(0)}\delta(t)$, of harmonic oscillators forming a fractal cluster results in the OFID of the form $P_\alpha(t) = \alpha_0 E_\alpha^{(0)} Re[f \exp\{-\gamma t - i\omega_0 t\}]$, where α_0 is the polarizability of an individual oscillator (with ω_0 being the resonant frequency) and $f \equiv f_1 + if_2$ is given by

$$f(t) = \left\langle \frac{1}{3} \sum_{nij} \exp\{-i\Omega_n t\} (i\alpha|n)(n|j\alpha) \right\rangle .$$

The frequencies $\Omega_n \equiv \omega_n - \omega_0 = \frac{1}{2}\omega_0 R_m^3 w_n$ characterize the shift (with respect to the central frequency ω_0) associated with the nth mode. (As above, w_n are the eigenfrequencies of the operator (5.28)). The authors showed that the OFID has no a characteristic time in the scaling domain, so that

$$P(t) \propto t^{-d_o}. \tag{5.46}$$

The simulations were performed for ballistic cluster-cluster aggregates ($D \approx 1.9$). The clusters were subjected to the dilution with $\beta = 64$ so that after the dilution each cluster consisted of $N = 512$ particles. The results were averaged over an ensemble of 100 random clusters.

In Fig. 9 the results of the simulations of optical free-induction decay, $f_1(t)/N$, are shown. At $t = 0$, one has $f = N$, i.e. all the dipoles are in phase. For $t > 0$, the quantity $f_1(t)$ decays, exhibiting a power-law dependence, $\propto t^{-d_0}$, within a certain time interval (the scaling region). For larger times $f(t)$ falls to zero, reflecting the complete dephasing of the dipole moments (not shown in the figure).

For the scaling region, the value -0.55 was found for the exponent in the power-law dependence of $f_1(t)$. In Ref. [33], the value $d_0 = 0.53 \pm 0.1$ was reported for the ballistic cluster-cluster aggregates. Thus, the exponent found from the OFID simulations coincides with $-d_0$, within the error interval.

Below we consider optical properties of original (non-diluted) aggregates of particles.

6. Optical properties of small-particle aggregates

In this section, following Ref. [102], we consider general solutions of the coupled-dipole equations for small-particle aggregates with the exact operator for the dipole interaction (including the near-, intermediate-, and far-zone terms). We discuss the results of simulations for original (non-diluted) clusters consisting of large numbers of particles, from 500 to 10000. It will be shown that in contrast to diluted clusters (see Section 5), the spectral dependence of absorption by original clusters significantly differs from that of the density of dipolar eigenmodes. This indicates the importance of symmetry properties of dipole modes in absorption by random fractals. Numerical simulations also demonstrate a significant difference in absorption spectra of fractal and non-fractal composites.

6.1. Coupled-dipole equations and optical cross sections

We consider the interaction of a plane electromagnetic wave $\boldsymbol{E}(\boldsymbol{r}, t) = \boldsymbol{E}^{(0)} \exp(i\boldsymbol{k}\cdot\boldsymbol{r} - i\omega t)$ with a cluster of N particles (monomers) located at points $\boldsymbol{r}_1, \ldots, \boldsymbol{r}_N$. As above, the monomers are assumed to be spherical with diameter much less than the wavelength of light. The particles are polarizable, with the light-induced dipoles given by $\boldsymbol{d}_i = \alpha_0 \boldsymbol{E}_i$, where $\boldsymbol{E}_i$ is the local field acting on the ith particle of isotropic polarizability α_0. The local field at any point is a superposition of the incident wave and all secondary waves scattered by the dipoles. Thus, dipole moments interact with each other and with the incident field, and obey the coupled-dipole equations (CDE):

$$d_{i\alpha} = \alpha_0 \left[E_\alpha^{(0)} \exp(i\boldsymbol{k}\cdot\boldsymbol{r}_i) + \sum_{j=1}^{N}{}' G_{\alpha\beta}(\boldsymbol{r}_{ij}) d_{j\beta} \right], \tag{6.1}$$

where the time-dependent term, $\exp(-i\omega t)$, is omitted, $\boldsymbol{r}_{ij} \equiv \boldsymbol{r}_i - \boldsymbol{r}_j$ and $\sum'$ denotes the sum over all values of index j except $j = i$. The interaction tensor $G_{\alpha\beta}$ is defined as (cf. Eq. (5.28)):

$$G_{\alpha\beta}(\boldsymbol{r}) = k^3 \left[A(kr)\delta_{\alpha\beta} + B(kr)\frac{r_\alpha r_\beta}{r^2} \right], \tag{6.2}$$

$$A(x) = [x^{-1} + ix^{-2} - x^{-3}] \exp(ix), \tag{6.3}$$

$$B(x) = [-x^{-1} - 3ix^{-2} + 3x^{-3}] \exp(ix), \tag{6.4}$$

where α and β denote Cartesian components. Summation over repeated Greek indices is implied.

We introduce a $3N$-dimensional complex vector space C^{3N} and an orthogonal basis $|i\alpha)$. Vectors $|d)$ and $|E) \in C^{3N}$ and their components in this basis are $(i\alpha|d) = d_{i,\alpha}$ and $(i\alpha|E) = E_{i,\alpha} = E_\alpha^{(0)} \exp(i\boldsymbol{k}\cdot\boldsymbol{r}_i)$. Similarly, we introduce a $3N\times 3N$ operator $\hat{V}$, which in the $|i\alpha)$ basis has components $(i\alpha|\hat{V}|j\beta) = -G_{\alpha\beta}(\boldsymbol{r}_{ij})$ where $G_{\alpha\beta}(\boldsymbol{r}_{ij})$ is defined in Eqs. (6.2)–(6.4). Then, Eqs. (6.1) acquire the form of a matrix equation:

$$(Z + \hat{V})|d) = |E), \tag{6.5}$$

where $Z = 1/\alpha_0$. Note that Eq. (6.5) is equivalent to Eq. (5.6) with a significant difference, however. In contrast to W defined in (5.28) and describing interaction in the near zone only, the operator $\hat{V}$ includes the near-, intermediate-, and far-zone terms and it is symmetric but not Hermitian. Thus, Eqs. (6.1) and (6.5) are exact and describe the dipolar interaction in the general case.

The solution of Eq. (6.5) has the form [102]:

$$|d) = \sum_n \frac{|n)(\bar{n}|E)}{(\bar{n}|n)} \frac{1}{Z + v_n}, \tag{6.6}$$

where v_n are the eigenvalues of $\hat{V}$ defined by $\hat{V}|n) = v_n|n)$ and the "bar" sign denotes complex conjugation of all components of a vector. Thus, if $|n)$ is a column vector, $(\bar{n}|$ is a row vector with the same entries as $|n)$. Although the $|n)$ basis is not, in general, orthogonal it can be shown that $(\bar{m}|n) = 0$ for $m \neq n$ [102].

In the $|i\alpha)$ basis the solution (6.6) acquires the form (cf. Eq. (5.29))

$$d_{i,\alpha} = \sum_{n,j} \frac{(i\alpha|n)(\bar{n}|j\beta)E_{j,\beta}}{[\sum_{i'}(\bar{n}|i'\alpha')(i'\alpha'|n)]} \frac{1}{Z + v_n}. \tag{6.7}$$

Formulas (6.6) and (6.7) indicate that, for an arbitrary collection of N interacting particles, there are $3N$ eigenmodes with resonant eigenfrequencies defined by $Re(Z) + v_n = 0$. The weight with which a mode contributes to the resultant optical response depends on the scalar product $(\bar{n}|E)$ and, thus, on the symmetry properties of the eigenvectors $|n)$.

Once the CDE (6.1) are solved for dipole moments $\boldsymbol{d}_i$, extinction and absorption cross sections (σ_e and σ_s, respectively) can be obtained from the optical theorem [102–104]:

$$\sigma_e = 4\pi k|E^{(0)}|^{-2} Im \sum_{i=1}^{N} \boldsymbol{d}_i \cdot \boldsymbol{E}^{(0)*} \exp(-\boldsymbol{k}\cdot\boldsymbol{r}_i) = 4\pi k|E^{(0)}|^{-2} Im(d|E), \tag{6.8}$$

$$\sigma_a = 4\pi k|E^{(0)}|^{-2} y_a \sum_{i=1}^{N} |d_i|^2 = 4\pi k|E^{(0)}|^{-2} y_a (d|d), \tag{6.9}$$

where

$$y_a = -Im(Z) - 2k^3/3 \tag{6.10}$$

is a non-negative constant characterizing the absorption strength. (The scattering cross section σ_s is defined by $\sigma_s = \sigma_e - \sigma_a$.) Note that each term in the sum (6.9) characterizes absorption by a single monomer; however, individual terms of the sum (6.8) have no independent physical significance, since scattering (and, therefore, extinction) is in general a collective phenomenon.

If clusters are much smaller than the wavelength of the incident wave and $y_a \gg 2k^3/3$, then we can use the quasi-static limit for the dipole interaction matrix [105]. This means that we can omit terms $1/x$, $1/x^2$ and $\exp(ix)$ in Eqs. (6.3), (6.4) and put $\exp(\pm i\boldsymbol{k}\cdot\boldsymbol{r}_i) = 1$ in formulas (6.1) and (6.8). We use below the notations $\hat{W}$ and w_n (similar to the notations of Section 5) for the quasi-static limit of the interaction operator, $\hat{V}$, and its eigenvalues, v_n. After averaging over the orientations of a cluster as a whole the extinction cross section is expressed as

$$\sigma_e = 4\pi k N \, Im\, \alpha, \tag{6.11}$$

where

$$\alpha = (1/3N) \sum_i Tr[\alpha_{\alpha\beta}^{(i)}], \tag{6.12}$$

and $\alpha_{\alpha\beta}^{(i)}$ are related to $d_{i\alpha}$ via

$$d_{i\alpha} = \sum_\beta \alpha_{\alpha\beta}^{(i)} E_\beta^{(0)}. \tag{6.13}$$

The $d_{i\alpha}$ are to be found from the solution of (6.1)–(6.4). Thus, with the trivial pre-factor $4\pi kN$, the extinction cross section is proportional to $Im\,\alpha$.

We also define three normalized vectors, one for each direction $\alpha = x, y, z$ as follows:

$$|\phi_\alpha) = \frac{1}{\sqrt{N}} \sum_i |i\alpha).$$

Then, it is easy to show that

$$\alpha = \left(\phi_\alpha \left| \frac{1}{\hat{W} + Z} \right| \phi_\alpha\right) = \sum_n \frac{(\phi_\alpha|n)(n|\phi_\alpha)}{\alpha_0^{-1} + w_n}. \tag{6.14}$$

The basic formulas (6.6)–(6.14) presented in this section will be applied below for numerical simulations of optical properties of fractal composites.

The CDE (6.1) are general in the sense that they place no restrictions on the geometry of the aggregates. In particular, the system of Eqs. (6.1) can be applied for finding the optical response of a fractal aggregate of particles.

We performed numerical simulations for a number of computer-generated clusters, both fractal and non-fractal ones. Below we briefly describe the computer models used for small-particle aggregates.

Random cluster-cluster aggregates (CCA) were simulated using a well-known numerical algorithm (see, for example, Ref. [98]). The fractal dimension of CCA is $D \approx 1.78$, and the length constant $R_0 \approx a/3$ where a is the lattice period (equal to the particle diameter). We generated various assemblies of CCA consisting of different numbers of particles: $N = 500$, 1000 and 10000. Note, that the model of CCA provides an excellent simulation of empirically observed aggregates of metal particles in solution [106]. In this model, encounters of randomly walking particles result in their sticking together, first to form small groups, which then aggregate into larger formations, and so on.

We also simulated other types of fractals, including Witten-Sander aggregates (WSA) and random-walk aggregates (RWA). WSA result from diffusion-limited cluster-particle aggregation and have fractal dimension $D \approx 2.5$ (see, for example, Ref. [107]). RWA were generated based on the model

of self-avoiding random walks; the fractal dimension in this case is $D \approx 1.7$. The WSA were built on a simple cubic lattice while the RWA were off-lattice.

To compare fractal and non-fractal composites, we also simulated a random gas of particles (RGP) and a close-packed sphere of particles (CPSP). While RGP is a very dilute system of particles randomly distributed in space, CPSP represents a dense (but still random) system of particles. In both cases $D = d = 3$ and the correlation function $g(r)$ is constant. The particles were assumed to be hard spheres. To provide better comparison with CCA, the RGP was generated in a spherical volume that would be occupied by a CCA with the same number of particles; this means that particles in CCA and RGP fill the same volume fraction, p (p was small, $p \approx 0.05$ for $N = 500$.) In contrast, a fairly dense packing of spherical particles, with $p \approx 0.44$, was used for CPSP.

To solve Eqs. (6.1) for the aggregates described above we used different numerical methods: diagonalization of the interaction matrix [24,26], the conjugate-gradient method [103], and the Lanczos algorithm [108,109].

6.2. Optical properties of small-particle composites in the quasi-static approximation

We discuss here linear optical properties of small-particle composites in the quasi-static approximation. General properties of the solutions of Eqs. (6.1) in the quasi-static approximation were considered in Section 5. Here we recapitulate some formulas that are relevant to the subsequent numerical results.

In the quasi-static approximation, the interaction tensor $\hat{W}$ does not depend on $k = \omega/c$, and the only dependence of $Im\,\alpha$ on ω is through the monomer polarizability α_0. As in Section 5, we introduce real, X, and imaginary, δ, parts of $Z = 1/\alpha_0$ so that

$$Z = 1/\alpha_0 = -(X + i\delta). \tag{6.15}$$

Note that solutions of the CDE can be expressed in terms of X and δ for an arbitrary form of the polarizability, α_0. Alternatively, defining α_0, one can always specify the frequency dependence of the spectral variable X and decay parameter δ. Thus, the solutions of the CDE, expressed in terms of X and δ, have an universal character, while their specific frequency (or wavelength) dependence is determined by the corresponding frequency dependence of $\alpha_0 = \alpha_0(\omega)$ (which, in general, depends on the specific particles aggregated into a cluster). For example, in the vicinity of an isolated resonance the polarizability can be represented as

$$\alpha_0 = \frac{R_m^3 \omega_m}{(\omega_0 - \omega) - i\Gamma}, \tag{6.16}$$

where ω_0 is the resonance frequency of an individual monomer, Γ is the resonance half-width, and ω_m, R_m are the characteristic excitation frequency and geometrical size of a particle, respectively (in particular, in a two-level model, $R_m^3 \omega_m = |d_{12}|^2/\hbar$, where d_{12} is the dipole moment of the transition.) Then, $X = R_m^{-3}(\omega - \omega_0)/\omega_m$ and $\delta = R_m^{-3}(\Gamma/\omega_m)$. In the next Section we consider X and δ for another important case where the particles are dielectric spheres.

As follows from Eqs. (6.10) and (6.15), the decay constant δ is related to y_a by $\delta = y_a + 2k^3/3$. Since we assume strong absorption, i.e. $2k^3/3 \ll y_a$, the approximation $\delta = y_a$ is valid within the precision of the quasi-static approximation.

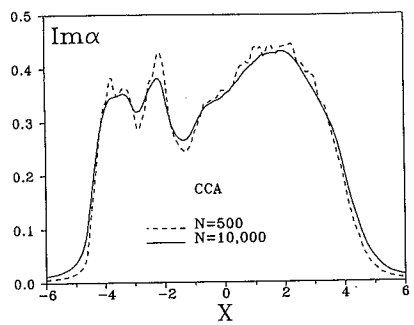

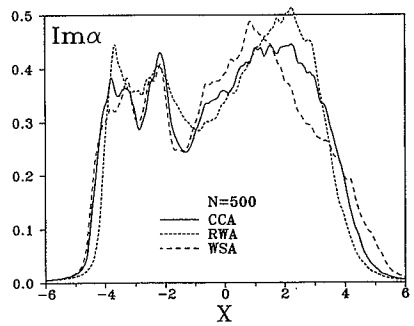

Fig. 10. Calculated absorption spectra, $Im\,\alpha(X)$, for cluster-cluster aggregates (CCA) containing different number of particles, $N = 500$ and $N = 10000$.

Fig. 11. Calculated absorption spectra, $Im\,\alpha(X)$, for various fractals consisting of $N = 500$ particles: cluster-cluster aggregates (CCA), random-walk aggregates (RWA) and Witten-Sander aggregates (WSA).

As was shown in Ref. [24], the exact property of the CDE solutions in the quasi-static approximation is

$$N^{-1} \sum_i |d_i|^2 = |E^{(0)}|^2 Im\,\alpha/\delta. \tag{6.17}$$

Taking into account Eqs. (6.8)–(6.13), (6.15) and (6.17), we conclude that in the quasi-static approximation, the extinction and the absorption cross sections are equal, and the scattering cross section is zero. In order to obtain a non-zero scattering cross section, the first non-trivial correction to the quasi-static solution must be determined, which turns out to be of the order of $(k^3/y_a)\sigma_e$.

In general, the decay parameter δ depends on ω. However, we first present our results as functions of $X = X(\omega)$, assuming that $\delta = const$ (this is the case, in particular, for a two-level system). As was mentioned above, in terms of X, the spectra exhibit a universal behavior since they are determined only by aggregate morphology, and do not depend on material properties. Material properties of monomers and the corresponding λ-dependence for aggregates of metal particles will be considered in Section 6.3.

All quantities below are given in units such that the diameter of a particle (equivalent to the lattice period for lattice clusters) is equal to one, $a = 1$. (Note that in Section 5, where we considered scaling properties of diluted fractals, different units, with $R_0 = 1$, were used; for CCA, in particular, one has $R_0 \approx a/3$). In the calculations presented here the value of the decay constant was $\delta = 0.1$ for all clusters except the ones consisting of 10000 particles, for which we used the value $\delta \approx 0.2$. The results of simulations were averaged over 10 random realizations for each type of clusters, except for the 10000 particle CCA, where the averaging was performed over 4 random realizations.

In Fig. 10, a plot of $Im\,\alpha$ as a function of X is presented for CCA with different number of particles, $N = 500$ and 10000 [102]. (The calculations with the 10000-particle CCA were performed by using the Lanczos algorithm [108,109].) The absorption $Im\,\alpha(X)$ exhibits little variation with N; however, the shape of the function $Im\,\alpha(X)$ is much more complicated than for diluted CCA (cf. Fig. 6a).

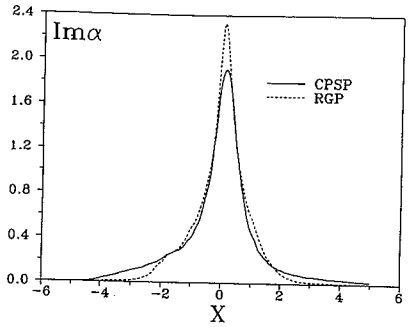

Fig. 12. Calculated absorption spectra for non-fractal 500-particle aggregates: a close-packed sphere of particles (CPSP) and random gas of particles (RGP).

The absorption $Im\,\alpha(X)$ for the diluted CCA (DCCA) has one maximum near $X = 0$ and is nearly symmetrical. For the original CCA there are at least 3 well-pronounced maxima significantly shifted from $X = 0$, and the symmetry is broken. These differences in the spectra of diluted and original clusters arise from the fact that the process of dilution does not conserve the local structure of clusters (although, the global fractal morphology is conserved).

Note that the exact properties for the first two moments of the quasi-static solutions (see Eqs. (5.30) and (5.31))

$$\int Im\,\alpha(X) = \pi, \quad \int X\,Im\,\alpha(X)\,dX = 0$$

hold for the functions shown in Fig. 10; the higher odd moments of $Im\,\alpha(X)$, however, are non-zero.

The three-maxima structure holds for various types of fractal clusters as can be seen from Fig. 11 where $Im\,\alpha(X)$ is plotted for different 500 particle fractal clusters, CCA, WSA, and RWA [102]. However, there are shifts in positions of the maxima for different types of clusters (especially, for positive X). For all fractals considered, there is a large inhomogeneous broadening; the absorption is reduced only for $|X| > 5$ (while the homogeneous half-width δ is very small, $\delta = 0.1$).

The spectral dependence of $Im\,\alpha(X)$ for trivial clusters ($D = d = 3$) is very different from those for fractals [102]. In Fig. 12, we plot $Im\,\alpha(X)$ for RGP and CPSP with the same number of particles, $N = 500$. Both spectra are nearly symmetrical and narrow (the half-width is $\approx 5\delta$ for both.) Thus, in contrast to fractal aggregates, such clusters do not show large inhomogeneous broadening. (In fact, for $a \to 0$ and $N \to \infty$ one anticipates that the spectra in both cases will be similar to that of isolated spherical particles.)

Thus, dipole-dipole interactions in fractals, in contrast to non-fractal composites (sparse, like RGP, or compact, like CPSP), lead to significantly larger inhomogeneous broadening. (In terms of the optical wavelength, the eigenmodes of silver CCA, for example, span the visible and infrared parts of the spectrum, while modes in non-fractal silver CPSP and RGP are positioned in a narrow range between approximately 350 nm and 450 nm.) This results from the fact that, for fractals, the dipole-dipole interaction is not long range, and therefore most of the eigenmodes are localized in some

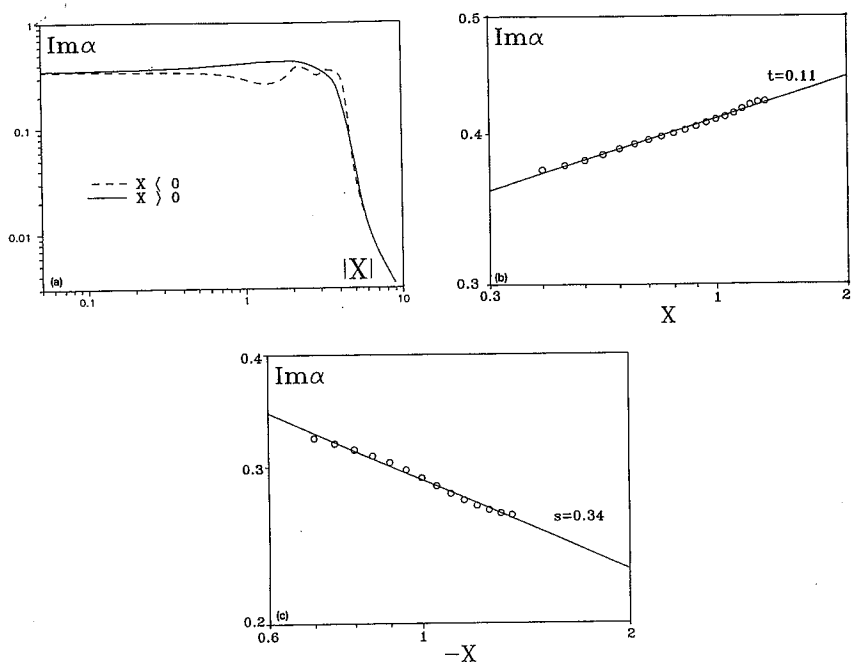

Fig. 13. Log–log plot of the absorption contour, $Im\,\alpha(X)$, for 10 000-particle CCA aggregates for the whole range of X (a), and in the vicinity of the critical point: $0.4 \leqslant X \leqslant 1.3$ (b) and $-1.4 \leqslant X \leqslant -0.7$ (c). The slopes in the figures (b) and (c) are $t = 0.11$ and $s = -0.34$ for positive and negative values of X, respectively.

small area of a fractal aggregate; these areas have very different local structures and, accordingly, they resonate at different frequencies. In contrast, in compact non-fractal aggregates (with $D = d = 3$) dipolar modes are delocalized over the whole sample, and they absorb light within a narrow spectral interval.

We next consider scaling properties of $Im\,\alpha$. The scaling theory discussed in Section 5 asserts that, for a fractal cluster, $Im\,\alpha(X)$ must, for small $|X|$, exhibit a power-law dependence of the form $|X|^{d_o-1}$; d_o is the optical spectral dimension, which must lie in the interval $0 \leqslant d_o \leqslant 1$. The same spectral behavior was predicted for the density of eigenstates $\rho(X)$, i.e. $Im\,\alpha(X) \approx \rho(X)$ (see Eq. (5.37). The numerical results presented in Section 5 showed that these predictions are approximately valid for diluted fractal clusters. As follows from the simulations shown below, these results fail for non-diluted clusters.

In Fig. 13 we present a double-logarithmic plot of $Im\,\alpha(X)$ for 10 000 particle CCA for the whole

region of eigenfrequencies (a) and, separately, for small negative (b) and small positive (c) values of X [102].

The point $X = 0$ can be considered as a special point in the spectral contour. In the range $-1.4 \leqslant X \leqslant -0.7$, the function $Im\,\alpha$ increases with increasing X, approximately following the power-law dependence, $Im\,\alpha \propto |X|^{-s}$, with $s = 0.34 \pm 0.01$ (see Figs. 10 and 13b). In the region near $X = 0$, the rate of increase becomes significantly smaller (see Fig. 10). The absorption again increases in the range $0.4 \leqslant X \leqslant 1.3$ as a power-law function, $Im\,\alpha \propto X^t$, with $t = 0.11 \pm 0.01$ (see Figs. 10 and 13 c). Qualitatively similar behavior for small $|X|$ was also obtained for RWA and WSA clusters (see Fig. 11). We note that such behavior resembles the dependence of conductivity on $p - p_c$ in the vicinity of the percolation threshold p_c (see Section 2).

The power-law dependence of the absorption near the "critical" point $X = 0$ might be due to scale invariance, similar to the metal-insulator transition in a percolation system. However, despite the fact that power-law dependences can be deduced for small regions near the center $X = 0$ (see Figs. 13b and 13c), it must be noted that these regions occupy a very small part of the whole spectrum ($\approx 15\%$ in terms of X). (Therefore, we conclude that convincing evidence of scaling for non-diluted fractals was not observed in our simulations.)

Note that for RWA (both original and diluted) the scaling $Im\,\alpha \propto |X|^{-(1+D/3)}$ for large $|X|$ was reported in Ref. [34]. The exponent $1 + D/3$ is in agreement with that predicted by the binary theory [22,24].

Next we discuss the density of dipolar eigenstates, $\rho(X) = (\pi/3N)dn/dX$, where dn is the number of eigenvalues in the interval dX. The coefficient $\pi/3$ was chosen so that $\rho(X)$ has the same normalization as $Im\,\alpha(X)$:

$$\int \nu(X)dX = \pi.$$

(This definition differs by the factor $\pi/3$ from that given in Section 5; cf. Eqs. (5.18) and (5.36).) Figs. 14a and 14b show the density of eigenstates $\rho(X)$ and $Im\,\alpha(X)$ for 500-particle CCA and CPSP, respectively [102]. It is apparent from Fig. 14a that the distribution of eigenmodes in CCA is not symmetric and differs significantly from $Im\,\alpha(X)$. This implies that selection rules are of importance and the density of eigenstates itself does not determine $Im\,\alpha(X)$. Thus, the conclusion of Refs. [24,25,34] that $Im\,\alpha(X) \approx \rho(X)$ is not correct, in general, and different modes of CCA contribute to $Im\,\alpha(X)$ with a different weight, in contrast to DCCA. The greatest difference in $Im\,\alpha$ and ρ is near the point $X = -1$. While $\rho(X)$ has a maximum near this point, $Im\,\alpha$ has a minimum there. (It is worth noting that a pair of monomers separated by unit distance has an eigenstate with $w = -1$ which is antisymmetrical (total dipole moment zero) with polarization orthogonal to the line connecting the monomers [105].)

As follows from Fig. 14b, the difference between $Im\,\alpha(X)$ and $\rho(X)$ is especially large for non-fractal CPSP. This result was anticipated for the following reason. For a continuous dielectric sphere, there is only one dipole eigenstate with non-zero total dipole moment (i.e. the selection rules are of great importance); since the CPSP can be considered as a discrete model for such a sphere, we conclude that selection rules are important in CPSP. Thus, despite the fact that our calculations demonstrate the significance of the selection rules for CCA, their role is not as important as for the case of non-fractal aggregates, such as CPSP. In particular, as follows from Fig. 14a, almost all eigenmodes within the interval $|X| < 5$ contribute significantly to the absorption.

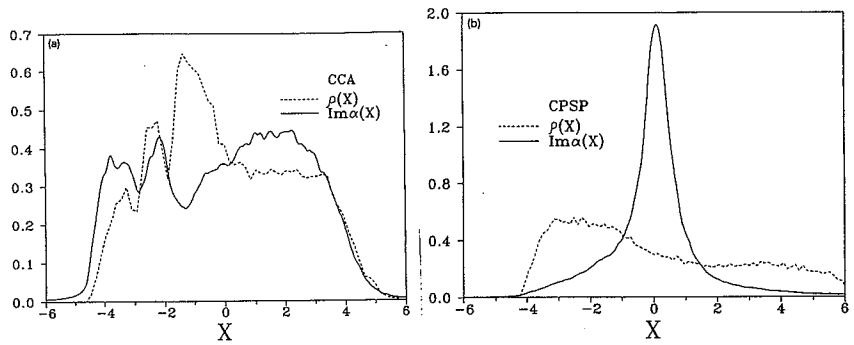

Fig. 14. Spectral dependence of the absorption, $Im\,\alpha(X)$, and the density of dipolar eigenmodes, $\rho(X)$, for 500-particle CCA (a) and CPSP (b).

We finally consider the localization length, $L(w_n) \equiv L_n$, characterizing a quasi-static eigenstate $|n)$. The $3N$ projections of the $|n)$ vector on the orthonormal basis $|i\alpha)$ determine its spatial behavior. The weight with which a given nth eigenstate is localized on the ith monomer is given by $m_n(\boldsymbol{r}_i) \equiv m_n(i) = \sum_\alpha [(i\alpha|n)]^2$; they are normalized by the condition $\sum_i m_n(i) = 1$. In terms of these weights, the localization length L_n of the nth eigenmode is defined as [24,25,29]

$$L_n \equiv L(w_n) = \sum_{i=1}^{N} m_n(i)\boldsymbol{r}_i^2 - \left[\sum_{i=1}^{N} m_n(i)\boldsymbol{r}_i\right]^2 . \tag{6.18}$$

This formula is actually a discrete function of its argument w_n. One can obtain a smooth localization function $L(X)$ by averaging $L(w_n)$ over some given interval ΔX for an ensemble of clusters

$$L(X) = \left\langle [K(X, \Delta X)]^{-1} \sum L(w_n) \right\rangle , \tag{6.19}$$

where the summation is taken over all n satisfying the condition $|X - w_n| \leqslant \Delta X$ and $K(X, \Delta X)$ is the number of terms in this sum (cf. (5.45)). The symbol $\langle \ldots \rangle$ denotes an average over an ensemble of random clusters.

In Fig. 15 we present the results of simulations for $L(X)$ for 500-particle CCA ($\Delta X \approx 0.6$) [102]. The points indicate values of the original function $L(w_n)$ for one particular cluster while the solid line shows the result of averaging over 10 random cluster realizations.

From Fig. 15 we see that $L(X)$ exhibits large fluctuations, especially near the central point $X = 0$. There are modes that are strongly localized and those that are delocalized. The mode localization increases, on average, toward larger values of $|X|$, so that for the most localized modes $L(X)$ reduces to a dimension comparable to the size of a monomer, a. Thus, similar to the case of diluted clusters, a significant fraction of eigenmodes in original clusters is also strongly localized.

To conclude this section, we note the following. While the predicted scaling was previously obtained for diluted clusters, the optical properties of original, non-diluted, clusters do not show convincing evidence of scaling. A possible reason for the absence of strong scaling may be related to the fact that

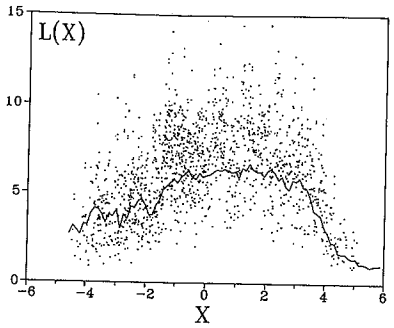

Fig. 15. The localization lengths, $L(X)$, of dipole eigenmodes versus their eigenvalues X for 500-particle CCA. The dependence $L(X)$ averaged over an interval of $\Delta X = 0.6$ for 10 random cluster realizations is shown by the solid line.

for all values of X there are modes that are sufficiently localized (see Fig. 15), so that only a few particles are involved in the excitation, and scale invariance does not manifest itself distinctively for such small distances. Another possible reason is due to symmetry properties of the eigenmodes. As our simulations show, eigenmodes are strongly asymmetric in contrast to the assumption of Ref. [24] of the spherical, on average, symmetry of modes. Scaling in this case might occur individually for modes with a certain degree of asymmetry (some effective "aspect ratio") while the overall spectrum, formed from modes of different symmetries, may exhibit multifractal scaling. (Note that multifractality of giant electric field fluctuations in semiconductor films was considered recently in Ref. [110].)

6.3. *Dipole interactions in silver nanocomposites: Numerical simulations and experimental data*

Now we calculate the optical cross section as a function of wavelength, λ, for silver CCA. The results of our simulations will be compared with experimental data for silver colloid aggregates. Optical properties of metallic particles and their aggregates were studied experimentally by a number of researchers, in particular, by Kreibig and co-workers [111].

First, we specify the dependence of α_0 on λ. An expression for the dipole polarizability of a dielectric sphere of radius R_m, which takes into account the radiative reaction correction, has the form [103]

$$\alpha_0 = R_m^3 \frac{\epsilon - \epsilon_h}{\epsilon + 2\epsilon_h - i(2/3)(kR_m)^3(\epsilon - \epsilon_h)}, \tag{6.20}$$

where $\epsilon = \epsilon' + i\epsilon''$ is the dielectric function of a monomer and ϵ_h is the dielectric constant of a host medium, which we assume to be water. The dielectric constant of water is real and nearly constant, $\epsilon_h \equiv \epsilon_w = 1.78$, in the spectral range under consideration (from 200 nm to 1000 nm).

The radiation correction introduced above results in the expression for α_0 satisfying the optical theorem and the energy conservation law. From Eqs. (6.10), (6.15) and (6.21) we obtain

$$\delta = R_m^{-3} \frac{3\epsilon_h \epsilon''}{|\epsilon - \epsilon_h|^2} + 2k^3/3, \quad y_a = R_m^{-3} \frac{3\epsilon_h \epsilon''}{|\epsilon - \epsilon_h|^2} > 0 \tag{6.21}$$

and

$$X = -R_m^{-3} \left[1 + \frac{3\epsilon_h(\epsilon' - \epsilon_h)}{|\epsilon - \epsilon_h|^2} \right]. \tag{6.22}$$

The dielectric function in a metal is well described by the Drude formula (cf. Eq. (2.1))

$$\epsilon = \epsilon_0 - \frac{\omega_p^2}{\omega(\omega + i\gamma)}, \tag{6.23}$$

where ϵ_0 includes the contribution to the dielectric constant associated with interband transitions in bulk material, ω_p is the plasma frequency and γ is the relaxation constant.

To simulate the silver colloid aggregates studied in our experiment, we used the CCA model described in Section 3. CCA have fractal dimension, structure, and aggregation pattern very similar to those observed in the experiment. This model contains two adjustable parameters, the lattice period, a, which defines the relative distances, r_{ij}, between particles, and the radius of a monomer, R_m. Clearly, solutions of the CDE are very sensitive to the ratio a/R_m, because this parameter determines the interaction strength. The model of geometrically touching spheres, which seems to be the most natural, implies that $a/R_m = 2$. However, as was shown in Ref. [112], this model fails to describe the long-wavelength resonances observed in a group of particles; it also fails to describe the long-wavelength tail observed in the absorption spectra of colloid aggregates (see, e.g., Refs. [100,111,104]).

The physical reason for the failure of this model is that the dipole approximation is not strictly applicable for touching spheres [112–116]. Indeed, the dipole field produced by one of the touching monomers is highly inhomogeneous ($\propto r^{-3}$) within the volume of the other one. This inhomogeneous field should result in high-order multipole moments, coupled both to each other and to the incident field. The high-order moments, when they are taken into account, effectively increase depolarization factors, and lead to the low-frequency resonances observed in experiments [112]. However, incorporating these high-order moments into the calculation results in an essentially intractable problem for the large fractal clusters considered here.

As suggested by Purcell and Pennypacker [117], and developed by Draine [103], a description of the optical response of an arbitrary shaped object can be obtained, remaining within the dipole approximation. (It is worth noting that the macroscopic Maxwell equations also contain only dipolar terms, i.e. polarization.) Below we generalize these ideas for fractal aggregates.

To account for multipolar effects in the CDE, real touching spheres may be replaced by effective spheres which geometrically intersect. Formally, this requires the ratio a/R_m to be taken less than 2. The physical reason underlying this procedure can be understood from the following arguments. Consider a pair of touching spheres and ascribe to the first sphere a dipole moment d located at its center. Since we would like to remain within the dipole approximation, the second sphere should also be replaced by a point dipole located at a certain distance from the first sphere. Clearly, because the field associated with the first sphere decreases non-linearly, $\sim d/r^3$, the second dipole should be placed somewhere closer than $2R_m$ from the center of the first sphere (otherwise, the interaction between the spheres would be underestimated). In other words, in order to correctly describe the

interaction between the spheres remaining within the dipolar approximation, the distance between the dipoles must be taken less than $2R_m$. This is equivalent to replacing the original touching spheres by overlapping spheres with the dipole moments located at their centers.

To gain insight concerning selection of the ratio a/R_m, we first consider cases for which a/R_m is known exactly. As shown in Refs. [103,117,118], the correct description of the optical response of a small object of arbitrary shape was obtained by considering dipolar interactions of a set of spherical monomers placed on a simple cubic lattice inside the volume of the object; the lattice period, a, was chosen such that $a^3 = (4\pi/3)R_m^3$. This relation, which provides equality of the total volume of the spheres and the original object under consideration, gives the ratio $a/R_m = (4\pi/3)^{1/3} \approx 1.612$. In Ref. [119] it was shown that, within the dipole approximation, correct depolarization coefficients for a linear array of spherical monomers are obtained provided a/R_m is chosen to be $(4\zeta_3)^{1/3} \approx 1.688$ ($\zeta_3 = \sum_k k^{-3}$), i.e. close to the above mentioned value. We used $a/R_m = (4\pi/3)^{1/3}$ in our calculations.

We also require that the radius of gyration and the total mass of clusters used in simulations must be the same as in the experiment. This condition, combined with $a/R_m = (4\pi/3)^{1/3}$, can be satisfied for fractals ($D \neq 3$) if one chooses $R_m = R_{exp}(\pi/6)^{D/[3(3-D)]}$, where R_{exp} is the radius of monomers used in experiments. In our experiments described below, the radius of silver particles forming colloidal aggregates was $R_{exp} \approx 7$ nm, so that $R_m \approx 5$ nm for $D = 1.78$.

For a light beam propagating in a system which contains randomly distributed clusters far away from each other (so that the clusters do not interact), the intensity dependence is given by the expression $I(z) = I(0)\exp(-\sigma_e \varsigma z)$, where ς is the cluster density; $\varsigma = p/[(4\pi/3)R_{exp}^3\langle N\rangle]$, where p is the volume fraction filled by spherical particles. Introducing the extinction efficiency,

$$Q_e = \frac{\langle\sigma_e\rangle}{\langle N\rangle\pi R_{exp}^2} = \frac{4kIm\,\alpha}{R_{exp}^2}, \tag{6.24}$$

the intensity dependence $I(z)$ acquires the form

$$I(z) = I(0)\exp[-\tfrac{3}{4}Q_e p(z/R_{exp})]. \tag{6.25}$$

As follows from (6.25) the extinction efficiency Q_e is the quantity that is measured in experiments on light transmission (rather than σ_e).

In Fig. 16a and 16b we plot the frequency variable X and relaxation parameter δ against wavelength (see Eqs. (6.21) and (6.22); $a^3/R_m^3 = 4\pi/3$ was used; for optical constants of silver, the data of Ref. [120] were used.) The λ-dependence of X and δ near 400 nm, and towards longer wavelengths, are associated with collective surface plasmon resonances. As seen in Fig. 16a, X changes significantly from 400 to 800 nm; hence, different dipole eigenmodes of a cluster can be excited by applied fields at different λ. In the wavelength region from 800 nm toward longer wavelength, X is almost constant ($X \approx X_0 = -a^3/R_m^3 = -4\pi/3$). This means that a change in λ in this region does not change the resonant dipole mode, which can be referred to as the "zero-frequency mode", or more simply as the "zero-mode". (Note, however, that whereas $X \approx const$ for $\lambda > 800$ nm, the relaxation constant δ significantly decreases from 800 nm towards the longer wavelengths, leading to a decreased decay parameter.) Since in the long-wavelength region the value of X (and, therefore, the mode excited) does not change with λ, the corresponding local field distribution in a cluster is also independent of the wavelength.

The enhanced far-infrared absorption (see Section 3.2), generally attributed to clustering, can be related to the excitation of the zero-mode of a cluster. Interactions between particles aggregated into

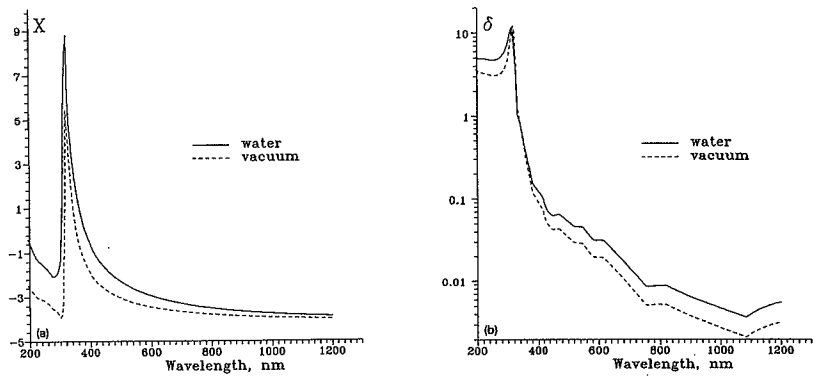

Fig. 16. The spectral variable X (a) and decay constant δ (b) versus wavelength for silver particles in vacuum and water.

a cluster lead to the formation of eigenmodes, including the zero-mode. The latter mode occurs in the long-wavelength part of the spectrum, where $X(\lambda) \approx X_0$ for all λ. When the cluster is excited by a low-frequency applied field, so that $X(\omega) \approx X_0$, absorption is primarily due to zero-mode excitation and is large because of its resonant character. For non-aggregated, well-separated particles, the absorption spectrum is centered in the narrow region near the center $X(\lambda_0) = 0$ (e.g., $\lambda_0 \approx 400$ nm for silver particles in water); therefore, there are no resonances in the long-wavelength part of the spectrum, where $X(\lambda) \approx X_0$, and, therefore, the absorption is small. Thus, the zero-mode formation, which accompanies particle clustering, results in the enhanced far-infrared absorption.

Provided the dependences $X = X(\lambda)$ and $\delta = \delta(\lambda)$ are specified, one can express the solutions of the CDE (expressed in terms of X and δ; see Eqs. (6.6)–(6.14)) as explicit functions of wavelength.

In Fig. 17, we plot the extinction efficiency, Q_e, as a function of λ calculated on the basis of the exact and quasi-static dipolar interaction [102]. The solution in the quasi-static limit was obtained by the Jacobi diagonalization method for 500-particle clusters. The solution of the CDE with the exact dipolar interaction (6.2)–(6.4) was obtained by the conjugate gradient method for 1000 particle clusters (for a control, Q_e was also calculated at two different wavelength for 10 000 particle clusters.) As seen in the figure, these solutions are in a good agreement. As was shown in Ref. [26], the quasi-static approximation is, under certain conditions, a good approximation for the description of dipolar excitations on fractals. This occurs because most eigenmodes are localized in areas smaller than the wavelength, λ, and, accordingly, the contributions to the local field of dipoles at distances that are comparable with or larger than λ are of no importance.

In Fig. 17, we also present the scattering efficiency $Q_s = \langle\sigma_s\rangle/[\langle N\rangle\pi R_{exp}^2]$, where the scattering cross section σ_s is given by $\sigma_s = \sigma_e - \sigma_a$. (Cross sections σ_e and σ_a are defined by (6.8) and (6.9), respectively.) As follows from the figure, the scattering is small so that in this case $\sigma_e \approx \sigma_a$. (Note that to obtain this and the next figure, the data of Ref. [121], rather than Ref. [120], were used for the optical constants of silver. These data are slightly different; however, this does not much affect the spectra presented in Figs. 17 and 18a.)

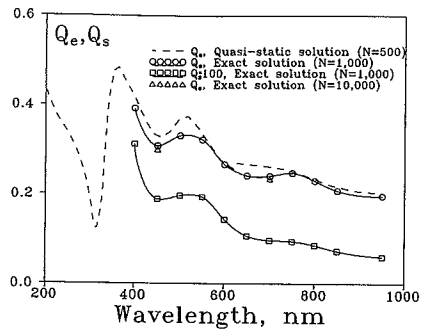

Fig. 17. Extinction efficiency Q_e and scattering efficiency Q_s versus wavelength. Q_e is calculated in the quasi-static approximation for 500-particle CCA and on the basis of the exact dipolar interaction for 1000-particle and 10000-particle CCA. Q_s is calculated for 1000-particle CCA with the exact dipole interaction.

In Ref. [102] experiments were performed to measure extinction in silver colloid aggregates. Fractal aggregates of silver colloid particles were produced from a silver sol generated by reducing silver nitrate with sodium borohydride [106]. The color of fresh (non-aggregated) colloidal solution is opaque yellow; the corresponding extinction spectrum (see Fig. 18a) peaks at 400 nm with the halfwidth about 40 nm. Addition of adsorbent (fumaric acid) promoted aggregation, and fractal colloid clusters formed. When adding the fumaric acid (0.1 cm^3 of 0.5 M aqueous solution) into the colloids (2.0 cm^3), the colloid's color changed through dark orange and violet to dark grey over 10 hours. Following aggregation, large wing in the long-wavelength part of the spectrum appeared in the extinction, as seen from Fig. 18a.

The process of aggregation can be described as follows. A large number of initially isolated silver nanoparticles execute random walks in the solution. Encounters with other nanoparticles result in their sticking together, first to form small groups, which then aggregate into larger formations, and so on. The CCA having fractal dimension $D \approx 1.78$ were eventually obtained. An electron micrograph of a typical silver colloid aggregate is shown in Fig. 18b.

Experimental extinction spectra are compared with numerical simulations in Fig. 18a. The calculations were performed for 500-particle CCA (solid line with a large wing) and for 10000 particle CCA (circles). For comparison, the measured and calculated spectra for non-aggregated monomers are also presented in the figure. Clearly, the aggregation results in a large tail in the red and infra-red part of the spectrum, which is well described by the simulations. The discrepancy in the central part of the spectrum probably occurs because, in the experiments, a number of particles remained non-aggregated and led to additional (not related to fractal aggregates) absorption near 400 nm.

To conclude this subsection, we consider two experimental observations that support the theoretical predictions of mode localization in fractals and frequency and polarization dependence of spatial locations of the light-induced dipole modes.

If the laser field creates hot spots in aggregates, then the corresponding parts of a cluster can be damaged (or modified) by a sufficiently powerful laser beam. As a result, the absorption corresponding to these parts will disappear, and there will be spectral holes left in the absorption for a

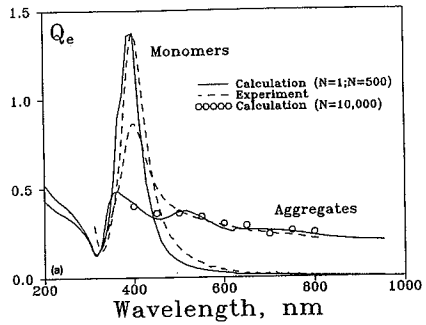

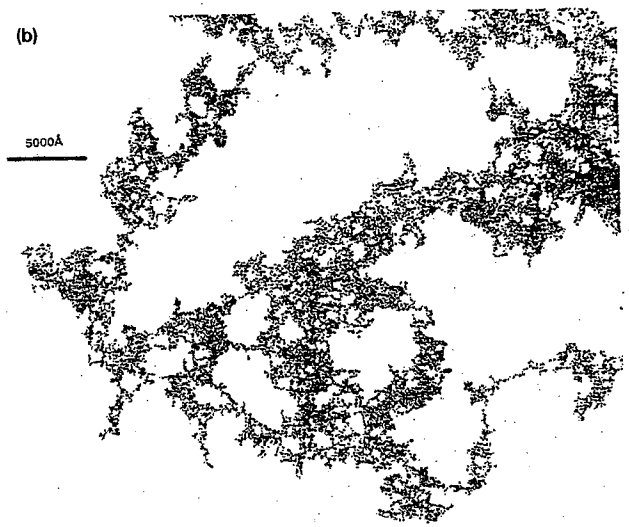

Fig. 18. (a) Experimental and calculated extinction spectra of silver colloid CCA. The theoretical spectra are presented for 500-particle and 10000-particle CCA. (b) Electron micrograph of a typical silver colloid aggregate.

given frequency and polarization. In Fig. 19 the transmission spectrum of silver colloid aggregates (fixed in gelatin) before and after irradiation by a series of strong laser pulses is shown [100,122]. Two independent dips were recorded at $\lambda = 540$ nm and $\lambda = 641$ nm. The dip width is close to the absorption line width and is only a small fraction of the cluster absorption band, i.e. the photomodification is selective over the wavelength. With increasing number of pulses or growing pulse power, the

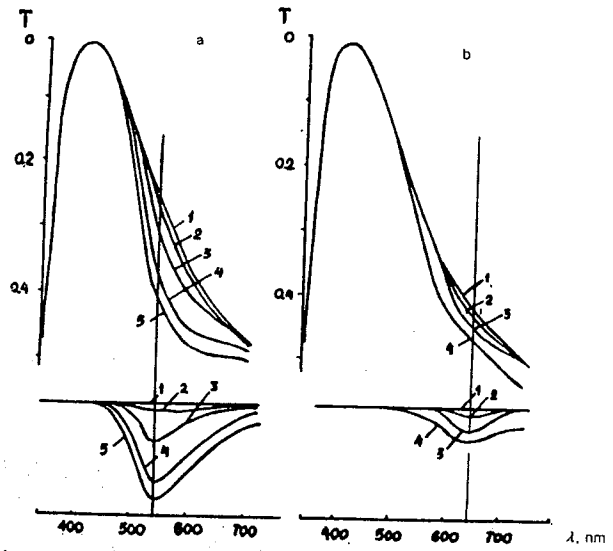

Fig. 19. Transmission spectrum (above) and spectral dependence of the difference in absorption (below) of non-irradiated (curves 1) and irradiated ($\tau = 30$ ps, $W = 2 \cdot 10^{-3}$ J/cm^2) samples (silver aggregates fixed in gelatin): (a) $\lambda = 540$ nm, curves 2,3,4, and 5 correspond to 1, 20, 80, and 230 pulses, respectively; (b) $\lambda = 641$ nm, curves 2 and 3 correspond to 20 and 120 pulses, and curve 4 to 120 pulses with $W = 8 \cdot 10^{-3}$ J/cm^2. Taken from Ref. [122].

dip becomes deeper and broader. Selective modification of the optical absorption spectrum in small-particle aggregates is observed only for identical polarizations of the light and the laser radiation. For orthogonal polarization of the probe beam no dip is observed in the absorption spectrum.

Recently, using a photon scanning tunneling microscope (PSTM), laser-excited localized optical modes on a silver colloid fractal aggregate have been observed [123]. The clusters were generated in a solution by diffusion-limited CCA, and then deposited onto the hypotenuse face of a total reflection prism. (As the simulations showed [123], large fractions of the dipolar modes are localized on deposited fractal aggregates as well as on the original 3d fractal clusters.) The evanescent field associated with the reflected beam induced dipole modes on a deposited fractal cluster and the corresponding local-field distribution was measured by a tapered optical fiber. The images of the "hot zones" demonstrated the localization of modes as well as the high frequency and polarization sensitivity of their spatial location. Since the PSTM operated in a pre-set constant optical intensity mode, it gave magnified images of the "hot spots". When approaching the excited mode, the PSTM tip pulled up and moved along a bell-like surface defined by the requirement of a constant detected intensity. This was a very large enhancement at the "hot spots" that caused the tip retraction to several hundreds of nm in the experiment [123] and resulted in magnification of the images. As

was estimated in Ref. [123], the magnification factor was approximately 5; the actual size of the high-local-field zones obtained in the experiment [123] was estimated to range between 50 nm and 200 nm, i.e. well beyond the wavelength limit.

7. Enhanced optical processes in small-particle composites

Non-linear electrical and optical properties of nanostructured composites have attracted much attention in recent years [21,23,30,33,99,100,124–133]. Composite materials may have much larger non-linear susceptibilities than those of ordinary bulk materials. The enhancement of the non-linear optical response in composites is due to strong fluctuations of the local fields, and these fluctuations are especially high in composites with fractal morphology [22,24,31,33,34]. Nanostructured composite materials are potentially of great practical importance as media with intensity-dependent dielectric functions and, in particular, as non-linear filters and optically bistable elements. A typical system under consideration is a composite in which a non-linear material is embedded in a host medium which can be linear or non-linear. The response of a non-linear composite can be tuned by controlling the volume fraction and morphology of constituents.

Stroud and Hui [124], and Flytzanis et al. [125] considered the electromagnetic response of non-linear particles randomly embedded in a linear host in the dilute limit (i.e. when the interaction among the particles is small. Perturbation expansions that allow one to determine small corrective terms for non-linear susceptibility were developed by Yu, Hui, Stroud and co-workers [126]. They also considered the case where inclusions and host material may possess non-linearities up to fifth order.

Sipe and Boyd studied non-linear susceptibilities of composites within the Maxwell-Garnet model [127]. Hui and Stroud generalized the differential effective-medium approximation, which they developed previously to model the effective linear response of a fractal cluster (see Section 3) to treat the effective non-linear response [128]. Their analysis showed that the clustering of particles can result in an appreciable enhancement of the non-linear response per particle (relative to the totally random case) only when the host is a better conductor than the non-linear inclusion. Yu came to a similar conclusion by applying a multifractal analysis of the voltage distribution to a deterministic fractal cluster embedded in the hierarchical lattice [129].

Strong enhancement of non-linear susceptibilities at zero frequency near a percolation threshold was pointed out by Zhang and Stroud [130]. Critical behavior of non-linear composites near the percolation threshold was also analyzed by Hui and by Yu and co-workers [131]. Using the effective-medium approximation (EMA) and numerical simulations on the basis of the transfer-matrix algorithm for random networks, Zhang and Stroud have also obtained a strong enhancement of the cubic non-linear susceptibility in a metal-insulator composite near surface-plasmon resonances [130]. Recently, Levy, Bergman, and Stroud showed that an induced cubic non-linearity can be generated in a composite, even though none of its components possess it intrinsically [132].

The aggregation of particles often results in clusters having a fractal morphology. Shalaev and co-workers [23,30,33,99,100,133] studied non-linear optical properties of fractal aggregates and showed that the aggregation of initially isolated particles into fractal clusters results in a huge enhancement of the non-linear response within the spectral range of the collective dipolar resonances (e.g., surface-plasmon resonances). The eigenmodes were obtained by diagonalizing the operator of the interaction between the light-induced dipoles on particles forming the cluster. Giant fluctuations of the local fields

responsible for enhancements in fractals were studied by Stockman and co-workers [31]. Many of the dipolar eigenmodes are strongly localized in different regions of a cluster with random local structure [24,29,123] (note that there are delocalized modes as well); this leads ultimately to strong fluctuations of local fields in fractals. A strongly varying, patchwork-like field distribution occurs because of the "hot zones" associated with the localized modes.

The prediction of a huge enhancement of optical non-linearities in fractal clusters [23] was then confirmed experimentally [99,100] for the example of degenerate four-wave mixing (DFWM). Aggregation of initially isolated silver particles into fractal clusters in this experiment led to a 10^6-fold enhancement of the efficiency of the non-linear four-wave process.

Numerical simulations of the non-linear optical response in diluted fractal clusters were reported in Ref. [30]. In the central part of the diluted cluster spectrum, the non-linear optical response scales as a function of the generalized frequency variable [30], whereas, in the wing, the response can be well described by the binary approximation [23].

Below, following Ref. [133], we consider a number of enhanced optical processes in composite materials consisting of original non-diluted aggregates of particles. The processes under consideration include four-wave mixing (FWM), third harmonic generation (THG), Raman and Rayleigh scattering, and non-linear refraction and absorption in Kerr media.

7.1. Local field enhancement

The enhancement of optical processes in small-particle composites occurs because local fields exhibit strong fluctuations that significantly exceed the applied field. The local fields can be found from linear optical response theory. We consider the response to electromagnetic waves at optical frequencies by a system of N polarizable particles (monomers), with dipole-dipole coupling between the particles. The monomers are positioned at the points $\boldsymbol{r}_i$ ($i = 1, \ldots, N$) and assumed to be much smaller than the wavelength, λ, of the incident wave.

For the sake of simplicity we also assume that λ is much greater than the cluster gyration radius R_c. For fractal clusters, however, the main results presented below are qualitatively valid even if $R_c \gg \lambda$. This is because most of the optical excitations in fractals are localized in sub-wavelength areas [24,29,123] and the interaction of monomers at distances greater than λ can be neglected [26].

The local field E_i acting on the ith monomer is expressed as (cf. Eq. (6.13))

$$E_{i\alpha} = \alpha_0^{-1} d_{i\alpha} = \alpha_0^{-1} \alpha_{i,\alpha\beta} E_\beta^{(0)}, \tag{7.1}$$

where $\alpha_{i,\alpha\beta}$ is the polarizability associated with the ith monomer in a cluster (cf. Eq. (5.29) and (6.14))

$$\alpha_{i,\alpha\beta} = \sum_{nj} \frac{(i\alpha|n)\,(n|j\beta)}{(w_n - X) - i\delta}\,. \tag{7.2}$$

We now discuss the enhancement of local fields in small-particle composites. The parameter characterizing the enhancement of local field intensity can be defined as

$$G = \langle |E_i|^2 \rangle / |E^{(0)}|^2. \tag{7.3}$$

As was shown in Ref. [24], the enhancement G is related to $Im\,\alpha(X)$ as follows (cf. Eq. (6.17)):

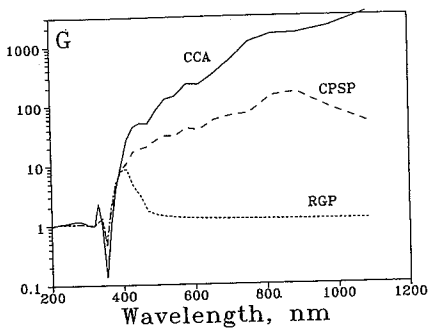

Fig. 20. Enhancement factors, G, of local field intensities plotted against λ for 500-particle aggregates: CCA (solid line), a random gas of particles (RGP) with the same as for CCA volume fraction of metal (short-dashed line), and a close-packed sphere of particles, CPSP (long-dashed line).

$$G = \delta[1 + X^2/\delta^2]\,Im\,\alpha. \tag{7.4}$$

According to Eq. (7.4), the enhancement factor $G \approx (X^2/\delta)\,Im\,\alpha$ for $|X| \gg \delta$, i.e. it can be very large. (Far in the Lorentz wing, for $|X| \gg 1$, the absorption is $Im\,\alpha \approx \delta/X^2$ and $G \approx 1$.)

Note that, since in fractals the fluctuations are very large so that $\langle |E|^2 \rangle \gg \langle |E| \rangle^2$ [33,24], we have $\langle |\Delta E|^2 \rangle \approx \langle |E|^2 \rangle$; therefore, in this case, G characterizes both the enhancement of local fields and their fluctuations as well. In other words, the larger fluctuations, the stronger enhancement.

Below we consider the results of numerical simulations of G for cluster-cluster aggregates (CCA) having fractal dimension $D \approx 1.78$, and for two non-fractal ensembles of particles: a random gas of particles (RGP) and a close-packed sphere of particles (CPSP). (For details of the numerical calculations, see Section 6.1.) As above we use units where the lattice period $a = 1$.

In Fig. 20 the results of simulations for the enhancement factor G in silver CCA in vacuum are compared with those for non-fractal composites, RGP and CPSP [133]. (The material optical constants for silver were taken here from Ref. [120].) As seen in Fig. 20, the enhancement of local-field intensities in fractal CCA is significantly larger than in non-fractal RGP and CPSP clusters, as was anticipated. The enhancement can reach very high values, $\sim 10^3$, and increases with λ. This occurs because both the localization of fractal eigenmodes and their mode quality factor ($q \sim 1/\delta \sim |\epsilon - \epsilon_h|^2/3\epsilon''\epsilon_h$) increase for the modes located in the long-wavelength part of the spectrum.

We next consider a more detailed comparison between fractal small-particle composites and non-fractal inhomogeneous media. The simulations were performed for RGP and CCA having the same volume fraction p filled by metal. The volume fraction p of particles in a fractal cluster is very small. (In fact, $p \to 0$ at $R_c \to \infty$; but p is, of course, finite for a finite number of particles.) According to the Maxwell-Garnett theory (see Section 3.1), there is only one resonant frequency in conventional ($d = D$) media with $p \ll 1$; the resonance is just slightly shifted from the resonance of an isolated particle at $X(\omega) = 0$. In contrast, in fractal media, despite the fact that p is asymptotically zero, there is a high probability of finding a number of particles close to any chosen one. (This is because the pair correlation function, $g(r) \propto r^{D-d}$, increases with decreasing distance r between particles.)

Thus, in fractals there is always a strong interaction of a particle with others distributed in its random neighborhood. As a result, there exist localized eigenmodes with distinct spatial orientations in different parts of a cluster, where the location depends on the frequency and polarization characteristics of the mode. As mentioned above, some of these modes are significantly shifted to the red part of the spectrum where their quality factors q are much larger than that at $X(\omega) = 0$, for a non-interacting particle. Thus, the dipole-dipole interactions of constituent particles in a fractal cluster "generate" a wide spectral range of resonant modes with enhanced quality factors and with spatial locations which are very sensitive to the frequency and polarization of the applied field. The localization of modes in various random parts of a cluster also brings about giant spatial fluctuations of the local fields, when one moves from "hot" to "cold" zones corresponding to high and low field-intensity areas, respectively.

In the case of a CPSP, the volume fraction, p, is not small. However, since the dipole-dipole interaction for a three-dimensional CPSP is long range, one expects that eigenmodes are delocalized over the whole sample so that all particles are involved in the excitation. Accordingly, fluctuations (and enhancements) of local fields are much smaller than in a fractal aggregate where the modes are localized.

As seen in Fig. 20, enhancements and fluctuations of local fields in non-fractal CPSP and RGP are significantly less than those in the case of fractal CCA, in accordance with the above arguments.

The enhanced local fields result in enhancements of the optical processes considered below. Based on the simulations presented above, one anticipates that in fractal composites, where the fluctuations are strong, the enhancements can be very large. Below, we analyze various enhanced optical phenomena in a composite material consisting of fractal CCA.

7.2. *Four-wave mixing*

Four-wave mixing (FWM) is determined by the non-linear polarizability [134,135]

$$\beta^{(3)}_{\alpha\beta\gamma\delta}(-\omega_s;\omega_1,\omega_1,-\omega_2), \tag{7.5}$$

where $\omega_s = 2\omega_1 - \omega_2$ is the generated frequency, and ω_1 and ω_2 are the frequencies of the applied waves. Coherent anti-Stokes Raman scattering (CARS) is an example of FWM. In one elementary CARS process, two ω_1 photons are transformed into ω_2 and ω_s photons. Another example is degenerate FWM (DFWM); this process is used for optical phase conjugation (OPC) which results in complete removal of optical aberrations [134]. In DFWM, all waves have the same frequency ($\omega_s = \omega_1 = \omega_2$) differing only in their propagation directions (although, generally, the polarizations are also different). In a typical OPC experiment, two oppositely directed pump beams, with field amplitudes $\boldsymbol{E}^{(1)}$ and $\boldsymbol{E}'^{(1)}$, and a probe beam, with amplitude $\boldsymbol{E}^{(2)}$ and propagating at a small angle to the pump beams, result in a OPC beam propagating against the probe beam. Because of the interaction geometry, the wave vectors satisfy the relation: $\boldsymbol{k}_1 + \boldsymbol{k}'_1 = \boldsymbol{k}_2 + \boldsymbol{k}_s = 0$. Clearly, for the two pairs of oppositely directed beams that have the same frequency ω, the phase-matching conditions are automatically fulfilled [134].

Below we consider the DFWM process where the total applied field is $\boldsymbol{E}^{(0)} = \boldsymbol{E}^{(1)} + \boldsymbol{E}'^{(1)} + \boldsymbol{E}^{(2)}$. The polarizability $\beta^{(3)}$, that results in DFWM, leads also to non-linear refraction and absorption (to be considered below) and is associated, in general, with the Kerr optical non-linearity. For coherent effects, including the ones discussed in this section, averaging is performed over a generated

field amplitude, i.e. non-linear polarization. Note also that the non-linear polarizability, $\beta^{(3)}$, can be associated either with monomers forming a cluster or with molecules adsorbed on the monomers.

We consider the enhancement of DFWM that accompanies the aggregation of particles into clusters. Let particles first be randomly embedded in a linear host medium so that there is no clustering. We assume that the volume fraction p that the particles occupy is small so that we can neglect their interaction. Then let particles aggregate in many random clusters that are relatively far from each other (i.e. the intercluster interaction is still negligible). Thus, after the aggregation one obtains a trivial mixture of many clusters (each cluster may consist of thousands of particles). The average volume fraction p filled by particles obviously remains the same. However, the particles within one cluster now strongly interact via light-induced dipolar fields. The described scenario of aggregation occurs, for example, in a silver colloid solution. In that case one first produces a silver sol (non-aggregated particles in solution), for example, by reducing silver nitrate with sodium borohydride [106]. Addition of an adsorbent (like phthalizine) promotes aggregation, forming fractal colloid clusters with fractal dimension $D \approx 1.78$ (see also Section 6.3).

The orientation-averaged non-linear polarizability in an isotropic medium can be expressed, in general, through two independent scalar functions f_s and f_a as [134]

$$\langle\beta^{(3)}_{\alpha\beta\gamma\delta}\rangle_0 = f_s\Delta^+_{\alpha\beta\gamma\delta} + f_a\Delta^-_{\alpha\beta\gamma\delta}, \tag{7.6}$$

$$\Delta^+_{\alpha\beta\gamma\delta} = \tfrac{1}{3}\{\delta_{\alpha\beta}\delta_{\gamma\delta} + \delta_{\alpha\gamma}\delta_{\beta\delta} + \delta_{\alpha\delta}\delta_{\beta\gamma}\}, \tag{7.7}$$

$$\Delta^-_{\alpha\beta\gamma\delta} = \tfrac{1}{3}\{\delta_{\alpha\beta}\delta_{\gamma\delta} + \delta_{\alpha\gamma}\delta_{\beta\delta} - 2\delta_{\alpha\delta}\delta_{\beta\gamma}\}, \tag{7.8}$$

where the sign $\langle\ldots\rangle_0$ denotes an average over orientations. The terms $f_s\Delta^+$ and $f_a\Delta^-$ are totally and partially symmetric parts of $\beta^{(3)}_{\alpha\beta\gamma\delta}$ (over $\alpha\beta$ and $\gamma\delta$), respectively.

When a cluster consists of monomers, the field acting upon them is the local field $\boldsymbol{E}_i$ rather than the applied field $\boldsymbol{E}^{(0)}$. Also, the dipolar interaction of non-linear dipoles should be included. Taking these arguments into account, we can write the following system of equations for the light-induced non-linear dipoles:

$$d^{NL}_{i,\alpha} = 3\beta^{(3)}_{\alpha\beta\gamma\delta}E_{i,\beta}E_{i,\gamma}E^*_{i,\delta} + \alpha(\omega_s)\sum_j W^{ij}_{\alpha\beta}d^{NL}_{j,\beta}, \tag{7.9}$$

where the pre-factor 3 represents the degeneracy factor that gives the number of distinct permutations of the frequencies ω, ω, and $-\omega$ [134].

The non-linear polarization $P^{(3c)}$ of an isotropic (on average) composite material consisting of particles aggregated into clusters has the form [135]

$$\boldsymbol{P}^{(3c)}(\omega) = A\boldsymbol{E}^{(0)}(\boldsymbol{E}^{(0)}\cdot\boldsymbol{E}^{(0)*}) + \tfrac{1}{2}B\boldsymbol{E}^{(0)*}(\boldsymbol{E}^{(0)}\cdot\boldsymbol{E}^{(0)}) \tag{7.10}$$

where A and B, are given by

$$A = \tfrac{2}{3}(F_s + F_a)pv_0^{-1}, \quad B = \tfrac{2}{3}(F_s - 2F_a)pv_0^{-1}, \tag{7.11}$$

v_0 is the volume of a particle, and F_s and F_a are totally and partially symmetric parts of the cluster polarizability $\beta^{(3c)}_{\alpha\beta\gamma\delta}$ having the form similar to (7.6)–(7.8), so that

$$\langle\beta^{(3c)}_{\alpha\beta\gamma\delta}\rangle = F_s\Delta^+_{\alpha\beta\gamma\delta} + F_a\Delta^-_{\alpha\beta\gamma\delta}.$$

The factors F_s and F_a can be expressed in terms of the products of the linear polarizabilities as follows [133]

$$\langle\beta^{(3c)}_{\alpha\beta\gamma\delta}\rangle = F_s\Delta^{+}_{\alpha\beta\gamma\delta} + F_a\Delta^{-}_{\alpha\beta\gamma\delta}, \tag{7.12}$$

where

$$F_s = \tfrac{1}{15}Z^3Z^*f_s\langle Tr(\hat{\alpha}_i^T\hat{\alpha}_i)Tr(\hat{\alpha}_i^T\hat{\alpha}_i^*) + 2Tr(\hat{\alpha}_i^T\hat{\alpha}_i\hat{\alpha}_i^T\hat{\alpha}_i^*)\rangle,$$
$$F_a = \tfrac{1}{6}Z^3Z^*f_a\langle Tr(\hat{\alpha}_i^T\hat{\alpha}_i)Tr(\hat{\alpha}_i^T\hat{\alpha}_i^*) - Tr(\hat{\alpha}_i^T\hat{\alpha}_i\hat{\alpha}_i^T\hat{\alpha}_i^*)\rangle, \tag{7.13}$$

where $(\hat{\alpha}_j^T\hat{\alpha}_j)_{\alpha\beta} \equiv \alpha_{j,\alpha'\alpha}\alpha_{j,\alpha'\beta}$, $(\hat{\alpha}_j^T\hat{\alpha}_j^*)_{\gamma\delta} \equiv \alpha_{j,\beta'\gamma}\alpha^*_{j,\beta'\delta}$, and $(\hat{\alpha}_j^T\hat{\alpha}_j\hat{\alpha}_j^T\hat{\alpha}_j^*)_{\alpha\beta} \equiv \alpha_{j,\alpha'\alpha}\alpha_{j,\alpha'\beta'}\alpha_{j,\gamma\beta'}\alpha^*_{j,\gamma\beta}$ (the T-symbol in $\hat{\alpha}^T$ denotes a transposition of the matrix $\hat{\alpha}$). According to (7.12) and (7.13), the symmetry of the non-linear polarizability of an isolated monomer (see Eqs. (7.6)–(7.8)), is reproduced in the polarizability of a cluster. The totally symmetric part of a monomer's non-linear polarizability "generates" a totally symmetric part of the cluster polarizability ($F_s \propto f_s$); the same is true for the partially symmetrical parts ($F_a \propto f_a$).

The non-linear susceptibility $\bar{\chi}^{(3c)}_{\alpha\beta\gamma\delta}$ of a composite material is defined via the relation

$$P^{(3c)}_{\alpha}(\omega) = 3\bar{\chi}^{(3c)}_{\alpha\beta\gamma\delta}(-\omega;\omega,\omega,-\omega)E^{(0)}_{\beta}E^{(0)}_{\gamma}E^{(0)*}_{\delta},$$

where $\bar{\chi}^{(3c)}_{\alpha\beta\gamma\delta}$ can be expressed in terms of the non-linear polarizability averaged over an ensemble of clusters $\langle\beta^{(3c)}_{\alpha\beta\gamma\delta}\rangle$ as follows:

$$\bar{\chi}^{(3c)}_{\alpha\beta\gamma\delta}(-\omega;\omega,\omega,-\omega) = pv_0^{-1}\langle\beta^{(3c)}_{\alpha\beta\gamma\delta}(-\omega;\omega,\omega,-\omega)\rangle. \tag{7.14}$$

In particular, if $\beta^{(3)}$ is due to the non-resonant electronic response (the low-frequency limit), then $f_a = 0$ [134,135]. Accordingly, we obtain in this case

$$\frac{A}{a} = \frac{B}{b} = \frac{F_s}{f_s}. \tag{7.15}$$

Thus, the efficiency of four-wave mixing (which is proportional to the generated amplitude squared) is enhanced due to the clustering of particles in a composite material by the factor

$$G_{FWM} = |F_s/f_s|^2 \simeq \frac{(X^2+\delta^2)^4}{225} \times |\langle Tr(\hat{\alpha}_i^T\hat{\alpha}_i)Tr(\hat{\alpha}_i^T\hat{\alpha}_i^*) + 2Tr(\hat{\alpha}_i^T\hat{\alpha}_i\hat{\alpha}_i^T\hat{\alpha}_i^*)\rangle|^2. \tag{7.16}$$

Thus, according to Eq. (7.16), the enhancement due to the particle clustering can be expressed via the product of linear polarizabilities α_i (averaged over an ensemble of clusters); these polarizabilities, in turn, represent the ratio of the corresponding local fields and the applied field (cf. Eq. (7.1)).

It was conjectured in Ref. [133] that the enhancement factor (7.16) can be approximated by the formula

$$G_{FWM} \approx C_{FWM}\frac{(X^2+\delta^2)^4}{\delta^6}[Im\,\alpha(X)]^2, \tag{7.17}$$

where the pre-factor C_{FWM} should be considered as an adjustable parameter. The X- and δ-dependence predicted by Eq. (7.17) can be obtained analytically by assuming that the resonant modes give a

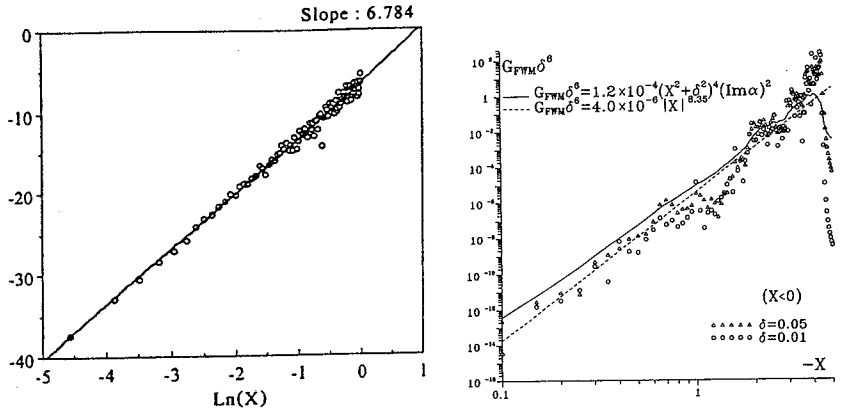

Fig. 21. The enhancement of degenerate or nearly-degenerate four-wave mixing in CCA, G_{FWM}, for diluted CCA ($X < 0$). The simulations were performed with $\delta = 0.005$. Units in which $R_0 = 1$ were used. Taken from Ref. [30].

Fig. 22. The enhancement of degenerate four-wave mixing, G_{FWM}, for original, non-diluted, CCA. Units in which $a = 1$ were used.

dominant contribution to the enhancement. For diluted clusters, when the scaling is well pronounced (see Section 5) the dependence (7.17) can be also obtained from the scaling arguments [30].

The results of the numerical simulations of G_{FWM} for diluted (Fig. 21) and non-diluted (Fig. 22) cluster-cluster aggregates (DCCA and CCA, respectively) are shown above. In both cases the results are shown for $X < 0$ that correspond to the red shift with respect to the resonance of an isolated monomer $X = 0$ (the results for $X > 0$ are similar). The simulations were performed based on the general formulas (7.2) and (7.16). The solid line in Fig. 22 describes the results of calculations with the use of formula (7.17), where C_{FWM} was found from the requirement that $G_{FWM}\delta^6 = 1$ at its maxima, $X \approx \pm 4$. The dashed line in Fig. 22 represents a power-law fit for the results of numerical simulations for $0.1 \leqslant |X| \leqslant 3$ and $\delta = 0.05$. (Note that different units were used for DCCA and CCA, $R_0 = 1$ and $a = 1$, respectively.)

In both cases the X-dependence is well reproduced by $X^8[Im\,\alpha(X)]^2$. Recall that for DCCA, $Im\,\alpha \propto |X|^{d_o-1}$ with $d_o = 0.3 \pm 0.1$ (see Section 5) so that $G_{FWM} \propto |X|^{6+2d_o}$ [30]. For non-diluted CCA, the dependence associated with $Im\,\alpha$ (see Fig. 10) is weak in comparison with the factor X^8.

As follows from Figs. 21 and 22, the enhancement increases strongly towards larger values of $|X|$. This occurs because the local fields become stronger for larger values of $|X|$. (As seen in Fig. 20, the local field intensities increase towards the long-wavelength part of the spectrum, which corresponds to larger $|X|$ for $X < 0$.)

We also conclude from Figs. 21 and 22 that the enhancement, in accordance with Eq. (7.17), is proportional to the sixth power of the resonance quality factor: $G_{FWM} \propto q^6$ ($q \sim \delta^{-1}$) and reaches huge values in the maxima occurring at $X \approx \pm 4$.

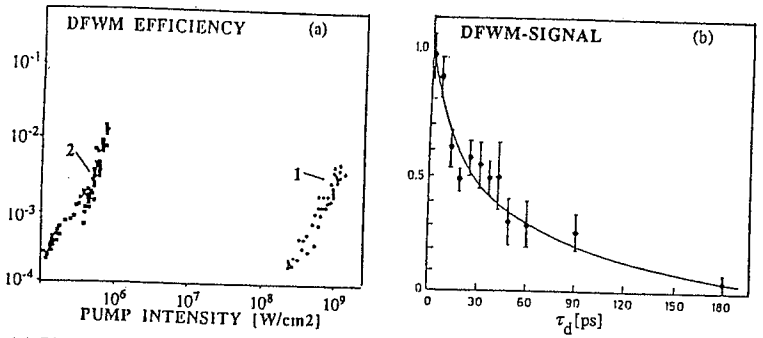

Fig. 23. (a) DFWM efficiency vs pump intensity for silver particles which are isolated (1) and aggregated into fractal clusters (2) ($\lambda = 532$ nm); (b) DFWM signal vs the time delay of one of the pumps ($\lambda = 540$ nm; pulse duration $\tau \approx 30$ ps). Taken from Ref. [100].

A million-fold enhancement of DFWM due to the clustering of initially isolated silver particles in colloidal solution was experimentally obtained [99,100]. In Fig. 23a we plot the experimental data for conversion efficiency $\eta = I_s/I_1 \propto I_0^2$ (I_s, I_1 and I_0 are the intensities of the DFWM signal, probe beam, and pump beam, respectively). As seen in the figure, similar values of η can be obtained in silver particles aggregated into fractal clusters at pump intensities $\sim 10^3$ times less than in the case of non-aggregated, isolated, particles. Since $\eta \propto I_0^2$, we conclude that the enhancement factor for silver fractal composites is $G \sim 10^6$. As follows from Fig. 16, the value of X and δ at the laser wavelength, $\lambda = 532$ nm, are $X \approx -2.55$ and $\delta \approx 0.05$, respectively. According to Fig. 22, $G_{FWM} \sim 10^6$ for these values of X and δ, in agreement with the experimental observations.

The value obtained in Ref. [100] for the non-linear susceptibility in silver fractal composites is $\bar{\chi}^{(3c)} \sim p \times 10^{-5}$ e.s.u. at $\lambda = 532$ nm. Even for a very small metal fraction used in the experiment of Ref. [100], $p \sim 10^{-5}$, this gives $\bar{\chi}^{(3c)} \sim 10^{-10}$ e.s.u. (cf. a typical value of $\chi^{(3)}$ in crystals is $\sim 10^{-15}$ e.s.u.). Moreover, p is a variable quantity and can be increased. We can assigned the value 10^{-5} e.s.u. to the non-linear susceptibility, $\chi^{(3c)}$, of silver fractal clusters; the quantity $\chi^{(3c)}$ is related to the non-linear susceptibility, $\bar{\chi}^{(3c)}$, of the composite (silver aggregates in water) via the relation $\bar{\chi}^{(3c)} = p \times \chi^{(3c)}$.

Rapid non-linear response of silver CCA was tested in the OPC scheme when one of the input pulses was delayed by moving the mirror that reflected the input beam back to the sample. As follows from Fig. 23b, the DFWM signal is twice decreased with the time delay τ_d increasing up to 30 ps, which coincides with the pulse duration (pulse duration of the used laser, 30 ps, did not allow one to measure shorter non-linear responses). Hence, the relaxation time of the non-linear response does not exceed 30 ps. The huge non-linearity, $\chi^{(3c)} \sim 10^{-5}$ e.s.u., with a time of the non-linear response $\leqslant 30$ ps [100], makes metal fractal aggregates very interesting for potential applications.

In the long-wavelength range of the spectrum, $\lambda > 1000$ nm, the quantity X is almost constant: $X(\lambda) \approx X_0$, where $a^3 X_0 = -4\pi/3$ (i.e. $X_0 = -4\pi/3$ in $a = 1$ units). The excitation in this spectral region, when $X(\lambda) \approx X_0$ for all λ, can be described in terms of the single mode, called "zero-mode" (see Section 6.3). In this case, all the spectral dependence for G_{FWM} is due to a λ-dependence of the factor δ^{-6} in (7.17). Since $G_{FWM} \sim |\bar{\chi}^{(3c)} v_0/\beta^{(3)}|^2$, we conclude that $\bar{\chi}^{(3c)} \propto \delta^{-3}$ in the long-wavelength part of the spectrum. For the Drude model, $\delta \propto \lambda$ in the infrared part of the spectrum; thus, $\bar{\chi}^{(3c)}$ strongly increases towards the longer wavelengths, $\propto \lambda^3$.

7.3. Enhanced harmonic generation

We consider now harmonic generation, beginning with third harmonic generation (THG). We assume that the phase-matching condition is fulfilled. The THG process is due to a third-order non-linearity. The corresponding non-linear dipole moment is

$$d_{i,\alpha}^{NL} = \beta_{\alpha\beta\gamma\delta}^{(3)} E_{i,\beta} E_{i,\gamma} E_{i,\delta}. \tag{7.18}$$

For isotropic media, the orientation-averaged non-linear polarizability may be expressed in terms of one independent constant [135]

$$\langle \beta_{\alpha\beta\gamma\delta}^{(3)}(-3\omega;\omega,\omega,\omega)\rangle_0 = f \Delta_{\alpha\beta\gamma\delta}^{+}. \tag{7.19}$$

We first assume that the generated signal $\omega_s = 3\omega$ lies outside the cluster band of resonant modes and, therefore, we neglect the interaction of non-linear dipoles oscillating at the frequency ω_s (cf. Eqs. (7.9) and (7.19)).

The polarizability of a small-particle aggregate has the form [133]

$$\langle \beta_{\alpha\beta\gamma\delta}^{(3c)} \rangle = F \Delta_{\alpha\beta\gamma\delta}^{+}, \tag{7.20}$$

where

$$F = \tfrac{1}{15} Z^3 f_s \langle Tr(\hat{\alpha}_i) Tr(\hat{\alpha}_i^T \hat{\alpha}_i) + 2Tr(\hat{\alpha}_i \hat{\alpha}_i^T \hat{\alpha}_i)\rangle. \tag{7.21}$$

Note that the cluster polarizability, $\langle \beta_{\alpha\beta\gamma\delta}^{(3c)} \rangle$, is totally symmetric as well as the polarizability of an isolated monomer, $\langle \beta_{\alpha\beta\gamma\delta}^{(3)} \rangle_0$; either is characterized by a single amplitude.

Enhancement of the third-harmonic generation process is given by $G_{THG} = |\langle F/f \rangle|^2$. Using (7.21) this results in

$$G_{THG} = \frac{(X^2+\delta^2)^3}{225} |\langle Tr(\hat{\alpha}_i) Tr(\hat{\alpha}_i^T \hat{\alpha}_i) + 2Tr(\hat{\alpha}_i \hat{\alpha}_i^T \hat{\alpha}_i)\rangle|^2. \tag{7.22}$$

For the excitation outside the cluster band of resonant modes, $\alpha_i \approx \alpha_0$ and $G_{THG} = 1$.

In Fig. 24 a log–log plot of G_{THG} as a function of negative X is presented for three very different values of δ (the results for $X > 0$ are similar). Despite the strong fluctuations, we conclude from Fig. 24 that, on average, the product $G_{THG}\delta^4$ does not depend on δ. Thus, in contrast to the binary theory [23], which predicts a small enhancement for the highest-order harmonic generation, the present results demonstrate a possibility of a very strong enhancement: $G_{THG} \propto \delta^{-4}$.

Based on the simulations, the following expression for the enhancement factor within a band of the eigenmodes was suggested in Ref. [133]:

$$G_{THG} \approx C_{THG} \frac{(X^2+\delta^2)^3}{\delta^4} [Im\, \alpha(X)]^2, \tag{7.23}$$

where the pre-factor C_{THG} is an adjustable parameter. Formula (7.23) reflects, in particular, the indicated dependence $G_{THG} \propto \delta^{-4}$. As follows from Eq. (7.23), the resultant enhancement can be

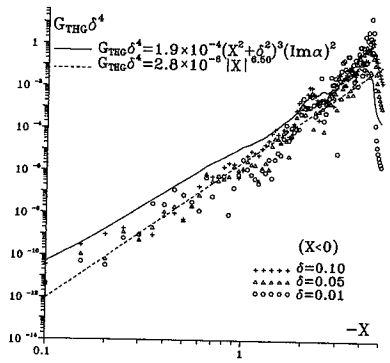

Fig. 24. The enhancement of the third-harmonic generation in CCA, G_{THG}, for negative X.

expressed via the frequency parameter X raised to some power and the linear absorption $Im\,\alpha(X)$ (cf. Eq. (7.17)). In addition, it contains a high power of the quality factor (q^5 for the DFWM and q^4 for the THG).

The solid line in Fig. 24 represents the results calculated from Eq. (7.23) with C_{THG} found from the relation $G_{THG}\delta^4 = 0.1$ at its maximum (at $X \approx -4$). The dashed line in Fig. 24 is a power-law fit for $0.1 \leqslant |X| \leqslant 3$ and $\delta = 0.05$.

In general, enhancement of nth harmonic generation may be estimated by

$$G_{nHG} \sim \left|\left\langle \frac{E_i^n}{[E^{(0)}]^n}\right\rangle\right|^2 \sim |\alpha_0|^{-2n}|\langle\alpha_i^n\rangle|^2. \tag{7.24}$$

The estimate (7.24) is based on the assumption that the interaction of non-linear dipoles oscillating at the frequency $\omega_s = n\omega$ can be ignored. If this interaction is of importance, the estimate (7.24) should be replaced by

$$G_{nHG} \sim |\alpha_0(\omega)|^{-2n}|\alpha_0(\omega_s)|^{-2}|\langle\alpha_i^n(\omega)\alpha_i(\omega_s)\rangle|^2. \tag{7.25}$$

Experimental observation of second harmonic generation that was enhanced (by three orders of magnitude) because of the clustering of silver colloidal particles was reported in Ref. [136].

7.4. Enhanced Raman scattering

In this section we consider the enhancement of Raman scattering, G_{RS}, in particles aggregated into clusters. In Ref. [28] the simulations of the enhancement of Raman scattering were performed for diluted cluster-cluster aggregates. Below we consider G_{RS} for original (non-diluted) CCA and compare the results with the experimental observations [133].

We assume that each monomer of a cluster, apart from the linear polarizability α_0, possesses also a Raman polarizability ζ. This means that the exciting field $\boldsymbol{E}^{(0)}$, applied to an isolated monomer, induces a dipole moment $\boldsymbol{d}^s$ oscillating with the Stokes-shifted frequency ω_s. To avoid unessential

complications, we suppose ζ to be a scalar; this gives $\boldsymbol{d}^s = \zeta\boldsymbol{E}$. The Raman polarizability may either be due to the polarizability of a monomer itself or to an impurity bound to the monomer.

We consider spontaneous Raman scattering, which is an incoherent optical process. This means that the Raman polarizabilities ζ_i corresponding to different monomers possess uncorrelated random phases:

$$\langle\zeta_i^*\zeta_j\rangle = |\zeta|^2\delta_{ij}. \tag{7.26}$$

This feature constitutes the principal distinction between ζ and the linear polarizability α. It ensures that there exists no interference of the Stokes waves generated by different monomers.

As was pointed out above, when the monomers are the constituents of a cluster, the field acting upon an ith monomer is the local field $\boldsymbol{E}_i$ rather than the external field $\boldsymbol{E}^{(0)}$. Also, the dipole interaction of the monomers at the Stokes-shifted frequency ω_s should be included. Taking these arguments into account, we can write the following system of equations:

$$d_{i\alpha}^s = \zeta_i E_{i\alpha} + \alpha_0^s \sum_{j\beta}(i\alpha|W|j\beta)d_{j\beta}^s, \tag{7.27}$$

where α_0^s is the linear polarizability of an isolated monomer at the Stokes-shifted frequency ω_s.

The total Stokes dipole moment $\boldsymbol{D}^s$, found by solving Eq. (7.27), is [28]

$$D_\alpha^s = \sum_i d_{i\alpha}^s = Z_s Z \sum_j \zeta_j \alpha_{j,\beta\alpha}^s \alpha_{j,\beta\beta'} E_{\beta'}^{(0)}, \tag{7.28}$$

where $Z_s = (\alpha_0^s)^{-1}$, $\alpha_i^s \equiv \alpha_i(X_s)$, and α_i are defined in (7.2).

The RS enhancement associated with particle clustering is defined as [28]

$$G_{RS} = \frac{\langle|\boldsymbol{D}_s|^2\rangle}{N|\zeta|^2|\boldsymbol{E}^{(0)}|^2}. \tag{7.29}$$

The above formulas (7.27)–(7.29) are exact and valid for any cluster. If the Stokes shift is so large that the Raman-scattered light is well out of the absorption band of the cluster, the polarizability α_i^s in (7.28) and (7.29) can be approximated as $\alpha_{i,\alpha\beta}^s \approx Z_s^{-1}\delta_{\alpha\beta}$, and the enhancement (7.29) acquires the following form after averaging over orientations [28]:

$$G_{RS} = |Z|^2\frac{1}{3N}\left\langle\sum_i|\alpha_{i,\alpha\beta}|^2\right\rangle = \delta\left(1 + X^2/\delta^2\right) Im\,\alpha. \tag{7.30}$$

Thus, if the Raman-scattered light does not interact with the cluster, the Raman scattering intensity is simply proportional to the mean square of the local fields (see Eq. (7.4)) [28].

However, in more interesting cases, the Stokes shift is small, and the Stokes amplitudes are also enhanced. Then, the general expression (7.29) is needed; after averaging over orientations, this gives

$$G_{RS} = \frac{(X^2+\delta^2)^2}{3}\langle Tr[(\hat{\alpha}_i^T\hat{\alpha}_i\hat{\alpha}_i^{T*}\hat{\alpha}_i^*]\rangle. \tag{7.31}$$

(For the non-resonant case, $|X| \gg |w_n|$, we have $\alpha_i = \alpha_0$ and, therefore, $G_{RS} = 1$ in Eq. (7.31).) According to (7.31), the enhancement of Raman scattering is determined by the enhanced local fields raised to the fourth power and averaged over an ensemble of clusters

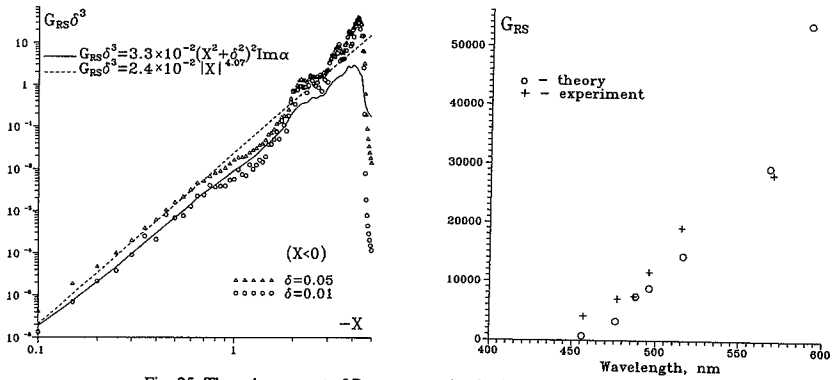

Fig. 25. The enhancement of Raman scattering in CCA, G_{RS}, for negative X.

Fig. 26. Theoretical and experimental enhancement factors for silver colloid aggregates as functions of wavelength, λ.

$$G_{RS} \sim \left\langle \frac{|E_i|^4}{|E^{(0)}|^4} \right\rangle \sim |\alpha_0^{-1}|^4 \langle |\alpha_i|^4 \rangle. \tag{7.32}$$

We conjecture the following formula for G_{RS} [133]:

$$G_{RS} \approx C_{RS} \frac{(X^2+\delta^2)^2}{\delta^3} Im\,\alpha(X), \tag{7.33}$$

with C_{RS} being an adjustable parameter. The X- and δ-dependence as in Eq. (7.33) can be obtained by assuming that resonant modes in (7.31) give the dominant contribution [133]. For diluted aggregates the formula (7.33) can be derived from scaling arguments [28].

In Fig. 25 the results of simulations of G_{RS}, defined in (7.31), are shown for negative X (the results for positive X are similar). The solid line in Fig. 25 gives the enhancement found from (7.33) with C_{RS} obtained from the relation $G_{RS}\delta^3 = 3$ at the maxima $X \approx -4$. The dashed line represents a power-law fit for the results of the simulations of $G_{RS}\delta^3$ with $\delta = 0.05$ in the interval $0.1 \leqslant |X| \leqslant 3$. The exponent obtained (4.07 ± 0.70) is close to 4. As was indicated above, the dependence associated with a pre-factor (in this case, X^4) dominates the weak spectral dependence originating from $Im\,\alpha(X)$.

As seen in Fig. 25, the product $G_{RS}\delta^3$, on average, does not depend on δ in the region close to the maxima, and its value there is close to unity. Thus, the strong enhancement of Raman scattering, $G_{RS} \sim \delta^{-3}$, can be obtained due to aggregation of particles into fractal clusters.

In Fig. 26, experimental RS enhancement data, obtained for silver colloid solution in Ref. [137], are compared with G_{RS} calculated using Eq. (7.31). (The values of X and δ for various λ were found using the data of Ref. [120]; see Fig. 16.) Only the spectral dependence of G_{RS} is informative in this figure since only relative values of G_{RS} are reported in Ref. [137]. The experimental data presented

in Fig. 26 are normalized by setting $G_{RS} \simeq 3 \times 10^{-4}$ at 570 nm, which is a reasonable value. Clearly, the present theory successfully explains the giant enhancement accompanying aggregation and the observed increase of G_{RS} towards the red part of the spectrum. The strong enhancement towards the red occurs because the local fields associated with collective dipolar modes in a CCA become significantly larger in this part of the spectrum (see Fig. 20).

7.5. Non-linear refraction and absorption

In this section we consider the enhancement of the optical Kerr non-linearity. The Kerr polarizability has, in general, the form $\beta^{(3)}_{\alpha\beta\gamma\delta}(-\omega;\omega,\omega,-\omega)$, and it determines the non-linear correction (proportional to the field intensity) to the refractive index and absorption. The Kerr-type non-linearity can also result in degenerate four-wave mixing (DFWM) considered above. Composite materials with large values of the Kerr non-linearity can be used as non-linear optical filters. Under certain conditions, they also manifest optical bistability [132] which can be utilized to build an optical analog of the electric transistor. Therefore, there is significant interest in developing materials with a large Kerr non-linearity.

We consider the enhancement of the Kerr susceptibility due to the clustering of small particles embedded in a linear host material. We assume that the volume fraction, p, filled by particles is small, and that they are initially randomly distributed in the host. Since p is small, the interaction between particles before aggregation is negligible. The aggregation results in many well-separated random clusters. The interactions between the light-induced dipoles on particles in a cluster lead to the formation of collective eigenmodes; their resonant excitation results in high local fields and the enhanced Kerr susceptibility.

The Kerr non-linear polarizability, $\beta^{(3)}$, has the same structure (see Eq. (7.5)) as the one describing DFWM. (In the present case, however, we assume that there is only one applied field, $\mathbf{E}^{(0)}$.) Although in Section 6.1 we considered only one specific process, DFWM, the analysis presented there was general and most of the obtained results are applicable to other phenomena associated with the Kerr susceptibility.

For isotropic media, the Kerr polarizability can be written in the form (7.6), with two independent constants, f_s and f_a. The polarization of the clusterized composite is

$$P^{(3c)}_\alpha(\omega) = 3\bar{\chi}^{(3c)}_{\alpha\beta\gamma\delta}(-\omega;\omega,\omega,-\omega) E^{(0)}_\beta E^{(0)}_\gamma E^{(0)*}_\delta.$$

The effective Kerr susceptibility, $\bar{\chi}^{(3c)}$, of the composite has the form

$$\bar{\chi}^{(3c)}_{\alpha\beta\gamma\delta} = G_{K,s} p\phi_s \Delta^+_{\alpha\beta\gamma\delta} + G_{K,a} p\phi_a \Delta^-_{\alpha\beta\gamma\delta}, \tag{7.34}$$

where $\phi_{s,a} = v_0^{-1} f_{s,a}$, with v_0 being the volume of a particle, and

$$G_{K,s} = \tfrac{1}{15} Z^3 Z^* \langle Tr(\hat{\alpha}_i^T \hat{\alpha}_i) Tr(\hat{\alpha}_i^T \hat{\alpha}_i^*) + 2Tr(\hat{\alpha}_i^T \hat{\alpha}_i \hat{\alpha}_i^T \hat{\alpha}_i^*) \rangle, \tag{7.35}$$

and

$$G_{K,a} = \tfrac{1}{6} Z^3 Z^* \langle Tr(\hat{\alpha}_i^T \hat{\alpha}_i) Tr(\hat{\alpha}_i^T \hat{\alpha}_i^*) - Tr(\hat{\alpha}_i^T \hat{\alpha}_i \hat{\alpha}_i^T \hat{\alpha}_i^*) \rangle. \tag{7.36}$$

The factors G_s and G_a are identical to F_s/f_s and F_a/f_a, respectively (see Eqs. (7.13)), and the enhancement for the DFWM process can be expressed in terms of $G_{K,s}$ as $G_{FWM} = |G_{K,s}|^2$.

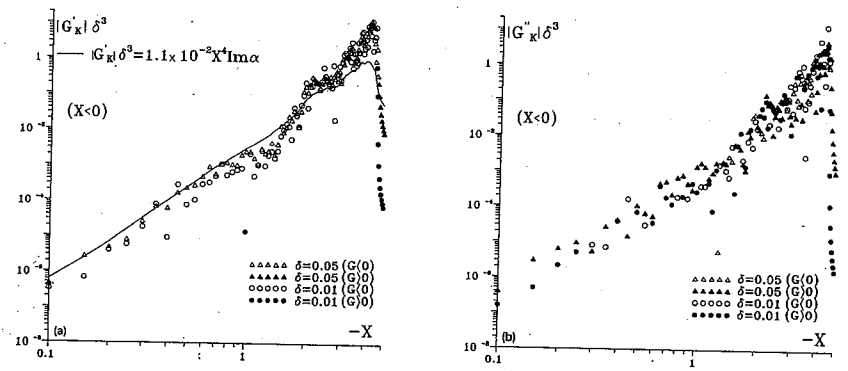

Fig. 27. The enhancement of the Kerr optical susceptibility in CCA: (a) the real part G'_K and (b) the imaginary part G''_K.

In general, according to Eqs. (7.34)–(7.36), there are two different enhancement coefficients for totally symmetric ($\propto \Delta^{+}_{\alpha\beta\gamma\delta}$) and partially symmetric ($\propto \Delta^{-}_{\alpha\beta\gamma\delta}$) parts of the susceptibility in an isotropic system. The fact that there are two different independent constants for the Kerr response in an isotropic medium results, in particular, in a rotation of the polarization ellipse [134].) If the field $E^{(0)}$ is polarized linearly or circularly, the non-linear polarization $P^{(3c)}$ can be expressed in terms of only one independent constant [134] (F_s and $[F_s + F_a]$, respectively). Also, in the low-frequency limit (where $\beta^{(3)}$ is due to the non-resonant electron response), the non-linear susceptibility tensor must be fully symmetrical, i.e. $F_a = 0$, for an arbitrary light polarization [134].

Below we consider the enhancement associated with $G_{K,s} \equiv G_K$. The enhancement factor is, in general, complex: $G_K \equiv G'_K + iG''_K$. If $\beta^{(3)}$ is real, the real part, G'_K, and the imaginary part, G''_K, determine the enhancement for the non-linear refraction and for the non-linear correction to absorption, respectively.

In accordance with Eq. (7.17), we assume that G'_K is larger than G''_K and can be approximated by

$$G'_K \approx C_K \frac{X^4}{\delta^3} Im\,\alpha(X). \tag{7.37}$$

In Fig. 27, a plot of G'_K (a) and G''_K (b) is presented for $X < 0$ (the results of the simulations for $X > 0$ are similar to those for $X < 0$) calculated from Eq. (7.35). The solid line in Fig. 27a represents the calculations based on Eq. (7.37) with the C_K chosen to satisfy the relation $|G'_K\delta^3| = 1$ in its maximum at $X \approx -4$. From the figure we conclude that Eq. (7.37) approximates the exact results reasonably well. Also, both real and imaginary parts of the enhancement are approximately proportional to the third power of the quality factor, $q^3 \sim \delta^{-3}$, and the following estimates are valid in the maxima: $G'_K\delta^3 \sim 1$ and $G''_K\delta^3 \sim 1$. (Actually, G'_K is several times larger than G''_K, in accordance with the assumption made above.) For metal particles, in particular, the decay parameter varies from $\delta = 0.01$ to $\delta = 0.1$ in the infrared and visible parts of the spectrum; accordingly, the enhancement associated with the clustering of particles ranges from $|G_K| \sim 10^3$ to $|G_K| \sim 10^6$ in this spectral range. Such a giant enhancement indicates that optical materials based on composites consisting

of small-particle clusters possess a high potential for various applications based on the large Kerr optical susceptibility. For $G'_K < 0$, the non-linear correction Δn to the refractive index is negative, if $\beta^{(3c)} > 0$, and positive, if $\beta^{(3c)} < 0$ (leading, respectively, to self-defocusing and self-focusing of the light beam). Interestingly, the imaginary part, G''_K, changes its sign as a function of X very rapidly. Thus, a non-linear correction to the absorption coefficient (given by G''_K for real $\beta^{(3c)}$) is a very strong function of the laser frequency and can be both positive and negative. The fact that a non-linear contribution to the absorption can have a different sign is not surprising: there are non-linear optical processes (associated with the Kerr-type non-linearity) leading to both positive and negative non-linear contributions to absorption. In particular, processes such as the saturation effect or the Rayleigh resonance (stimulated Rayleigh scattering) lead to negative corrections to the absorption, whereas two-photon absorption, for example, results in a positive correction [134]. Clearly, the light excites simultaneously many resonant modes in a cluster leading to a competition between various contributions associated with different resonant optical processes; this probably results in the strong dependence of G''_K on X.

7.6. Enhanced Rayleigh scattering and Anderson light localization

Resonant Rayleigh scattering by fractal clusters was studied by Shalaev et al. [26]. They showed that the scattering cross section of small-particle aggregates has the form [26]

$$\sigma_s = \frac{2\pi}{15} k^4 N (K_1 \langle Tr(\hat{\alpha}^i \hat{\alpha}^{i'*})\rangle + K_2 \langle Tr\,\hat{\alpha}^i Tr\,\hat{\alpha}^{i'*}\rangle), \tag{7.38}$$

$$K_1 = \begin{cases} C(kR_0)^{-D}\left(\dfrac{7}{2-D} - \dfrac{2}{4-D} + \dfrac{2}{6-D}\right), & \text{if } (D<2); \\ \frac{7}{2}(kR_0)^{-2}\ln((kR_0)^2 N), & \text{if } (D=2); \\ \dfrac{7}{2}\dfrac{D}{D-2}(kR_0)^{-2}N^{1-D/2}, & \text{if } (D>2). \end{cases} \tag{7.39}$$

$$K_2 = \begin{cases} C(kR_0)^{-D}\left(\dfrac{1}{2-D} - \dfrac{6}{4-D} + \dfrac{6}{6-D}\right), & \text{if } (D<2); \\ \frac{1}{2}(kR_0)^{-2}\ln((kR_0)^2 N), & \text{if } (D=2); \\ \dfrac{1}{2}\dfrac{D}{D-2}(kR_0)^{-2}N^{1-2/D}, & \text{if } (D>2) \end{cases} \tag{7.40}$$

where $C = D\Gamma(D-1)2^{1-D}\cos\frac{1}{2}\pi(D-2)$ and $\Gamma(\ldots)$ is the Gamma function.

The scattering enhancement factor, F_R, is defined as $F_R = \sigma_s/N\sigma_s^{(0)}$, where $\sigma_s^{(0)}$ is the single-particle scattering cross section, $\sigma_s^{(0)} = \frac{8}{3}\pi k^4|\alpha_0|^2$. From (7.38) we have

$$F_R = \tfrac{1}{20}|\alpha_0|^{-2}(K_1\langle Tr(\hat{\alpha}^i\hat{\alpha}^{i'*})\rangle + K_2\langle Tr\,\hat{\alpha}^i Tr\,\hat{\alpha}^{i'*}\rangle). \tag{7.41}$$

In the limit of non-resonant scattering Eq. (7.41) reduces to the result obtained first by Berry and Percival [138], $F_R = \frac{3}{20}(K_1 + 3K_2)$.

It was shown in Ref. [26] that the enhancement for diluted fractal clusters can be estimated as

$$F_R \sim \frac{N}{R_0^3\delta}(R_0^3|X|)^{d_o+1}, \tag{7.42}$$

for small clusters ($kR_c \ll 1$), and as

$$F_R \sim \frac{(kR_0)^{-D}}{R_0^3\delta}(R_0^3|X|)^{d_o+1} \quad (D<2); \tag{7.43}$$

$$F_R \sim \frac{(kR_0)^{-2}}{R_0^3\delta}\ln((kR_0)^2N)(R_0^3|X|)^{d_o+1}, \quad (D=2); \tag{7.44}$$

$$F_R \sim \frac{(kR_0)^{-2}}{R_0^3\delta}N^{1-2/D}(R_0^3|X|)^{d_o+1}, \quad (D>2), \tag{7.45}$$

for large aggregates ($kR_c \gg 1$). Here d_o is the optical spectral dimension (see Eq. (5.37) and the accompanying discussion). Thus, according to Eqs. (7.42)–(7.45), the scattering cross section per particle is enhanced by coherence due to the fractality (factor $(kR_0)^{-D}$ in Eq. (7.43) and factor $(kR_0)^{-2}N^{1-2/D}$ in Eq. (7.45)) and, in addition, by the resonance character of the scattering by dipolar eigenmodes in fractal clusters (factor δ^{-1}). Formulas (7.42)–(7.45) are supported by numerical simulations of Ref. [26]. We mention that Rayleigh scattering by colloidal gold was studied experimentally in Ref. [139].

To conclude this section we briefly consider the possibility of observation of light localization in fractals suggested in Ref. [140]. (For other papers and references on light localization in various media see, for example, Refs. [141–148]; multiple and cooperative scattering was also considered in Refs. [149,150].) Light localization is an effect that arises entirely from coherent multiple scattering and interference when the radiation elastic mean-free path l reduces to the wavelength λ. This effect is similar to Anderson localization of electrons in disordered solids [151]. Achieving the condition $l \sim \lambda$ needed for observation of localized light modes is experimentally rather difficult since usually $l \gg \lambda$. Small-particle fractal composites are thought to be promising media for light localization because of the strong enhancement of the light scattering in these objects [26,140].

To observe the light localization, we suggested [140] to use a mixture of small-particle fractal aggregates with the intercluster distance of the order of the cluster size R_c ("fractal gel"). The elastic mean-free path in this case is $l \sim (\sigma_s n_c)^{-1} \sim R_c^3/\sigma_s$, where n_c is the concentration of clusters (aggregates) and σ_s is given in Eqs. (7.38)–(7.40). As shown in Ref. [140], the requirement $l \sim \lambda$ can be fulfilled in the fractal gel under reasonable conditions, whereas the absorption remains small. In the vicinity of the mobility edge, anomalous behavior for the light transmission and absorption was predicted in Ref. [140].

7.7. Discussion

As shown above, the clustering of small particles embedded in a host material may result in a giant enhancement of both linear (e.g., Rayleigh and Raman scattering) and non-linear (four-wave mixing, harmonic generation, and non-linear refraction and absorption) optical effects. The enhancement occurs because of strongly fluctuating local fields that can have very large values in particle aggregates (see Fig. 20). Non-linearities emphasize these fluctuations, leading to giant enhancements.

If particles aggregate into fractal clusters, fluctuations of the local fields are especially large (see Fig. 20). This is because the dipole interactions in fractals are not long range (as they are in conventional three-dimensional media) and many of the collective eigenmodes are localized in different parts of a cluster with various random structures. This ultimately leads to strong spatial fluctuations of the fields. In contrast, in compact three-dimensional clusters of particles, the long-range dipolar interaction involves all particles into the excitation of eigenmodes, thereby suppressing the fluctuations (see Fig. 20).

Enhancement in small-particle clusters can be understood and roughly estimated using the following simple arguments. Consider the enhancement for an arbitrary non-linear optical process $\propto E^n$. As discussed above, for the resonant dipolar eigenmodes on fractals, local fields, E_i, exceed the external field, $E^{(0)}$, by the factor $\sim |\alpha_0^{-1}/\delta| = |X + i\delta|/\delta$, i.e. $\sim |X|/\delta$ for $|X| \gg \delta$. However, the fraction of the monomers involved in the resonant optical excitation is small, $\sim \delta Im\,\alpha(X)$.

For a non-linear optical process, $\propto |E|^n$, one can estimate the ensemble average of the enhancement, $\langle|E_i/E^{(0)}|^n\rangle$, as the resonant value, $|E_i/E^{(0)}|^n_{res}$, multiplied by the fraction of the resonant modes (in other words, the fraction of particles involved in the resonant excitation). This gives for the enhancement the following estimate:

$$\langle|E_i/E^{(0)}|^n\rangle \sim |X|^n\delta^{-n} \times \delta Im\,\alpha(X) \sim |X|^n\delta^{1-n}Im\,\alpha(X), \tag{7.46}$$

which is $\gg 1$ for $n > 1$. Since this is only a rough estimation, an adjustable constant, C, should in general be added as a pre-factor.

The non-linear dipole amplitude can be enhanced along with the linear local fields provided the generated frequency lies within the spectral region of the cluster eigenmodes. For enhancements of incoherent processes, such as Raman scattering and non-linear refraction and absorption in Kerr media, we obtain from Eq. (7.46): $G \sim CX^4\delta^{-3}Im\,\alpha(X)$ (cf. Eqs. (7.33) and (7.37)). For coherent processes, the resultant enhancement $\sim |\langle|E_i/E^{(0)}|^n\rangle|^2$; accordingly, the enhancement factor $\sim CX^6\delta^{-4}[Im\,\alpha(X)]^2$ for the third harmonic generation (cf. Eq. (7.23)), and $\sim CX^8\delta^{-6}[Im\,\alpha(X)]^2$ for degenerate four-wave mixing (cf. Eq. (7.17)). (The latter enhancement is larger because of the "additional" enhancement of the generated non-linear amplitudes oscillating at the same frequency as the applied field.)

There are other optical phenomena (not considered here) that can be also enhanced in small-particle composites. For example, fluorescence (from molecules adsorbed on a small-particle aggregate) following the two-photon absorption by the aggregate is enhanced by the factor $G_F \sim \langle|E_i/E^{(0)}|^4\rangle \sim |\alpha_0|^{-4}\langle|\alpha_i|^4\rangle \propto \delta^{-3}$.

8. Concluding remarks

In this paper we have presented some recent advances in the electromagnetics of small-particle composites. The emphasis was on theoretical approaches that are currently used and, especially, on those which have been recently employed to describe optical properties of small-particle aggregates.

As is well known, there is only one dipolar mode that can be excited by a homogeneous field in a spherical particle (in a spheroid there are three dipole modes). For a three-dimensional collection of small particles, such as the random close-packed sphere of particles (CPSP) and the random gas of particles (RGP), the absorption spectra are still peaked near the relatively narrow surface plasmon

resonance of the individual particles, i.e. all eigenmodes of the collection of particles are located in a small spectral interval.

In contrast to conventional three-dimensional systems, the dipolar interaction in low-dimensional fractals is not long range, which results in localization of the corresponding eigenmodes at various random locations in the cluster. These modes form the optical spectrum of fractal aggregates which is characterized by strong inhomogeneous broadening. It is important to note that, despite the asymptotically zero density of particles in a fractal cluster, there is always a high probability of finding a number of particles in close proximity to any given one ($g \propto r^{D-3}$, i.e. g becomes large at small r). Therefore, there are strong interactions between neighboring particles, which lead to the formation of eigenmodes covering a broad spectral range. The large variety of different local configurations in a fractal cluster leads to the wide spectral interval covered by the eigenmodes. We emphasize that this behavior is different from non-fractal composites (such as RGP and CPSP) where dipolar eigenmodes typically occupy a narrow spectral interval. Thus, in objects with fractal morphology, the density-density correlation, $g(r) \propto r^{D-d}$, results in an unusual combination of properties: whereas the volume fraction filled by particles in a fractal is very small (as in gases), there are strong interactions between neighboring particles (as in crystals).

Localization of eigenmodes in fractals leads to a patchwork-like distribution of local fields associated with "hot" and "cold" zones in fractals. This brings about large spatial fluctuations of local fields in fractal composites and huge enhancement of various optical effects.

In fractals formed, for example, by metal particles, the dipole eigenmodes cover the visible and infra-red parts of the spectrum; the mode quality-factors increase with the wavelength, i.e. the local fields are especially large in the long-wavelength part of the spectrum. High local fields result in giant enhancements of a number of optical processes in small-particle composites. This makes nanostructured composite materials, and, especially, those with fractal morphology, very attractive for many potential applications.

Note that a microscopically rough surface often has a fractal or self-affine structure (e.g., a thin film deposited on a cold substrate) [152–156]. Electromagnetic properties of rough surfaces were studied in a number of papers (see e.g. Refs. [157–169]. Optical excitations of a rough surface can also result in high local fields and large enhancement of many optical processes (see e.g. Refs. [170,171]).

Acknowledgement

This research was supported by NSF under grant DMR-9500258, EPA under grant R822658-01-0, and by NATO under grant CRG 950097. The author is very grateful to his collaborators and, especially, to M. Moskovits (University of Toronto), R. Botet (Paris-Sud Université, Orsay, France), M.I. Stockman and T.F. George (Washington State University), V.A. Markel and E.Y. Poliakov (New Mexico State University), V.V. Slabko and A.K. Popov (L.V. Kirensky Institute of Physics, Krasnoyarsk, Russia), V.P. Safonov (Institute of Automation and Electrometry, Novosibirsk, Russia), E.B. Stechel (Sandia National Laboratory, NM), and D.P. Tsai (National Chung Cheng University, Taiwan). Also, useful discussions with the following colleagues are highly appreciated: D. Stroud (Ohio State University), F. Brouers (Institut de Physique, Université de Liège, Belgium), R.K. Chang (Yale University), J. Martin (Sandia National Laboratory, NM), F. Claro (Universidad Catolica de Chile), R. Fuchs (Iowa State University), A.A. Maradudin (UC, Irvine), M.V. Berry (H.H. Wills Physics Laboratory, Bristol), C. Douketis and T. Haslett (University of Toronto), P. Sheng (Exxon Research), J. Sipe and A. Golubentsev (University of Toronto), A. Sarychev (Scientific Center for Applied Problems in Electrodynamics, Moscow, Russia), R.L. Armstrong, and P. Nachman (New Mexico State University).

References

[1] Electron Transport and Optical Properties of Inhomogeneous Media, eds. J.C. Garland and D.B. Tanner, AIP, New York (1978); Electron Transport and Optical Properties of Inhomogeneous Media (ETOPIM 3), eds. W.L. Mochan and R.G. Barrera, North-Holland, Amsterdam (1994).
[2] B.B. Mandelbrot, The Fractal Geometry of Nature (Freeman, San Francisco, 1982).
[3] B. Sapoval, Fractals (Aditech, Paris, 1990).
[4] A. Bunde and S. Havlin. In: Fractals and Disordered Systems (eds. A. Bunde and S. Havlin), Springer Verlag, Heidelberg 1991.
[5] S. Alexander and R. Orbach, J. Physique - Lettres 43 (1982) 625.
[6] R. Rammal and G. Toulouse, J. Physique - Lettres 44 (1983) 13.
[7] H.E. Stanley, J. Phys. A 10 (1977) L211.
[8] S. Kirkpatrick, Reviews of Modern Physics 45 (1973) 574.
[9] J.P. Clerc, G. Girard, J.M. Laugier and J.M. Luck, Advances in Physics 39 (1990) 191.
[10] A.L. Efros and B.I. Shklovskii, Phys. Stat. Sol. 76 (1976) 475.
[11] J.P. Straley, J. Phys. C: Solid State Phys. 9 (1976) 783.
[12] P.C. Hohenberg, B.I. Halperin, Reviews of Modern Physics 49 (1977) 435.
[13] Electrophysical Properties of Percolation Systems, ed: A. N. Lagar'kov (Moscow, 1990).
[14] D. Stroud and D. Bergman, Phys. Rev. B 25 (1982) 2061.
[15] Y. Yagil, M. Yosefin, D.J. Bergman, G. Deutscher, P. Gadenne, Phys. Rev. B 43 (1991) 11 342.
[16] Y. Gefen, A. Aharony, and S. Alexander, Phys. Rev. Lett. 50 (1983) 77.
[17] P.R. Devaty, Phys. Rev. B 44 (1991) 593.
[18] X. Zhang and D. Stroud, Phys. Rev. B 48 (1993) 6658.
[19] G.A. Niklasson, J. Appl. Phys. 62 (1987) R1; Physica D 38 (1989) 260.
[20] J.P. Straley, J. Phys. C 13 (1980) 819.
[21] D.J. Bergman and D. Stroud. In: Solid State Physics 46 (1992) 147.
[22] V.M. Shalaev, M.I. Stockman, Zh. Eksp. Teor. Fiz. 92 (1987) 509 [Sov. Phys. JETP 65 (1987) 287]; Z. Phys. D-Atoms, Molecules and Clusters, 10 (1988) 71.
[23] A.V. Butenko, V.M. Shalaev, M.I. Stockman, Zh. Eksp. Teor. Fiz. 94 (1988) 107 [Sov. Phys. JETP 67 (1988) 60]; Z. Phys. D - Atoms, Molecules and Clusters, 10 (1988) 81. [The spectral function $S_a(z)$ of Ref. [23] must be replaced by the function $S_D(z)$ of Ref. [24] that corrects the former one.]
[24] V.A. Markel, L.S. Muratov, and M.I. Stockman, Zh. Eksp. Teor. Fiz. 98 (1990) 819 (Sov. Phys. JETP 71 (1990) 455); V.A. Markel, L.S. Muratov, M.I. Stockman, and T.F. George, Phys. Rev. B 43 (1991) 8183.
[25] M.I. Stockman, T.F. George, and V.M. Shalaev, Phys. Rev. B 44 (1991) 115.
[26] V.M. Shalaev, R. Botet, and R. Jullien, Phys. Rev. B 44 (1991) 12216; ibid. 45 (1992) 7592(E).
[27] V.M. Shalaev, M. Moskovits, A.A. Golubentsev, and S. John, Physica A 191 (1992) 352.
[28] M.I. Stockman, V.M. Shalaev, M. Moskovits, R. Botet, and T.F. George, Phys. Rev. B 46 (1992) 2821.
[29] V.M. Shalaev, R. Botet, A.V. Butenko, Phys. Rev. B 48 (1993) 6662.
[30] V.M. Shalaev, M.I. Stockman, & R. Botet, Physica A 185 (1992) 181.
[31] M.I. Stockman, L.N. Pandey, L.S. Muratov, and T. F. George, Phys. Rev. Lett. 72 (1994) 2486.
[32] V.M. Shalaev, R. Botet, Phys. Rev. B 50 (1994) 12987.
[33] V.M. Shalaev, V.A. Markel, V.P. Safonov, Fractals 2 (1994) 201; V.M. Shalaev, R. Botet, D.P. Tsai, J. Kovacs, M. Moskovits, Physica A 207 (1994) 197.
[34] M.I. Stockman, L.N. Pandey, L.S. Muratov, and T. F. George, Phys. Rev. B 51 (1995).
[35] J.C. M. Garnett, Phil. Trans. R. Soc. L. 203 (1904) 385; ibid. 205 (1906) 237.

[36] R. Clausius, Mechanishe Warmetheorie, Brounschweig, 2 (1878) 62.
[37] O.F. Mossotti, Mem. Soc. Sci. Modena, 14 (1850) 49.
[38] H.A. Lorentz, Wiedem. Ann. 9 (1880) 641.
[39] L. Lorentz, Wieden. Ann. 11 (1881).
[40] D.A. G. Bruggeman, Ann. Physik. (Leipzig) 24 (1935) 636.
[41] D.J. Bergman, Physics Reports 43 (1978) 377.
[42] D. Stroud, Phys. Rev. B 19 (1979) 1783.
[43] K.D. Cummings, J.C. Garland, and D.B. Tanner, Phys. Rev. B 30 (1984) 4170.
[44] R. Ruppin, Phys. Rev. B 19 (1979) 1318.
[45] P.N. Sen and D.B. Tanner, Phys. Rev. B 26 (1982) 3582.
[46] D.M. Wood and N.W. Ashcroft, Phys. Rev. B 25 (1982) 6255.
[47] P. Chylek, D. Boice, and R.G. Pinnick, Phys. Rev. B 27 (1983) 5107.
[48] B.N. J. Persson and A. Liesch, Phys. Rev. B 28 (1983) 4247.
[49] D.B. Tanner, Phys. Rev. B 30 (1984) 1042.
[50] G.S. Agarwal and R. Ingura, Phys. Rev. B 30 (1984) 6108.
[51] A. Bittar, S. Berthier, and J. Lafait, J. Phys. (Paris) 45 (1984) 623.
[52] W.A. Curtin, R.C. Spitzer, N.W. Ashcroft, and A. J. Sievers, Phys. Rev. Lett. 54 (1985) 1071.
[53] R.S. Koss and D. Stroud, Phys. Rev. B 32 (1985) 3456.
[54] P.M. Hui and D. Stroud, Phys. Rev. B 33 (1986) 2163.
[55] G.A. Niklasson and C.G. Grankvist, Phys. Rev. Lett. 56 (1986) 256.
[56] V.A. Davis and L. Schwartz, Phys. Rev. B 31 (1985) 5155; ibid. 33 (1986) 6627.
[57] R. Fuchs, Phys. Rev. B 11 (1975) 1732.
[58] R. Fuchs, Phys. Rev. B 35 (1987) 7700.
[59] R. Rojas, F. Claro, and R. Fuchs, Phys. Rev. B 37 (1988) 6799.
[60] Zhe Chen, Ping Sheng, D.A. Wetz, H.M. Lindsay, M. Y. Lin, and P. Meakin, Phys. Rev. B 37 (1988) 5232.
[61] R.G. Barrera, G. Monsivais, and W.L. Mochan, Phys. Rev. B 38 (1988) 5371.
[62] P.N. Sen, C. Scala, and M.H. Cohen, Geophys. 46 (1981) 781.
[63] P. Sheng, X. Jing, M. Zhou, Physica A 207 (1994) 37.
[64] P. Sheng and Z. Chen, Phys. Rev. Lett. 60 (1988) 227.
[65] Z. Chen, P. Sheng, D.A. Weitz, H.M. Lindsay, M. Y. Lin, P. Meakin, Phys. Rev. B 37 (1988) 5232.
[66] S. Torquato, Physica A 207 (1994) 79.
[67] X.C. Zeng, P.M. Hui, D.J. Bergman, D. Stroud, Phys. Rev. B 39 (1989) 13224.
[68] B. Derrida and J. Vannimenus, J. Phys. A 15 (1982) L557; B. Derrida, D. Stauffer, H.J. Herrmann, and J. Vannimenus, J. Phys. Lett. 44 (1983) L701; H.J. Herrmann, B. Derrida, and J. Vannimenus, Phys. Rev. B 30 (1984) 4080.
[69] D.J. Frank and C.J. Lobb, Phys. Rev. B 37 (1988) 302.
[70] I. Hoffmann and D. Stroud, Phys. Rev. B 43 (1991) 9965.
[71] F. Brouers, J.P. Clerc, G. Giraud, J.M. Laugier, and Z.A. Randriamanantany, Phys. Rev. B 47 (1993) 666.
[72] F. Brouers, J.M. Jolet, G. Giraud, J.M. Laugier, and Z.A. Randriamanantany, Physica A 207 (1994) 100.
[73] Ping Sheng, Phys. Rev. Lett. 45 (1980) 60.
[74] X.C. Zeng, P.M. Hui, D. Stroud, Phys. Rev. B 39 (1989) 1063.
[75] I.H. H. Zabel and D. Stroud, Phys. Rev. B 46 (1992) 8132.
[76] S. Alexander, Phys. Rev. B 40 (1989) 7953.
[77] F. Brouers, D. Rauw, J.P. Clerc and G. Giraud, Phys. Rev. B 49 (1994) 14582.
[78] T. Robin and B. Souillard, Europhys. Lett. 21 (1993) 273.
[79] D.J. Bergman, Phys. Rev. B 14 (1976) 4304; D. J. Bergman. In: Electron Transport and Optical Properties of Inhomogeneous Media, Eds: J.C. Garland and D.B. Tanner, (AIP, New York, 1978) 46.
[80] R. Fuchs. In: Electron Transport and Optical Properties of Inhomogeneous Media, Eds: J.C. Garland and D.B. Tanner, (AIP, New York, 1978) 276.
[81] K. Ghosh and R. Fuchs, Phys. Rev. B 38 (1988) 5222.
[82] R. Fuchs, F. Claro, Phys. Rev. B 39 (1989) 3875.
[83] K. Ghosh, R. Fuchs, Phys. Rev. B 44 (1991) 7330.
[84] F. Claro, R. Fuchs, Phys. Rev. B 44 (1991) 4109.

[85] G. Milton, J. Appl. Phys. 52 (1981) 5286.
[86] D. Stroud, G.W. Milton, and B.R. De, Phys. Rev. B 34 (1986) 5145.
[87] R. Fuchs, K. Ghosh, Physica A 207 (1994) 185.
[88] T.C. Halsey, M.H. Jensen, L.P. Kadanoff, I. Procaccia, B.I. Shraiman, Phys. Rev. A 33 (1986) 1141.
[89] S. Alexander, C. Laermans, R. Orbach, and H. M. Rosenberg, Phys. Rev. B 28 (1983) 4615.
[90] E. Courtens, J. Pelous, J. Phalippou, R. Vacher, and T. Woignier, Phys. Rev. Lett 58 (1987) 128; E. Courtens, C. Lartigue, F. Mezei, R. Vacher, G. Goddens, M. Forret, J. Pelous, and T. Woignier, Z. Phys. B 79 (1990) 1; R. Vacher, E. Courtens, G. Goddens, J. Pelous, and T. Woignier, Phys. Rev. B 39 (1989) 7384.
[91] A. Boukenter, B. Champagnon, E. Duval, J. Dumas, J. F. Quinson, J. Serughetti, Phys. Rev. Lett. 57 (1986) 2391; E. Duval, G. Mariotto, M. Montagna, O. Pilla, G. Viliani, M. Barland, Europh. Lett. 3 (1987) 333; E. Duval, V.N. Novikov, and A. Boukenter, Phys. Rev. B 48 (1993) 16785.
[92] G. Mariotto, M. Montagna, G. Viliani, E. Duval, S. Lefrant, E. Rzepka, C. Mai, Europh. Lett. 6 (1988) 239; O. Pilla, G. Viliani, M. Montagna, V. Mazzcurati, G. Ruocco, G. Signorelli, Philosoph. Magaz. B 65 (1992) 243; P. Benassi, O. Pilla, V. Mazzacurati, M. Montagna, G. Ruocco, G. Signorelli, Phys. Rev. B 44 (1991) 11734.
[93] A. Alippi, G. Shkedrin, A. Bettucci, F. Craciun, E. Molinari, and A. Petri, Phys. Rev. Lett. 69 (1992) 3318.
[94] C.K. Harris, R.B. Stinchcombe, Phys. Rev. Lett., 50 (1983) 1399.
[95] A. Petri, L. Pietronero, Phys. Rev. B 45 (1992) 12864.
[96] A. Bunde, H.E. Roman, S. Russ, A. Aharoni, and A. B. Harris, Phys. Rev. Lett. 69 (1992) 3189.
[97] M.H. Jensen, G. Paladin, and A. Vulpani, Phys. Rev. Lett. 67 (1991) 208.
[98] R. Jullien and R. Botet, Aggregation and Fractal Aggregates (World Scientific, Singapore, 1987).
[99] S.G. Rautian, V.P. Safonov, P.A. Chubakov, V.M. Shalaev, M.I. Stockman, Pis'ma Zh. Eksp. Teor. Fiz. **47**, 243 (1988) [JETP Lett. **47**, 243 (1988)].
[100] A.V. Butenko, P.A. Chubakov, Yu. E. Danilova, S. V. Karpov, A.K. Popov, S.G. Rautian, V.P. Safonov, V.V. Slabko, V. M. Shalaev, and M.I. Stockman, Z. Phys. D Atoms, Molecules and Clusters 17 (1990) 283.
[101] J.E. Martin and J.P. Wilcoxon, Phys. Rev. Lett 61 (1988) 373; J.E. Martin, J. Wilcoxon, and J. Odinek, Phys. Rev. A 43 (1991) 858.
[102] V.A. Markel, V.M. Shalaev, E.B. Stechel, W. Kim, and R. Armstrong, Phys. Rev. B 53 (1996), in press.
[103] B. T. Draine, Astrophys.J. 333 (1988) 848.
[104] Yu. E. Danilova, V.A. Markel, V.P. Safonov, Atmos. Oceanic Opt. 6 (1993) 821.
[105] V.A. Markel, Journal of Modern Optics 39 (1992) 853.
[106] D. Weitz and M. Oliveria, Phys. Rev. Lett. 52 (1984) 1433 ; J.A. Creighton, Metal colloids, in: Surface Enhanced Raman Scattering, edited by R.K. Chang and T.E. Furtak, Plenum Press, New York, 1982.
[107] T.A. Witten and L.M. Sander, Phys. Rev. B 27 (1983) 5686.
[108] J.K. Collum and R.A. Willoughby, Lanczos Algorithm for Large Symmetric Eigenvalue Computations, Vol. 1, Theory; Birkhäuser, Boston (1985).
[109] Solid State Physics, Vol. 35, Academic Press, New York (1980).
[110] F. Brouers, S. Blacher, A. Sarychev, In: "Fractals in the Natural and Applied Sciences (in press).
[111] U. Kreibig and L. Genzel, Surf. Sci 156 (1985) 678; U. Kreibig, P. Zacharis, Z. Physik 231 (1970) 128; U. Kreibig, M. Vollmer, Optical Properties of Metal Clusters, Springer-Verlag, Berlin, Heidelberg (1995).
[112] J.E. Sansonetti, J.K. Furdyna, Phys. Rev. B 22 (1980) 2866.
[113] M. Ausloos, P. Clippe, A.A. Lucas, Phys. Rev. B 18 (1978) 7176.
[114] P. Clippe, R. Evrard, A.A. Lucas, Phys. Rev. B 14 (1976) 1751.
[115] J.M. Gerardy, M. Ausloos, Phys. Rev. B 22 (1980) 4950.
[116] F. Claro, Sol. St. Comm. 29 (1984) 229.
[117] E.M. Purcell, C.R. Pennypacker, Astrophys. J. 186 (1973) 705.
[118] S.B. Singham, C.F. Bohren, J. Opt. Soc. Am. A 5 1867.
[119] V.A. Markel, Journal of Modern Optics 40 (1993) 2281.
[120] P.B. Johnson and R.W. Christy, Phys. Rev. B 6 (1972) 4370 .
[121] Handbook of optical constants of solids, Ed: E.D. Palik (Academic Press, 1985).
[122] A.V. Karpov, A.K. Popov, V.V. Slabko, and V. M. Shalaev, Pis'ma Zh. Eksp. Teor. Fiz. 48 (1988) 528 [JETP Lett. 48 (1988) 571].

[123] D.P. Tsai, J. Kovacs, Z. Wang, M. Moskovits, V.M. Shalaev, J. Suh, and R. Botet, PRL 72 (1994) 4149; V.M. Shalaev and M. Moskovits, Phys. Rev. Lett. 75 (1995) 2451.
[124] D. Stroud, P.M. Hui, Phys. Rev. B 37 (1988) 8719.
[125] C. Flytzanis, Prog. Opt. 29 (1992) 2539; D. Ricard. Ph. Roussignol, C. Flytzanis, Optics Letters 10 (1985) 511; F. Hache, D. Ricard, C. Flytzanis, and U. Kreibig, Applied Physics A 47 (1988) 347.
[126] K.W. Yu, Y.C. Wang, P.M. Hui, G.Q. Gu, Phys. Rev. B 47 (1993) 1782; K.W. Yu. P.M. Hui, D. Stroud, Phys. Rev. B 47 (1993) 14150.
[127] J.E. Sipe, R.W. Boyd, Phys. Rev. A 46 (1992) 1614.
[128] P.M. Hui, D. Stroud, Phys. Rev B 49 (1994) 11729.
[129] K.W. Yu, Phys. Rev. B 49 (1994) 9989.
[130] D. Stroud, X. Zhang Physica A 207 (1994) 55; X. Zhang and D, Stroud, Phys. Rev. B 49 (1994) 944.
[131] P.M. Hui, Phys. Rev. B 49 (1994) 15344; K.W. Yu, Y. C. Chu, and Eliza M.Y. Chan, Phys. Rev. B 50 (1994) 7984.
[132] D. Bergman, O. Levy, D. Stroud, Phys. Rev. B 49 (1994) 129; O. Levy, D. Bergman, Physica A 207 (1994) 157; O. Levy, D. J. Bergman, D.G. Stroud, Phys. Rev. B 52 (1995) 3184.
[133] V.M. Shalaev, E.Y. Poliakov, and V.A. Markel, Phys. Rev. B. 53 (1996), in press.
[134] R.W. Boyd, Non-linear Optics, Academic Press, 1992.
[135] L.D. Landau, E.M. Lifshits and L.P. Pitaevskii, Electrodynamics of Continuous Media, 2nd Edition (Pergamon, Oxford, 1984).
[136] I.A. Akimov, A.V. Baranov, V.M. Dubkov, V.I. Petrov, and E.A. Sulabe, Opt. Spectrosc. (Russia) 63 (1987) 756.
[137] J.S. Suh and M. Moskovits, J. Phys. Chem. 58 (1984) 5526.
[138] M.V. Berry, I.C. Percival, Optica Acta 33 (1986) 577.
[139] J.P. Wilcoxon, J.E. Martin, and D.W. Schaefer, Phys. Rev. B 39 (1989) 2675.
[140] V.M. Shalaev, M. Moskovits, A.A. Golubentsev, and S. John, Physica A (1992) 352.
[141] S. John, Physics Today, May 1991; S. John, Phys. Rev. Lett. 58 (1987) 2486.
[142] A.Z. Genack, Phys. Rev. Lett. 58 (1987) 2043; M. Drake, A.Z. Genack, Phys. Rev. Lett. 63 (1989) 259.
[143] E. Yablonovich, Phys. Rev. Lett. 58 (1987) 2043; E. Yablonovich, T.J. Gmitter, Phys. Rev. Lett. 63 (1989) 1950.
[144] C.M. Soukoulis, S. Datta, E.N. Economou, Phys. Rev. B 49 (1994) 3800.
[145] A.R. McGurn and A.A. Maradudin, Physica A 207 (1994) 435; A.R. McGurn, K.T. Christensen, F.M. Mueller, A.A. Maradudin, Phys. Rev. B 47 (1993) 13120.
[146] Zhao-Qing Zhang and Ping Sheng, Phys. Rev. B 49 (1994) 83.
[147] A.K. Sarychev, D.J. Bergman, Y. Yagil, Physica A 207 (1994) 372.
[148] W. Gellermann, M. Kohmoto, B. Sutherland, and P. C. Taylor, Phys. Rev. Lett. 72 (1994) 633.
[149] S. Kawato, T. Hattori, T. Takemori, and H. Nakatsuka, Phys. Rev. B 49 (1994) 90.
[150] F.C. Spano, S. Mukamel, Phys. Rev. Lett. 66 (1991) 1197.
[151] P.W. Anderson, Phys. Rev. 109 (1958) 1492.
[152] R. Chiarello, V. Panella, J. Krim, C. Thompson, Phys. Rev. Lett. 67 (1991) 3408; J. Krim, I. Heyvaert, C. Van Haesendonck, and Y. Bruynseraede, Phys. Rev. Lett. 70 (1993) 57.
[153] M. Nakamura, Phys. Rev. B 41 (1990) 12 268.
[154] P. Meakin, CRC Critical Reviews in Solid State and Materials Sciences 13 (1987) 143.
[155] F. Family and T. Viscek, Dynamics of Fractal Surfaces (World Scientific, Singapore, 1990).
[156] C. Douketis, T.H. Haslett, V.M. Shalaev, Z. Wang, M. Moskovits, Physica A 207 (1994) 352.
[157] D.E. Aspnes, Thin Solid Films 89 (1982) 249.
[158] P Gadenne, A. Beghdadi and J. Lafait, Opt. Comm. 65 (1988) 17; P. Gadenne, Y. Yagil, and G. Deutscher, Physica A 157 (1989) 279; M. Gadenne and P. Gadenne, Physica A 157 (1989) 344; M. Gadenne, J. Lafait, and P. Gadenne, Physica A 157 (1989) 400; M. Gadenne, J. Lafait, and P. Gadenne, Opt. Comm. 71 (1989) 273; Y. Yagil, D. J. Bergman, and Y. Yagil, Physica A 207 (1994) 360; Y. Yagil, G. Deutscher, and D.J. Bergman, Physica A 207 (1994) 323.
[159] A.A. Maradudin, in: Topics in Condensed Matter Physics, M.P. Das, ed. (Nova, New York, 1994); G.A. Farias, E.F. Vasconcelos, S.L. Cesar, A.A. Maradudin, Physica A 207 (1994) 315.
[160] S.A. Akhmanov, V.N. Seminogov, V.I. Sokolov, ZhETF 93 (1987) 1654.
[161] T. Robin and B. Souillard, Physica A 157 (1989) 285; T. Robin and B. Souillard, Opt. Comm. 71 (1989) 15.
[162] G. Ritchie, E. Burstein, R.B. Stephens, J. Opt. Soc. Am. B 2 (1985) 544.

[163] C. Douketis, T.L. Haslett, J.T. Stuckless, M. Moskovits, and V.M. Shalaev, Surf. Sci. Lett. 297 (1993) L84.
[164] L.I. Daikhin and M.I. Urbakh, Surf. Sci. 236 (1990) 187; A.M. Brodsky and M.I. Urbakh, Surf. Sci. 115 (1982) 417.
[165] J.-J. Greffet, C. Baylard, and P. Versaevel, Opt. Lett. 17 (1992) 1740; J.-J. Greffet and Z. Maassarani, JOSA A 7 (1990) 1483; A. Sentenac and J.-J. Greffet, JOSA A 6 (1992) 996; J.-J. Greffet, Waves in Random Media 3 (1991) S65; J.-J. Greffet, Opt. Lett. 17 (1992) 238; F. Pincemin, J.-J. Greffet, Physica A 207 (1994) 146.
[166] N. Garcia and M. Nieto-Vesperinas, Phys. Rev. Lett. 71 (1993) 3645.
[167] T.C. Halsey and M. Leibig, Anals of Physics, 219 (1992) 109.
[168] Po-zen Wong, Phys. Rev. B 32 (1985) 7417.
[169] S. Wang and P. Halevi, Phys. Rev. B 47 (1993) 10815; G. H. Cocoletzi, S. Wang, Phys. Rev. B 48 (1993) 17413.
[170] Surface Enhanced Raman Scattering, edited by R.K. Chang and T.E. Furtak, Plenum Press, New York, 1982.
[171] M. Moskovits, Rev. Mod. Phys. 57 (1985) 783.

FORTHCOMING ISSUES

J. de Boer, F. Harmsze, T. Tjin. Non-linear finite W-symmetries and applications in elementary systems

G. Nägele. On the dynamics and structure of charge-stabilized suspensions

K. Jansen. Domain wall fermions and chiral gauge theories

J.P. Boon, D. Dab, R. Kapral, A. Lawniczak. Lattice gas automata for reactive systems

F.E. Wietfeldt, E.B. Norman. The 17 keV neutrino

T.P. Martin. Shells of atoms

J. Alam, S. Raha, B. Sinha. Electromagnetic probes of quark gluon plasma

C. Caccamo. Integral equation theory description of phase equilibria in classical fluids

W. Glöckle, H. Witala, D. Hüber, K. Kamada, J. Golak. The three-nucleon continuum: achievements, challenges and applications

S. Gentile, M. Pohl. Physics of tau leptons

Y. Abe, S. Ayik, P.-G. Reinhard, E. Suraud. On stochastic approaches of nuclear dynamics

C.-H. Lee. Kaon condensation in dense stellar matter

B.I. Sturman, S.G. Odoulov, M.Yu. Goulkov. Parametric four-wave processes in photorefractive crystals

V. Zelevinsky, B.A. Brown, N. Frazier, M. Horoi. The nuclear shell model as a testing ground for many-body quantum chaos

W.H. Zurek. Cosmological experiments in condensed matter systems

A. Hosaka, H. Toki. Chiral bag model for the nucleon

K. Richter, D. Ullmo, R.A. Jalabert. Orbital magnetism in the ballistic regime: geometrical effects

H. Albrecht et al. (ARGUS Collaboration). Physics with ARGUS

K.G. Chetyrkin, J.H. Kühn, A. Kwiatkowski. QCD corrections to the e^+e^- cross section and the Z boson decay rate: concepts and results

S. Singh. Curvature elasticity in liquid crystals

PHYSICS REPORTS

Instructions to Authors (short version)

(A more detailed version of these instructions is published in the preliminary pages to each volume)

Submission. In principle, papers are written and submitted on the invitation of one of the Editors, although the Editors would be glad to receive suggestions. Proposals for review articles (approximately 500–1000) words should be sent by the authors to one of the Editors (listed on page 2 of the cover). The Editor will evaluate proposals on the basis of timeliness and relevance and inform the author(s) as soon as possible.

All submitted papers are subject to a refereeing process.

Preparation of manuscripts. The requirements as regards presentation of the text and illustrations are described in full in the more detailed version of these instructions. Please note that the main text should be preceded by a separate title page containing title, author(s), affiliation(s), abstract, PACS codes and keywords.

–*Address*: The name, complete postal address, e-mail address, telephone and fax number of the corresponding author should be indicated on the manuscript.

–*Abstract*: A short informative abstract not exceeding approximately 150 words is required.

–*PACS codes/keywords*: Please supply one or more PACS-1996 classification codes and up to 4 keywords of your own choice for indexing purposes.

After acceptance.

–*Proofs*: Proofs will be sent to the author 6–8 weeks after acceptance. Proofs will usually be printed on low-quality paper. Please note that the proofs have been proofread by the Publisher and only a cursory check by the author is needed; we are unable to accept changes in, or additions to, the edited manuscript at this stage. In order to guarantee the fastest possible production times, the proofs must be returned within 48 hours after receipt, preferably by fax. If no reply is received, the Publisher assumes that there are no further corrections to be made and will proceed with publication of the article.

–*Copyright transfer*: The author(s) will receive a form with which they can transfer copyright of the article to the Publisher. This transfer will ensure the widest possible dissemination of information.

Electronic manuscripts. The Publisher welcomes the receipt of an electronic version of your accepted manuscript (encoded in LaTeX). If you have not already supplied the final, revised version of your article (on diskette) to the Journal Editor, you are requested herewith to send a file with the text of the accepted manuscript directly to the Publisher by e-mail or on diskette (allowed formats 3.5″ or 5.25″ MS-DOS, or 3.5″ Macintosh) to the address given below. Please note that no deviations from the version accepted by the Editor of the journal are permissible without the prior and explicit approval by the Editor. Such changes should be clearly indicated on an accompanying printout of the file.

Files sent via electronic mail should be accompanied by a clear identification of the article (name of journal, editor's reference number) in the "subject field" of the e-mail message. LaTeX articles should preferably use the Elsevier document class "elsart", or alternatively the standard document class "article" or the document style "revtex". The Elsevier LaTeX package (including detailed instructions to authors) can be obtained using anonymous FTP from the Comprehensive TeX Archive Network (CTAN), or from the Publisher (see detailed instructions).

Author benefits.

–*Free offprints.* For regular articles, the joint authors will receive 10 offprints free of charge of the journal issue containing their contribution; additional copies may be ordered at a reduced rate.

–*DISCOUNT. Contributors to Elsevier Science journals are entitled to a 30% discount on all Elsevier Science books.*

Further information. Mail: Elsevier Science B.V., Issue Management, Physics Reports, P.O. Box 2759, 1000 CT Amsterdam, The Netherlands.

E-mail: l.bakker@elsevier.nl (subject Physics Reports).

URL: http://www.elsevier.nl/

In all correspondence with the Publisher, please include full reference to the paper concerned, i.e. journal name, the name of the first author, title and manuscript reference number.

North-Holland, an imprint of Elsevier Science

PHYSICS REPORTS

A Review Section of Physics Letters

Volume 272, numbers 2 & 3, July 1996

Abstracted/Indexed in: Current Contents: Physical, Chemical & Earth Sciences/INSPEC/ Physics Briefs/Chemical Abstracts

Contents

◆ means that this issue falls in the subject area generally covered by 'Physics Letters A', viz. general physics, statistical physics, nonlinear science, atomic and molecular physics, plasma and fluid physics and condensed matter physics.

◆◆ means that this issue falls in the subject area generally covered by 'Physics Letters B', viz. nuclear physics and high energy physics.

0370-1573(199607)272:2&3;1-S